# Generator-Collector Sensors for Water Quality Monitoring

Lewis, Grace

*Award date:*
2015

*Awarding institution:*
University of Bath

# Generator-Collector Sensors for Water Quality Monitoring

**Grace Elizabeth Margaret Lewis**

A thesis submitted for the degree of Doctor of Philosophy
University of Bath
Department of Chemistry
April 2015

# Acknowledgments

I gratefully acknowledge Professor Frank Marken and Dr. Barbara Kasprzyk-Hordern for being such inspirational supervisors, who guided and supported me to achieve my PhD. I would also like to thank my co-supervisor Dr. Anneke Lubben for her encouragement and invaluable advice at times when it was most definitely needed. All three supervisors have played a vital role in enabling me to get to where I am today and I feel extremely privileged to have been given the opportunity to work with them. An extended thank you must go to all members of the Marken and Kasprzyk-Hordern groups (past and present) for making my postgraduate experience an enjoyable one.

A special mention must go to my fellow PhD student Sian Evans for keeping my sanity in check, even when enduring the horrendous smells of the wastewater treatment plant, and Dr. Sara Dale who continually motivated me and welcomed me whole-heartedly into the Marken group on my first day. I am delighted to have the friendship of both Sian and Sara and look forward to the many more laughs that lie ahead.

The continued love and support from family must not be missed as without them I would not have found the courage to pursue a career in science and believe that I am able to achieve my ambitions.

Finally, I acknowledge the NERC for funding my postgraduate research.

"*I have not failed. I've just found 10,000 ways that won't work.*"

- Thomas A. Edison (1847-1931)

# Abstract

The detection of emerging environmental contaminants at trace levels is a huge challenge for analytical research, and when expensive laboratory equipment is required, it is essential to provide a cheaper method that can ultimately undertake real-time sampling, whilst maintaining the sensitivity and reliability of current monitoring procedures. Electrochemical methods are a suitable candidate and studies into the development of submicron-gap generator-collector electrodes are provided alongside a variety of electrochemical methods.

The aim of this project is to fabricate novel, low-cost, electrochemical devices with the potential for development into sensors for water quality monitoring. Nitrobenzene, Phosphate and Hydroquinone are the analytes used as they have well-known redox pathways and are known environmental pollutants and/or markers for other emerging contaminants.

Initial studies examine the use of square wave voltammetry experiments in generator-collector mode, to provide information on either the fully reduced species or the intermediate species, depending on the buffered conditions used, with a view to detecting short-lived intermediates. Drawbacks with electrode geometry see the development of junction electrodes with larger active areas for greater sensitivity and changes in electrode materials for more robust device with a wider potential window. Generator-collector electrodes are also demonstrated as devices in electrochemical flow injection and for anion transfer at a triple phase boundary.

# List of Abbreviations

| | |
|---|---|
| AFM | Atomic force microscopy |
| BDD | Boron-doped diamond |
| CE | Counter electrode |
| CVD | Chemical vapour deposition |
| DCFE | Double channel flow electrode |
| EQSD | Environmental quality standards directive |
| GC-MS | Gas chromatography – mass spectrometry |
| LC-MS | Liquid chromatography – mass spectrometry |
| NAPQI | N-acetyl-p-benzoquinone imine |
| OHP | Outer Helmholtz Plane |
| PPP | 3-(4-phenylpropyl)-pyridine |
| RDX | Hexahydro-1,3,5-trinitro-1,3,5-triazine |
| RE | Reference electrode |
| RRDE | Rotating ring-disc electrode |
| SCE | Saturated calomel electrode |
| SEM | Scanning electron microscopy |
| SPE | Solid phase extraction |
| TNT | 2,4,6-trinotrotoluene |
| TPPMn | Tetraphenylporphyrinato manganese(II/III) |
| WE | Working electrode |
| WJRDE | Wall jet ring-disc electrode |
| WWTP | Wastewater treatment process |

# List of Chemical Symbols

| | |
|---|---|
| T | Absolute temperature |
| $i_{pa}$ | Anodic peak current |
| $E_{pa}$ | Anodic peak potential |
| $c$ | Bulk concentration |
| $i_{pc}$ | Cathodic peak current |
| $E_{pc}$ | Cathodic peak potential |
| $\Phi_{cavity}$ | Cavity transport coefficient |
| $\Delta G$ | Change in Gibbs free energy |
| N | Collection efficiency |
| $I_{col}$ | Collector current |
| [Ox] | Concentration of oxidized species |
| [Red] | Concentration of reduced species |
| i | Current density |
| d | Depth |
| D | Diffusion coefficient |
| j | Diffusional flux |
| x | Distance |
| A | Electrode area |
| $K_{eq}$ | Equilibrium constant |
| F | Faradays constant |
| $I_{gen}$ | Generator current |
| $\Delta E_H$ | Hysteresis effect |
| $\delta$ | Inter-electrode gap |

| | |
|---|---|
| l | Length |
| $I_{\mathrm{lim}}$ | Limiting current |
| $\phi_{\mathrm{m}}$ | Metal potential |
| $E_{\mathrm{mid}}$ | Midpoint potential |
| n | Number of electrons |
| $N_{gap}$ | Number of generator-collector gaps |
| $\left\lvert E_p^{ox} - E_p^{red} \right\rvert$ | Peak separation |
| $\Delta\Phi_{\mathrm{m/s}}$ | Potential difference between two phases |
| $\nu$ | Scan rate |
| $\phi_{\mathrm{s}}$ | Solution potential |
| $\Delta G°$ | Standard Gibbs free energy |
| E | Standard redox potential |
| t | Time |
| $A_{IDE}$ | Total active area of the interdigitated array |
| R | Universal gas constant |
| w | Width |

# Contents

# Chapter 1

# Introduction to Water Quality Monitoring

## Abstract

An introduction is given outlining the growing concern for the occurrence and fate of trace pollutants in the aquatic environment, focussing upon current water quality monitoring research. Electrochemical sensing methods for the detection of environmental contaminants will be presented with an emphasis on hydroquinone, phosphate and nitrobenzene, the target compounds this research is based upon.

## Contents

## 1.1 Water Quality Monitoring

Water quality monitoring measures the chemical, biological and physical properties of water to ensure its condition is fit for its intended use, i.e. human consumption. Over the last few decades, emerging contaminants in the aqueous environment have been a cause for concern and until recently, their presence at low concentration was not thought to have significant effects and only monitored for short-term exposure, overlooking the risk of long-term exposure. On-going investigations expand our knowledge of the occurrence, fate and potential ecological damage and/or human health risks, of a large number of known pollutants, with newfound compounds added frequently.

Pollutants are continually introduced into the aquatic environment either as the unaltered parent compounds, metabolites or conjugates, via various transport routes. Some sources of contamination include industrial applications such as hospital waste and manufacturing processes, pesticide run-off from agricultural land, leaching from landfill sites, human excretion of pharmaceuticals and poor removal of pollutants during the wastewater treatment process (WWTP). This results in a large array of chemicals and their various forms present in the environment, with compounds such as pharmaceuticals undergoing further transformation during the WWTP [1]. With the ingestion of water and food as the primary route for the uptake of pollutants in humans and the ecosystem, it is vital that water is clean. The EU Water Framework Directive [2] aims to determine and regulate priority substances that present a risk to the aquatic environment due to their persistence, bioaccumulation and toxicity. Limits on their concentration levels in surface waters (known as environmental quality standards) are established and controlled to ensure good ecological status. Current legislation (2012 Commission proposal on priority substances (COM(2011)876) and Environmental Quality Standards Directive (EQSD) 2008/105/EC) names around 40 priority

substances, with some identified as priority hazardous substances. These include a variety of metals and their compounds such as lead, cadmium, nickel and mercury, polyaromatic hydrocarbons, polybrominated biphenylethers (flame retardants), benzene, chloroform, and recently added diclofenac, a non-steroidal anti-inflammatory drug and 17β-estradiol, an endocrine disrupter. It is therefore of vital importance that the analytical methods used for the monitoring and detection of these pollutants provide reliable and sensitive data that can be applied worldwide.

## 1.2 Current Analytical Methods

With on-going research into the existence of pollutants within WWTP effluent, surface and drinking water, at concentrations ranging from $\mu gL^{-1}$ to $ngL^{-1}$, analytical methods are constantly evolving to improve detection limits and industry standard protocols. Common analytical techniques include liquid chromatography – mass spectrometry (LC-MS) [3, 4], gas chromatography – mass spectrometry (GC-MS) and capillary electrophoresis (CE). LC-MS has become the method of choice regarding polar organic compounds and with constant improvements towards method development; reliable, precise and sensitive results can be obtained [5]. It has an advantage, especially over GC-MS (mainly used for non-polar, volatile compounds), that no derivatisation step is necessary; therefore less time is needed on sample preparation and thus it is less labour intensive. In combination with sample pre-concentration steps, trace level (ng/L) detection limits can be reached. Sample preparation techniques are an important step in the analysis process; they are optimised to extract the analytes of interest from the bulk sample and incorporate a clean-up procedure to concentrate the analyte from the very low concentrations present so it is detectable by LC-MS [6-8]. Solid phase extraction

(SPE) is most frequently used, where an aqueous sample is passed through a solid sorbent to retain the pollutants on the membrane, followed by washing the analyte with an organic solvent to elute them. Although SPE provides better selectivity, sensitivity and accuracy of sample preparation than other extraction techniques, such as liquid-liquid extraction, it does require the selection of an appropriate sorbent and extraction conditions. As many target compounds are determined simultaneously, care must be taken in optimising the experimental conditions to provide the best recovery for all compounds, but unfortunately this is often a compromise and the best performance cannot be obtained for each compound. Despite this, SPE has proven to give high accuracy and precision for environmental water samples [9].

Despite major advances in analytical techniques, limitations still exist for environmental detection of trace pollutants. Improvements in method development [10] such as matrix effects, interferences [11] and extraction conditions need to be addressed [5], but also the time required to carry out such experiments is under scrutiny. Current methods are extremely time consuming because of the many stages a sample has to endure between sample collection and data handling. Sample collection is the only stage performed in the field therefore appropriate transportation and storage is needed to transfer the samples to the laboratory. Suitable storage is required throughout the process to avoid contamination or degradation of the sample and the active analyte contained within it. In order to carry out any of the sample collection, pre-treatment or analysis, skilled workers are required to operate instrumentation and implement the various methods throughout the proceedings. All of the aspects mentioned generate a large financial cost limiting the usage of current analytical techniques to developing countries [12]. The development of a system that is cost effective and portable, can perform real-time

sampling and does not require trained technicians would greatly benefit environmental research (see section 1.3).

## 1.3 Electrochemical Sensing and Target Pollutants

For the detection of emerging environmental pollutants, electrochemistry offers a low cost alternative to current practices offering potentially high accuracy and low detection limits. As electrons are the main reagent source, as opposed to organic chemicals, electrochemical technologies are "clean", therefore do not contribute to contamination of the sample during the experimental process. The equipment is easily automated, controlled and operated, generally without the need for high temperature and pressure, so the use of trained technicians is minimised again lowering the financial implications. Finally, with the adjustment of experimental conditions, electrochemical processes can be made more selective or alternatively can be optimised to detect a particular analyte or group of target compounds.

Environmental detection of emerging pollutants using electrochemical devices is a newly developing area of research that faces many challenges. The majority of these contaminants are relatively small molecules found at trace amounts and are therefore difficult to detect. A pre-concentration step or modification of an electrode surface is generally needed to enhance detection limits, for example DNA-aptamers immobilised onto the surface of gold electrodes were developed for the sensitive detection of chloramphenicol [13], and electrochemical aptasensors with carbon nanotube modifications were successfully developed for tetracyclines [14].

Electrochemical devices have been employed for a vast array of environmental applications for many years, especially for monitoring water quality parameters such as pH, dissolved oxygen and conductivity. This has led to the successful development of sensitive and selective field-based sensors for the detection and/or monitoring of emerging environmental pollutants. Electrochemical sensors can be designed for a particular function; for example, voltammetric/amperometric devices measure the rate of electron transfer which is proportional to the target analyte concentration, while potentiometric methods (mainly ion-selective electrodes) measures ionic concentration by converting the ion activity in the solution to an electrical potential. Stripping-based electrochemical sensors (where the target metal accumulates on the working electrode) have been successfully employed for the monitoring of heavy metals [15] such as mercury [16, 17], lead [17-20], cadmium [18-20], and copper [17, 20], with the advantage of being extremely sensitive and selective.

### 1.3.1 Nitro-based Explosives

The detection of nitro-based explosives is of particular importance for national security and environmental purposes [21]. Explosives such as 2,4,6-trinotrotoluene (TNT) and hexahydro-1,3,5-trinitro-1,3,5-triazine (RDX) are used widely within the military, construction and demolition, and are produced and used in large quantities. RDX, an explosive nitroamine, was widely used during World War II and developed to be more powerful than TNT (the most commonly used explosive). During their production, explosive compounds are released into the environment and lead to the contamination of groundwater and soil when concentrations reach toxic levels [22].

Nitro-based explosives are commonly monitored using sensitive analytical techniques such as ion mobility spectrometry [23, 24], mass spectrometry [25-27] and gas chromatography [28, 29]. However, continual threats of terrorist activity raises the need for a more rapid and sensitive detection device that can also be deployed on-site for the analysis of post explosion debris and at contaminated sites. Reliability, simplicity and low cost are among many requirements for a nitro-based explosive sensor along with the ability to detect bulk and trace concentrations.

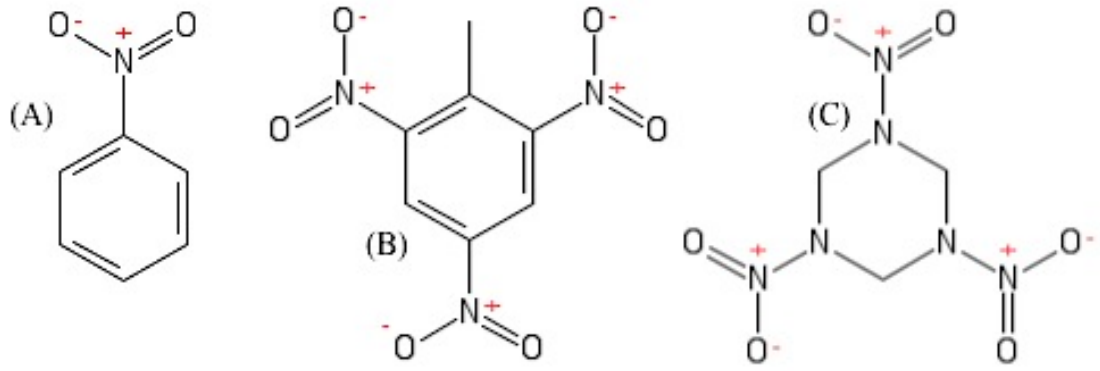


**Figure 1.1** Chemical structures of (A) nitrobenzene, (B) TNT and (C) RDX.

Electrochemical methods offer the advantage, over current detection techniques, of miniaturization to a portable/handheld device without compromising sensitivity and reliability. With advances in micro-fabrication [30, 31], analytical devices are developed for on-site testing, with a range of working electrode materials for the cathodic measurements of nitro-aromatic compounds. A commercial nitro-based explosive has well-known redox properties ideal for electrochemical detection and/or monitoring [32]. A nitro aromatic follows a reduction reaction pathway to form an amine via an electron transfer with a hydroxylamine intermediate [32, 33], and the nitro group contains an electron deficient nitrogen which acts as an electron acceptor. A

common electrode material used for nitro-aromatics is carbon in its various forms [32, 34], i.e. fibre, glassy carbon and graphene. These materials exhibit strong absorption of the nitro-compound onto the surface making them ideal for selective determination, and modification of these electrodes can further enhance their capabilities [35]. A commonly employed electrochemical technique for this application is square wave voltammetry [36], utilizing the options of faster scan rates, and greater sensitivity compared to other conventional voltammetric methods. Table 1.1 describes a variety of electrochemical tools used for the detection of nitro-based compounds and the environmental sample tested.

| **Electrode material** | **Nitro compound detected** | **Limit of Detection (µg/L)** | **Environmental sample tested** |
|---|---|---|---|
| Glassy carbon electrode modified with multi-wall carbon nanotubes [37] | TNT | 0.6 | Untreated nondeaerated seawater |
| Glassy carbon electrode modified with copper nanoparticles and single-wall carbon nanotubes, solubilised in nafion [38] | TNT | 1 | Tap water, river water and contaminated soil |
| Mercury film immobilised on glassy carbon electrode [39] | RDX | 120 | Soil |
| Screen printed carbon electrode [40] | TNT | 200 | Ground water and river water |
| Screen printed carbon electrode [41] | 2,6-DNT | 160 | N/A |
| Flow system for on-line monitoring with a carbon fibre detector [42] | TNT | 25 | Untreated seawater and river water |

| | | | |
|---|---|---|---|
| Micro-fabricated capillary electrophoresis chips with integrated electrochemical detection using a gold working electrode [43, 44] | TNT | 24 | Soil and ground water |
| Microfluidic device with a mercury/gold amalgam electrode [34] | TNT | 7 | N/A |
| Graphene film deposited onto a glassy carbon electrode [45] | TNT | 1 - 200 | N/A |
| Glassy carbon electrode modified with graphene nano-ribbons [46] | TNT | 1 | Untreated seawater |
| Glassy carbon electrode modified with (i) graphene nano-ribbons and (ii) graphene nano-sheets, plus a (iii) bare glassy carbon electrode [47] | TNT | (i) 0.14, (ii) 0.51, (iii) 0.52 | Seawater |
| Glassy carbon electrode modified with multi-wall carbon nanotubes [48] | RDX | 0.6 | Ground water and tap water |

**Table 1.1** Summary of carbon-based electrodes used for the detection of nitro-based explosives.

### 1.3.2 Phosphates

Nutrient pollution, such as nitrogen and phosphorus, is another challenging environmental issue that demands reliable and sensitive detection methods. Phosphorus is essential for living cells and supports the growth of algae and aquatic plants, providing food for aquatic organisms. However, excess phosphorus from human

activity, such as agriculture, pollutes water and results in faster algae growth. Algal blooms (large growths of algae) reduce the water quality and deplete dissolved oxygen, which is detrimental to all aquatic life and can be harmful to humans if they come into contact with polluted water or consume infected fish/shellfish.

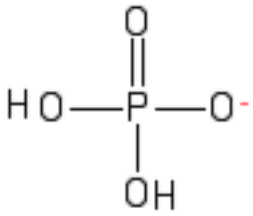


**Figure 1.1** Chemical structures of Phosphate,

Phosphates are formed from the element phosphorus and can occur as orthophosphates (found in sewage), polyphosphates (used in detergents) that are broken down by hydrolysis into the ortho form and organic phosphates (results from the breakdown of pesticides). Phosphate anions are found at approximately 63% in the soluble fraction of wastewater [49] and the EU water framework directive (EU Directive 98/15/EEC) states the maximum annual mean total phosphorus concentration is 2 mg/L. The recommended laboratory method used to determine the concentration of phosphates is colourimetric analysis [50]. The orthophosphate sample is added to a mixture of reagents, producing a blue coloured phosphomolybdate complex that can be measured optically with a spectrophotometer. This standard technique can be labour intensive and costly, so a sensor designed to be cheaper with continuous, real-time monitoring would be highly beneficial.

Various electrochemical sensor methodologies and electrodes have been reported and reviewed [51-54] for the detection of orthophosphate ions, with potentiometric, amperometric and voltammetric approaches, summarized in Table 1.2. Potentiometric methods have utilized ion-selective electrodes to facilitate the transfer of the ion via a central ionophore compound and solid-state electrodes, which offer greater durability and miniaturization capabilities. Unfortunately this technique offered limited success, with electrodes requiring pre-treatment, others had short lifetimes and some experienced sensitivity to interferences. Amperometric sensors have used enzymes immobilized onto the surface of the electrode for greater selectivity via molecular recognition and ferrocene based receptors. Voltammetry offers an indirect measurement of phosphate for example with the use of receptors on the surface of the electrode to attract the phosphate ion or the reaction of phosphate with metals and associated complexes. However both amperometric and voltammetric sensors also suffer from poor selectivity and therefore need greater revision before they are suitable for use in-field.

| **Electrochemical detection technique** | **Method/electrode** | **Limit of Detection (µg/L)** |
|---|---|---|
| Potentiometric Ion-selective electrodes | Organotin ionophore, PVC membrane [55] | 1000 |
| | Molybdenum acetylacetonate ionophore [56] | 30 |
| | Ferrocene / macrocyclic amide, PVC membrane [57] | 70 |
| Potentiometric Solid state electrodes | Cobalt electrode with oxide layer [58] | 160 |
| | Bisthiourea ionophore based screen printed electrode [59] | 120 |
| | Modified carbon paste electrodes with zeolite [60] | 400 |
| | Solid state membrane disk with aluminium copper and aluminium phosphate [61] | 30 |
| Amperometric | Enzyme based sensor that generates hydrogen peroxide [62] | 3 |
| | Anodic oxidation of molybdenum [63] | 4 |
| | Reduction of phosphomolybdate complex [64] | 30 |
| Voltammetric | Redox of molybdovanadophosphate [65] | 30 |
| | Inhibition of redox reaction of potassium hexacyanoferrate [66] | 1600 |
| | Inhibition of an enzyme based glucose electrode [67] | 9 |

**Table 1.2** Summary of electrochemical methods used for the detection of phosphates.

### 1.3.3 Hydroquinone

Hydroquinone (1,4-dihydroxy-benzene) and its oxidized derivative 1,4-benzoquinone are major benzene metabolites that are ubiquitous in the environment. Benzene is a well-known carcinogen that is readily released into the environment through emissions from burning coal and oil, gasoline stations, vehicle exhausts, and combustion processes. Metabolism of benzene in the body is enzymatically converted to hydroquinone, a redox active compound that promotes the formation of reactive oxygen species and accumulates in the urine. Further metabolism converts hydroquinone into 1,4-benzoquinone, a toxic metabolite found in human blood. Both metabolites can therefore be used as a biomarker for human exposure and can also be used to track the exposure of benzene, in mixtures such as petrol.

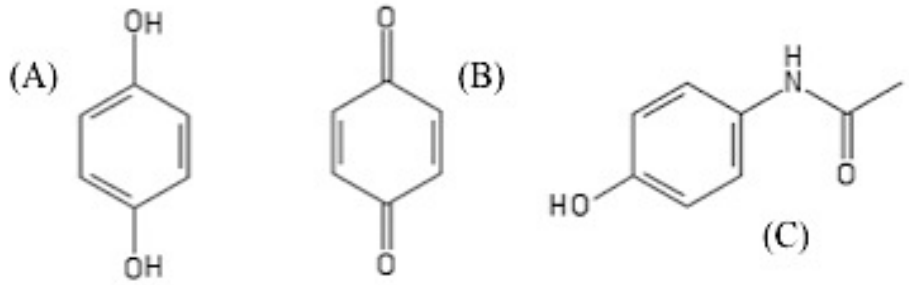


**Figure 1.3** Chemical structures of (A) hydroquinone, (B) benzoquinone and (C) paracetamol.

Hydroquinone also has many industrial applications; as a developing agent in black and white photography and x-ray films, an intermediate to produce antioxidants for rubber and food, and a dye intermediate. Exposure to hydroquinone alone can cause irritation to the skin and ingestion of large amounts results in various symptoms such as tinnitus (ringing of the ears), nausea, vomiting, convulsion and many more. 1,4-benzoquinone is

also a well know metabolite of paracetamol (also known as acetaminophen and N-acetyl-p-aminophenol). In the liver, during xenobiotic metabolism, a small fraction, about 5-10%, of paracetamol is oxidised to form the toxic and highly reactive para-quinone NAPQI (N-acetyl-p-benzoquinone imine) by-product. At therapeutic levels, the drug is almost immediately detoxified by conjugation with glutathione but excess levels in the body, see the glucuronidation and sulfation pathways saturated, increasing the amount of unchanged drug eliminated, which then oxidises to form NAPQI [68]. NAPQI depletes the glutathione stores in the liver and binds to cellular proteins resulting in hepatotoxicity [69].

Alongside parent compounds, there is a demand for the detection of their metabolites, which can be more toxic and environmentally damaging. Hydroquinone has a well-known oxidation pathway and is therefore suitable for electrochemical detection. Many reported electrochemical methods with applications in aqueous environmental samples focus on the simultaneous detection of hydroquinone and catechol due to their overlapping redox peaks. Table 1.3 describe electrode materials developed for the simultaneous detection of hydroquinone and catechol using differential pulse voltammetry.

With electrochemical methods offering valuable characteristics compared to conventional laboratory based technology, it is of utmost importance to develop novel devices that are sensitive and selective to low level concentrations of environmental pollutants. The work described throughout this thesis aims to provide experimental methods for the detection of a variety of redox analytes using various generator-collector electrode geometries with an aim of developing a simple and novel electrochemical sensor for the detection of nitrobenzene, phosphate and hydroquinone in wastewater and drinking water.

| **Electrode** | **Limit of Detection for HQ (µmol/L)** | **Sample tested for proposed method** |
|---|---|---|
| Modified glassy carbon with multi-wall carbon nanotubes [70] | 0.75 | Tap water. Recoveries of ca. 98-102% |
| Graphene-chitosan composite film modified glassy carbon electrode [71] | 0.75 | Tap, river and lake water. Recoveries of ca. 95-104% |
| Poly-amidosulfonic acid and multi-wall carbon nanotube composite modified glassy carbon electrode [72] | 1 | Tap water. Recoveries of ca. 98-103% |
| Poly(thionine) modified glassy carbon electrode [73] | 0.03 | Tap water. Recoveries of ca. 97-102% |
| Activated glassy carbon electrode [74] | 0.16 | Tap water. Recoveries of ca. 96-104% |
| Electrospun carbon nanofiber modified carbon paste electrode [75] | 0.4 | Lake water. Recoveries of ca. 96-102% |
| Glassy carbon electrode covalently modified with penicillamine [76] | 1 | Tap water. Recoveries of ca. 97-104% |
| Modified glassy carbon electrode with poly(diallyldimethylammonium chloride) functionalized graphene [77] | 0.25 | Yellow river water. Recoveries of ca. 97-103% |
| Gold electrode modified with carbon nanofibers and gold nanoparticles [78] | 0.86 | Tap water. Recoveries of ca. 95-104% |
| Graphene oxide-mesoporous $MnO_2$ nanocomposite modified glassy carbon electrode [79] | 0.007 | Filtered lake water. Recoveries of ca. 97-108% |

**Table 1.3** Summary of electrode materials developed for the simultaneous determination of hydroquinone and catechol using differential pulse voltammetry.

## 1.4 References

1. Kasprzyk-Hordern, B., *Pharmacologically active compounds in the environment and their chirality.* Chemical Society Reviews, 2010. **39**(11): p. 4466-4503.

2. *The EU Water Framework Directive*. Cited 2015; Available from: http://ec.europa.eu/environment/water/water-framework/index_en.html.

3. Gros, M., M. Petrovic, and D. Barcelo, *Multi-residue analytical methods using LC-tandem MS for the determination of pharmaceuticals in environmental and wastewater samples: a review.* Analytical and Bioanalytical Chemistry, 2006. **386**(4): p. 941-952.

4. Kim, S.C. and K. Carlson, *LC-MS2 for quantifying trace amounts of pharmaceutical compounds in soil and sediment matrices.* Trac-Trends in Analytical Chemistry, 2005. **24**(7): p. 635-644.

5. Primel, E.G., S.S. Caldas, and A.L.V. Escarrone, *Multi-residue analytical methods for the determination of pesticides and PPCPs in water by LC-MS/MS: a review.* Central European Journal of Chemistry, 2012. **10**(3): p. 876-899.

6. Barcelo, D., *LC-tandem MS.* Trac-Trends in Analytical Chemistry, 2005. **24**(7): p. 564-565.

7. Diaz-Cruz, M.S. and D. Barcelo, *LC-MS2 trace analysis of antimicrobials in water, sediment and soil.* Trac-Trends in Analytical Chemistry, 2005. **24**(7): p. 645-657.

8. Petrovic, M., M.D. Hernando, M.S. Diaz-Cruz, and D. Barcelo, *Liquid chromatography-tandem mass spectrometry for the analysis of pharmaceutical*

*residues in environmental samples: a review.* Journal of Chromatography A, 2005. **1067**(1-2): p. 1-14.

9. Marie-Claire, H., *Solid-phase extraction: method development, sorbents, and coupling with liquid chromatography.* Journal of Chromatography A, 1999. **856**(1–2): p. 3-54.

10. Baker, D.R. and B. Kasprzyk-Hordern, *Critical evaluation of methodology commonly used in sample collection, storage and preparation for the analysis of pharmaceuticals and illicit drugs in surface water and wastewater by solid phase extraction and liquid chromatography-mass spectrometry.* Journal of Chromatography A, 2011. **1218**(44): p. 8036-8059.

11. Keller, B.O., J. Sui, A.B. Young, and R.M. Whittal, *Interferences and contaminants encountered in modern mass spectrometry.* Analytica Chimica Acta, 2008. **627**(1): p. 71-81.

12. Jjemba, P., *Pharma-Ecology: The Occurrence and Fate of Pharmaceuticals and Personal Care Products in the Environment*. 2008, New Jersey: John Wiley & Sons, chapter 2.

13. Mehta, J., B. Van Dorst, E. Rouah-Martin, W. Herrebout, M.-L. Scippo, R. Blust, and J. Robbens, *In vitro selection and characterization of DNA aptamers recognizing chloramphenicol.* Journal of Biotechnology, 2011. **155**(4): p. 361-369.

14. Zhou, L., D.-J. Li, L. Gai, J.-P. Wang, and Y.-B. Li, *Electrochemical aptasensor for the detection of tetracycline with multi-walled carbon nanotubes amplification.* Sensors and Actuators B-Chemical, 2012. **162**(1): p. 201-208.

15. Chang, J., G. Zhou, E.R. Christensen, R. Heideman, and J. Chen, *Graphene-based sensors for detection of heavy metals in water: a review.* Analytical and Bioanalytical Chemistry, 2014. **406**(16): p. 3957-3975.

16. Zhou, L., W. Xiong, and S. Liu, *Preparation of a gold electrode modified with Au-TiO2 nanoparticles as an electrochemical sensor for the detection of mercury(II) ions.* Journal of Materials Science, 2015. **50**(2): p. 769-776.

17. Wang, S., E.S. Forzani, and N. Tao, *Detection of heavy metal ions in water by high-resolution surface plasmon resonance spectroscopy combined with anodic stripping voltammetry.* Analytical Chemistry, 2007. **79**(12): p. 4427-4432.

18. Tang, F.-J., F. Zhang, Q.-H. Jin, and J.-L. Zhao, *Determination of Trace Cadmium and Lead in Water Based on Graphene-modified Platinum Electrode Sensor.* Chinese Journal of Analytical Chemistry, 2013. **41**(2): p. 278-282.

19. dos Santos, V.B., E.L. Fava, N.S. de Miranda Curi, R.C. Faria, and O. Fatibello-Filho, *A thermostated electrochemical flow cell with a coupled bismuth film electrode for square-wave anodic stripping voltammetric determination of cadmium(II) and lead(II) in natural, wastewater and tap water samples.* Talanta, 2014. **126**: p. 82-90.

20. Palchetti, I., S. Laschi, and M. Mascini, *Miniaturised stripping-based carbon modified sensor for in field analysis of heavy metals.* Analytica Chimica Acta, 2005. **530**(1): p. 61-67.

21. Yinon, J., *Field detection and monitoring of explosives.* Trac-Trends in Analytical Chemistry, 2002. **21**(4): p. 292-301.

22. Pennington, J.C. and J.M. Brannon, *Environmental fate of explosives.* Thermochimica Acta, 2002. **384**(1-2): p. 163-172.

23. Khayamian, T., M. Tabrizchi, and M.T. Jafari, *Analysis of 2,4,6-trinitrotoluene, pentaerythritol tetranitrate and cyclo-1,3,5-trimethylene-2,4,6-trinitramine using negative corona discharge ion mobility spectrometry.* Talanta, 2003. **59**(2): p. 327-333.

24. Buryakov, I.A., *Detection of explosives by ion mobility spectrometry.* Journal of Analytical Chemistry, 2011. **66**(8): p. 674-694.

25. Zhao, X.M. and J. Yinon, *Characterization and origin identification of 2,4,6-trinitrotoluene through its by-product isomers by liquid chromatography-atmospheric pressure chemical ionization mass spectrometry.* Journal of Chromatography A, 2002. **946**(1-2): p. 125-132.

26. Evans, C.S., R. Sleeman, J. Luke, and B.J. Keely, *A rapid and efficient mass spectrometric method for the analysis of explosives.* Rapid Communications in Mass Spectrometry, 2002. **16**(19): p. 1883-1891.

27. Badjagbo, K. and S. Sauve, *Mass Spectrometry for Trace Analysis of Explosives in Water.* Critical Reviews in Analytical Chemistry, 2012. **42**(3): p. 257-271.

28. Ebrahimzadeh, H., Y. Yamini, and F. Kamarei, *Optimization of dispersive liquid-liquid microextraction combined with gas chromatography for the analysis of nitroaromatic compounds in water.* Talanta, 2009. **79**(5): p. 1472-1477.

29. Walsh, M.E., *Determination of nitroaromatic, nitramine, and nitrate ester explosives in soil by gas chromatography and an electron capture detector.* Talanta, 2001. **54**(3): p. 427-438.

30. Wang, J., *Portable electrochemical systems.* Trac-Trends in Analytical Chemistry, 2002. **21**(4): p. 226-232.

31. Wang, J., *Real-time electrochemical monitoring: Toward green analytical chemistry.* Accounts of Chemical Research, 2002. **35**(9): p. 811-816.

32. Bratin, K., P.T. Kissinger, R.C. Briner, and C.S. Bruntlett, *Determination of nitro aromatic, nitramine and nitrate ester explosive compounds in explosive mixtures and gunshot residue by liquid-chromatography and reductive electrochemical detection.* Analytica Chimica Acta, 1981. **130**(2): p. 295-311.

33. Chen, J.C., J.L. Shih, C.H. Liu, M.Y. Kuo, and J.M. Zen, *Disposable electrochemical sensor for determination of nitroaromatic compounds by a single-run approach.* Analytical Chemistry, 2006. **78**(11): p. 3752-3757.

34. Wang, J. and M. Pumera, *Microchip flow-injection analysis of trace 2,4,6-trinitrotoluene (TNT) using mercury-amalgam electrochemical detector.* Talanta, 2006. **69**(4): p. 984-987.

35. Agui, L., D. Vega-Montenegro, P. Yanez-Sedeno, and J.M. Pingarron, *Rapid voltammetric determination of nitroaromatic explosives at electrochemically activated carbon-fibre electrodes.* Analytical and Bioanalytical Chemistry, 2005. **382**(2): p. 381-387.

36. Wang, J., E. Ouziel, C. Yarnitzky, and M. Ariel, *Flow detector based on square-wave polarography at dropping mercury-electrode.* Analytica Chimica Acta, 1978. **102**(DEC): p. 99-112.

37. Wang, J., S.B. Hocevar, and B. Ogorevc, *Carbon nanotube-modified glassy carbon electrode for adsorptive stripping voltammetric detection of ultratrace levels of 2,4,6-trinitrotoluene.* Electrochemistry Communications, 2004. **6**(2): p. 176-179.

38. Hrapovic, S., E. Majid, Y. Liu, K. Male, and J.H.T. Luong, *Metallic nanoparticle-carbon nanotube composites for electrochemical determination of explosive nitroaromatic compounds.* Analytical Chemistry, 2006. **78**(15): p. 5504-5512.

39. Ly, S.Y., D.H. Kim, and M.H. Kim, *Square-wave cathodic stripping voltammetric analysis of RDX using mercury-film plated glassy carbon electrode.* Talanta, 2002. **58**(5): p. 919-926.

40. Wang, J., F. Lu, D. MacDonald, J.M. Lu, M.E.S. Ozsoz, and K.R. Rogers, *Screen-printed voltammetric sensor for TNT.* Talanta, 1998. **46**(6): p. 1405-1412.

41. Honeychurch, K.C., J.P. Hart, P.R.J. Pritchard, S.J. Hawkins, and N.M. Ratcliffe, *Development of an electrochemical assay for 2,6-dinitrotoluene, based on a screen-printed carbon electrode, and its potential application in bioanalysis, occupational and public health.* Biosensors & Bioelectronics, 2003. **19**(4): p. 305-312.

42. Wang, J. and S. Thongngamdee, *On-line electrochemical monitoring of (TNT) 2,4,6-trinitrotoluene in natural waters.* Analytica Chimica Acta, 2003. **485**(2): p. 139-144.

43. Hilmi, A. and J.H.T. Luong, *Electrochemical detectors prepared by electroless deposition for microfabricated electrophoresis chips.* Analytical Chemistry, 2000. **72**(19): p. 4677-4682.

44. Hilmi, A. and J.H.T. Luong, *Micromachined electrophoresis chips with electrochemical detectors for analysis of explosive compounds in soil and groundwater.* Environmental Science & Technology, 2000. **34**(14): p. 3046-3050.

45. Tang, L.H., H.B. Feng, J.S. Cheng, and J.H. Li, *Uniform and rich-wrinkled electrophoretic deposited graphene film: a robust electrochemical platform for TNT sensing.* Chemical Communications, 2010. **46**(32): p. 5882-5884.

46. Goh, M.S. and M. Pumera, *Graphene-based electrochemical sensor for detection of 2,4,6-trinitrotoluene (TNT) in seawater: the comparison of single-, few-, and multilayer graphene nanoribbons and graphite microparticles.* Analytical and Bioanalytical Chemistry, 2011. **399**(1): p. 127-131.

47. Tan, S.M., C.K. Chua, and M. Pumera, *Graphenes prepared from multi-walled carbon nanotubes and stacked graphene nanofibers for detection of 2,4,6-trinitrotoluene (TNT) in seawater.* Analyst, 2013. **138**(6): p. 1700-1704.

48. Rezaei, B. and S. Damiri, *Using of multi-walled carbon nanotubes electrode for adsorptive stripping voltammetric determination of ultratrace levels of RDX*

*explosive in the environmental samples.* Journal of Hazardous Materials, 2010. **183**(1-3): p. 138-144.

49. Parsons, S.A. and J.A. Smith, *Phosphorus removal and recovery from municipal wastewaters.* Elements, 2008. **4**(2): p. 109-112.

50. Murphy, J. and J.P. Riley, *A modified single solution method for the determination of phosphate in natural-waters.* Agriculture Biology & Environmental Sciences, 1986(12): p. 16-16.

51. Villalba, M.M., K.J. McKeegan, D.H. Vaughan, M.F. Cardosi, and J. Davis, *Bioelectroanalytical determination of phosphate: A review.* Journal of Molecular Catalysis B-Enzymatic, 2009. **59**(1-3): p. 1-8.

52. Engblom, S.O., *The phosphate sensor.* Biosensors & Bioelectronics, 1998. **13**(9): p. 981-994.

53. Midgley, D., *Sulfate and phosphate ion-selectove electrodes.* Ion-Selective Electrode Reviews, 1986. **8**(1): p. 3-54.

54. Warwick, C., A. Guerreiro, and A. Soares, *Sensing and analysis of soluble phosphates in environmental samples: A review.* Biosensors & Bioelectronics, 2013. **41**: p. 1-11.

55. Glazier, S.A. and M.A. Arnold, *Phosphate-selectove polymer membrane-ekectrode.* Analytical Chemistry, 1988. **60**(22): p. 2540-2542.

56. Ganjali, M.R., P. Norouzi, M. Ghomi, and M. Salavati-Niasari, *Highly selective and sensitive monohydrogen phosphate membrane sensor based on molybdenum acetylacetonate.* Analytica Chimica Acta, 2006. **567**(2): p. 196-201.

57. Liu, W., X. Li, M. Song, and Y. Wu, *A novel dibasic phosphate-selective electrode based on Ferrocene-bearing macrocyclic amide compound.* Sensors and Actuators B-Chemical, 2007. **126**(2): p. 609-615.

58. Meruva, R.K. and M.E. Meyerhoff, *Mixed potential response mechanism of cobalt electrodes toward inorganic phosphate.* Analytical Chemistry, 1996. **68**(13): p. 2022-2026.

59. Khaled, E., H.N.A. Hassan, A. Girgis, and R. Metelka, *Construction of novel simple phosphate screen-printed and carbon paste ion-selective electrodes.* Talanta, 2008. **77**(2): p. 737-743.

60. Ejhieh, A.N. and N. Masoudipour, *Application of a new potentiometric method for determination of phosphate based on a surfactant-modified zeolite carbon-paste electrode (SMZ-CPE).* Analytica Chimica Acta, 2010. **658**(1): p. 68-74.

61. Tafesse, F. and M. Enemchukwu, *Fabrication of new solid state phosphate selective electrodes for environmental monitoring.* Talanta, 2011. **83**(5): p. 1491-1495.

62. Durso, E.M. and P.R. Coulet, *Phosphate-sensitive enzyme electrode - A potential sensor for environment control.* Analytica Chimica Acta, 1990. **239**(1): p. 1-5.

63. Jonca, J., V. Leon Fernandez, D. Thouron, A. Paulmier, M. Graco, and V. Garcon, *Phosphate determination in seawater: Toward an autonomous electrochemical method.* Talanta, 2011. **87**: p. 161-167.

64. Udnan, Y., I.D. McKelvie, M.R. Grace, J. Jakmunee, and K. Grudpan, *Evaluation of on-line preconcentration and flow-injection amperometry for phosphate determination in fresh and marine waters.* Talanta, 2005. **66**(2): p. 461-466.

65. Fogg, A.G. and N.K. Bsebsu, *Differnetial-pulse voltammetric deterination of phosphate as molybdovanadophosphate at a glassy-carbon electrode and assessment of eluents for the flow-injection voltammetric determination of phosphate, silicate, arsenate and germanate.* Analyst, 1981. **106**(1269): p. 1288-1295.

66. Aoki, H., K. Hasegawa, K. Tohda, and Y. Umezawa, *Voltammetric detection of inorganic phosphate using ion-channel sensing with self-assembled monolayers of a hydrogen bond-forming receptor.* Biosensors & Bioelectronics, 2003. **18**(2-3): p. 261-267.

67. Cheng, W.-L., J.-W. Sue, W.-C. Chen, J.-L. Chang, and J.-M. Zen, *Activated Nickel Platform for Electrochemical Sensing of Phosphate.* Analytical Chemistry, 2010. **82**(3): p. 1157-1161.

68. Hodgman, M.J. and A.R. Garrard, *A Review of Acetaminophen Poisoning.* Critical Care Clinics, 2012. **28**(4): p. 499-516.

69. Black, M., *Acetaminophen hepatotoxicity.* Annual Review of Medicine, 1984. **35**: p. 577-593.

70. Qi, H.L. and C.X. Zhang, *Simultaneous determination of hydroquinone and catechol at a glassy carbon electrode modified with multiwall carbon nanotubes.* Electroanalysis, 2005. **17**(10): p. 832-838.

71. Yin, H., Q. Zhang, Y. Zhou, Q. Ma, T. Liu, L. Zhu, and S. Ai, *Electrochemical behavior of catechol, resorcinol and hydroquinone at graphene-chitosan composite film modified glassy carbon electrode and their simultaneous determination in water samples.* Electrochimica Acta, 2011. **56**(6): p. 2748-2753.

72. Zhao, D.-M., X.-H. Zhang, L.-J. Feng, L. Jia, and S.-F. Wang, *Simultaneous determination of hydroquinone and catechol at PASA/MWNTs composite film modified glassy carbon electrode.* Colloids and Surfaces B-Biointerfaces, 2009. **74**(1): p. 317-321.

73. Ahammad, A.J.S., M.M. Rahman, G.-R. Xu, S. Kim, and J.-J. Lee, *Highly sensitive and simultaneous determination of hydroquinone and catechol at poly(thionine) modified glassy carbon electrode.* Electrochimica Acta, 2011. **56**(14): p. 5266-5271.

74. Ahammad, A.J.S., S. Sarker, M.A. Rahman, and J.-J. Lee, *Simultaneous Determination of Hydroquinone and Catechol at an Activated Glassy Carbon Electrode.* Electroanalysis, 2010. **22**(6): p. 694-700.

75. Guo, Q., J. Huang, P. Chen, Y. Liu, H. Hou, and T. You, *Simultaneous determination of catechol and hydroquinone using electrospun carbon nanofibers modified electrode.* Sensors and Actuators B-Chemical, 2012. **163**(1): p. 179-185.

76. Wang, L., P.F. Huang, J.Y. Bai, H.J. Wang, L.Y. Zhang, and Y.Q. Zhao, *Covalent modification of a glassy carbon electrode with penicillamine for*

*simultaneous determination of hydroquinone and catechol.* Microchimica Acta, 2007. **158**(1-2): p. 151-157.

77. Wang, L., Y. Zhang, Y. Du, D. Lu, Y. Zhang, and C. Wang, *Simultaneous determination of catechol and hydroquinone based on poly (diallyldimethylammonium chloride) functionalized graphene-modified glassy carbon electrode.* Journal of Solid State Electrochemistry, 2012. **16**(4): p. 1323-1331.

78. Huo, Z., Y. Zhou, Q. Liu, X. He, Y. Liang, and M. Xu, *Sensitive simultaneous determination of catechol and hydroquinone using a gold electrode modified with carbon nanofibers and gold nanoparticles.* Microchimica Acta, 2011. **173**(1-2): p. 119-125.

79. Gan, T., J. Sun, K. Huang, L. Song, and Y. Li, *A graphene oxide-mesoporous MnO2 nanocomposite modified glassy carbon electrode as a novel and efficient voltammetric sensor for simultaneous determination of hydroquinone and catechol.* Sensors and Actuators B-Chemical, 2013. **177**: p. 412-418.

# Chapter 2

# Introduction to Electrochemical Methods with Single and Dual Electrode Devices

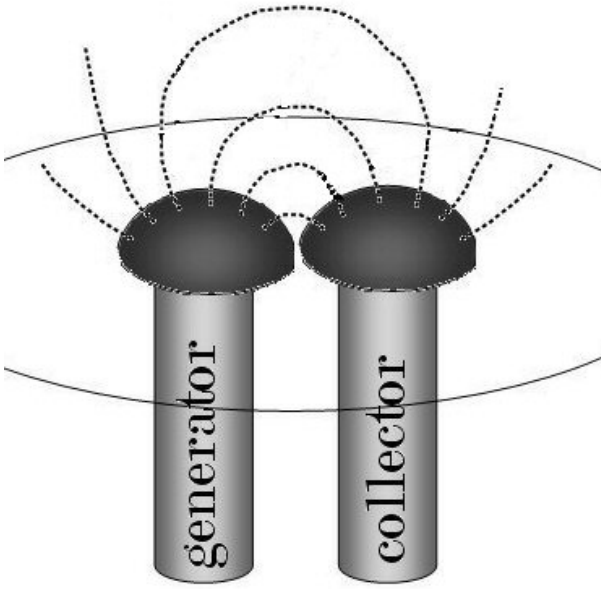


## Abstract

Electrochemical methods are based on the interaction of an electronic conductor (the working electrode) with the electrolyte solution. Charge transfer at this interface is coupled to many other processes and this chapter introduces the physico-chemical background, some important techniques, and the development of dual-electrode experiments.

# Contents

## 2.1 Electrochemical Equilibrium

Electrochemistry can be described as the study of charge transfer between electrodes and reactant molecules, usually in the solution phase [1] whether the reaction is a single electron transfer or a series of two or more steps. The charge transfer can occur in two directions; the redox species can gain an electron from the electrode to be reduced, (Equation 2.1), or it can donate an electron to the electrode surface to give the oxidised form, (Equation 2.2).

$$Fe^{3+}\ (aq) + e^{-}\ (m) \rightarrow Fe^{2+}\ (aq) \qquad (2.1)$$

$$Fe^{2+}\ (aq) \rightarrow Fe^{3+}\ (aq) + e^{-}\ (m) \qquad (2.2)$$

The electrode, an inert metal, must be immersed in an electrolyte containing solution and a voltage is applied to induce the exchange of electrons across the interface between the metallic and solution phases. At the electrode surface, equilibrium is established between the ions in solution and electrons within the metal, as illustrated by Equation 2.3.

$$Fe^{3+}\ (aq) + e^{-}\ (m) \leftrightharpoons Fe^{2+}\ (aq) \qquad (2.3)$$

As the reaction moves towards equilibrium, where the rate of oxidation and reduction is equal, a net electrical charge and potential gradient are established at the electrode-

solution interface to balance electron energies inside and outside of the metal. This charge gradient, also known as the potential difference, can be seen in Equation 2.4, Where: $\Delta\Phi_{m/s}$ is the potential difference between two phases; $\phi_s$ is the solution potential and $\phi_m$ is the metal potential. Although not directly measurable, this potential difference can be experimentally compared with that of a reference electrode.

$$\Delta\phi_{m/s} = \phi_m - \phi_s \tag{2.4}$$

The application of an external voltage is the main driving force of an electrode reaction as it provides the electrical energy needed to induce the charge transfer (electrons). It alters the energy of the electron within the electrode and the behaviour of this electrode can be understood by considering the Fermi Level.

Within a metal there are conduction bands which 'free moving' electrons occupy to bind the metal cations together. A change in electrical potential allows these electrons to move freely between these bands and a continuum of levels are filled up to an energy maximum, the Fermi Level [2]. The discrete energy levels within the ions in solution are known as unfilled molecular orbitals.

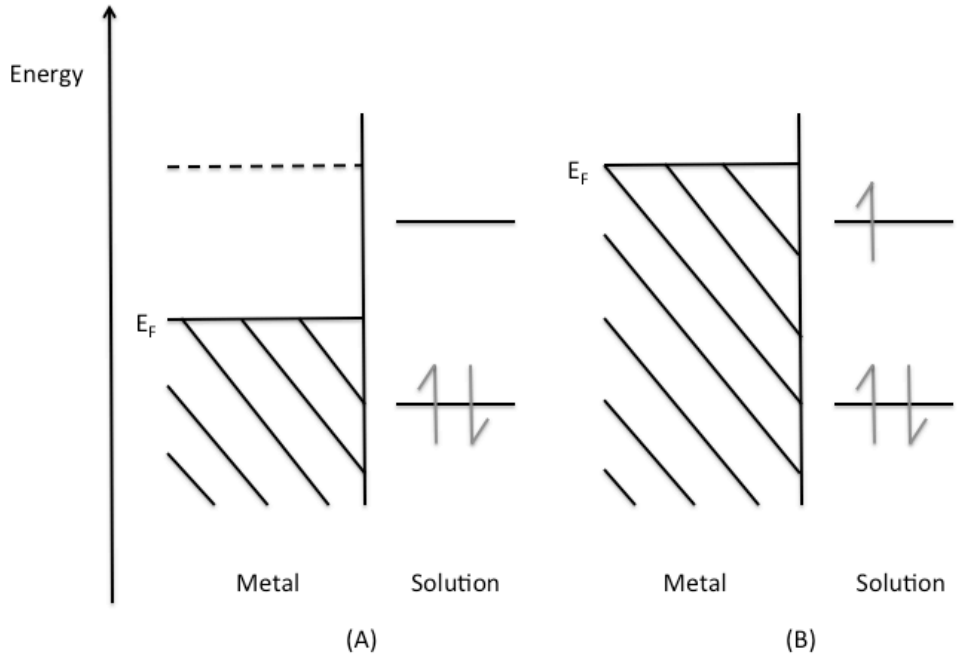


**Figure 2.1** Schematic showing the energy of electrons in the solution and the metal. (A) electrode potential is insufficient to drive the electron transfer (B) electrode potential is favourable to drive the electron transfer.

Figure 2.1(B) illustrates that by raising the energy (number of electrons) in the metal through the application of a negative potential, the Fermi level in that metal is higher than the vacant orbitals in the ions (solution phase). Therefore it is energetically favourable for the electron to transfer from the metal to the ion (solution phase), thus reducing the ion. This results in a positive charge upon the metal and an overall negative charge upon the solution. Consequently, the Fermi level in the metal is lowered and a higher energy level in solution can be seen, Figure 2.1(A).

### 2.1.1 The Nernst Equation

In the late 19$^{th}$ century, it was proposed that equilibrium is attained, under standard reaction conditions, when Gibbs free energy is at a minimum value. Chemical thermodynamics gives us the Gibbs free energy change when a general chemical reaction, (Equation 2.5), proceeds to the right, (Equation 2.6), where $\Delta G$ is the change in Gibbs free energy, $\Delta G°$ is the standard Gibbs free energy, R is the universal gas constant (8.314 J $K^{-1}$ $mol^{-1}$), T is the absolute temperature and Q is the reaction quotient.

$$\alpha A + \beta B \leftrightharpoons \gamma C + \delta D \tag{2.5}$$

$$\Delta G = \Delta G° + RT \ln Q \tag{2.6}$$

Once equilibrium is reached, the chemical and potential driving forces of the reaction are equal. We can relate potential, *E*, to Gibbs free energy change, $\Delta G$, given the following equations, where Equation 2.7 is under general conditions and Equation 2.8 under standard conditions, *n* is the number of electrons, and *F* is Faraday's constant.

$$\Delta G = -nFE \tag{2.7}$$

$$\Delta G° = -nFE° \tag{2.8}$$

By introducing Equations 2.7 and 2.8 into Equation 2.6, it can be rearranged to give the equation derived by Nernst, where *E* is the standard redox potential and [Ox] and [Red] are the concentrations of oxidised and reduced species, respectively.

$$E = E^\circ + \frac{RT}{nF} \ln \frac{[Ox]}{[Red]} \tag{2.9}$$

The Nernst equation relates the concentrations of the oxidised and reduced species to the applied potential difference from an electrochemical cell. It can be seen that small changes in potential can ultimately lead to large changes in concentration of the oxidised or reduced species.

## 2.2 Electrode Surface - Solution Interface

A charged interfacial region between the electrode and the solution is established from the movement of charged species between the two, creating parallel layers of opposite charge; one layer on the electrode surface and the other near to the surface [3]. To visualize this dynamic behaviour at the charged interface, mathematical models have been developed.

Helmholtz first identified interactions occurring at the interface, suggesting the presence of the double layer, and in 1853 proposed a model assuming that no Faradaic processes occur at the electrode. He hypothesized that the metal electrode possessed an excess charge density (positive or negative) at its surface and in order to maintain electrical

neutrality, it would be counteracted by an equal but opposite charge in the electrolyte solution [1]. Ions within the solution are attracted to the electrode so that they are the minimum distance away from the surface, and this distance is known as the Outer Helmholtz Plane (OHP). Helmholtz's double layer assumption is equivalent to that of a capacitor where some distance separates two layers of charge. The potential drop that occurs across the interface, between the two layers, is linear, Figure 2.2(A).

In the early 20$^{th}$ Century, Gouy and Chapman improved the Helmholtz model, determining that the charge density in solution was not solely located at the OHP but spread within a single 'diffuse layer' close to the electrode surface. It was suggested that this is due to the dispersion of excess ions caused by the random drifting of particles in solution, known as Brownian motion. Although the majority of the potential drop across this layer is located close to the surface, some of the charge is further away from the electrode than the OHP; therefore the potential drop decreases as it moves further into the diffuse layer, Figure 2.2(B).

In 1924, Stern combined the two aforementioned theories. He acknowledged Helmholtz's concept of the electrical double layer, where there was a minimum distance the ions were attracted close to the surface, but theorised this could not fully neutralise the surface of the electrode. It was Gouy and Chapman's idea that Brownian motion formed a diffuse layer that he postulated to counter-balance the remaining charge density. Subsequently, Stern's model shows an initial, linear potential drop between the electrode and the OHP after which it decreases, Figure 2.2(C).

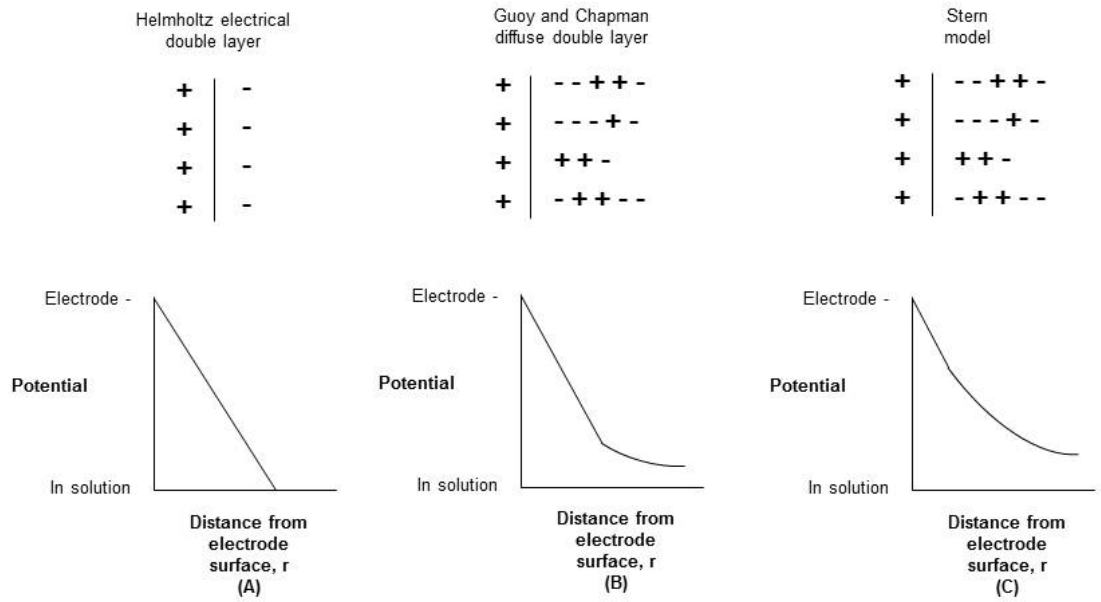


**Figure 2.2** Schematic representations of (A) Helmholtz, (B) Gouy and Chapman and (C) Stern models.

## 2.3 Mass Transport

### 2.3.1 Diffusion

Electrolysis requires the transportation of reactant molecules from the bulk solution to the electrode surface-solution interface for the reaction to occur. Mass transfer occurs for two main reasons; (i) there is movement of a species across a concentration gradient, or (ii) there is a difference between the electrical or chemical potential at either the electrode or the solution. Three significant mechanisms can influence an electrolysis reaction: diffusion, convection and migration.

Diffusion can be defined as the spontaneous movement of species along a concentration gradient, from an area of high concentration to an area of low concentration, in order to minimise uneven concentration distributions [2, 4]. In electrochemistry this is the

gradient of chemical potential. Fick's two laws can explain this. The 1st law, (Equation 2.10), represents the diffusional flux and shows that the rate of diffusion is dependant upon the concentration gradient at any given distance.

$$j = -D_{ox} \frac{\partial[ox]}{\partial x} \tag{2.10}$$

Here *j* is the diffusional flux (number of moles diffusing per unit per second), *D* is the diffusion coefficient (characteristic of the diffusing species), [ox] is the concentration of the oxidised species, *x* is the distance.

The negative concentration gradient indicates there are fewer particles on the right hand side of Equation 2.5 therefore the flux is down the concentration gradient (movement of particles from left to right) [3]. Fick's 2nd law, (Equation 2.11), allows us to evaluate the rate of change of concentration of the electro-active material close to the electrode surface as a function of time. Where t is time, *D* is the diffusion coefficient (characteristic of the diffusing species), [ox] is the concentration of the oxidised species, x is the distance.

$$\frac{\partial[ox]}{\partial t} = D_{ox} \frac{\partial^2[ox]}{\partial x^2} \tag{2.11}$$

### 2.3.2 Convection

This transport process arises when a mechanical force acts on the solution, and can be deemed natural or forced. Natural convection results from density differences (concentration of reaction products close to the electrode are of different density compared to those in the bulk solution) and/or thermal gradients (due to the exo- or endo-thermicity of the process) within the solution [1]. These effects are largely unpredictable, hence considered undesirable forces, but only have a significant impact with larger electrodes (electrodes with sizes of mm or more).

When an external force is acting upon the solution such as stirring, pumping or gas bubbling is acting upon the solution, then convection is forced. Involuntary forced convection is unfavourable, but when introduced deliberately, it can mask the effects from natural convection, allowing for reproducible experiments to be made above the 10-20 second limit.

### 2.3.3 Migration

Migration is the electrostatic effect that is brought about by the application of a voltage on the electrode, generating a charged interface. It concerns the movement of only the charged species (anions and cations) due to their attraction or repulsion near to this interface, in turn affecting the Faradaic current flow.

Migration is therefore problematic in electrochemical experiments so the addition of an electrolyte at high concentration (ca. 0.1M) eliminates these complex transport processes. A high concentration of electrolyte will increase the conductivity of the solution resulting in it being less resistive to the flow of current [1].

## 2.4 Electron Transfer Kinetics

The rate on an electrochemical reaction is controlled partly by the rate of electron transfer and partly by the rate at which the solution species is transported to the electrode surface. The electrochemical response is dominated by the rate-determining step, and here we consider an electron-transfer limited system where the transport of solution species is fast but the reaction process is slow. Consider a reversible redox reaction:

$$O\ (s) + e^-\ (m) \underset{k_{ox}}{\overset{k_{red}}{\rightleftharpoons}} R\ (s) \qquad (2.12)$$

The rate of reduction and oxidation are described by equations (2.14) and (2.15) respectively, given the magnitude of current, i, is:

$$i = FAj \qquad (2.13)$$

$$i_c = -FAk_{red}[O]_o \qquad (2.14)$$

$$i_a = FAk_{ox}[R]_o \qquad (2.15)$$

Where F is the Faraday constant (96485 C $mol^{-1}$), A is the electrode area ($cm^2$), j is the flux (amount of material undergoing electrochemical reaction per unit area within a unit

time), k is the rate constant for the electron transfer and $[O]_o/[R]_o$ is the surface concentration of the oxidised/reduced species.

Using the transition state theory of chemical kinetics, where a reaction proceeds via an energy barrier, we can relate the activation energy to the above rate constants by the Arrhenius equation (2.16):

$$k_{(ox\ OR\ red)} = A\exp\ \frac{-E_{A\ (ox\ OR\ red)}}{RT} \qquad (2.16)$$

In which $E_A$ is the activation energy and A is the pre-exponential factor (units are dependant on the order of the reaction).

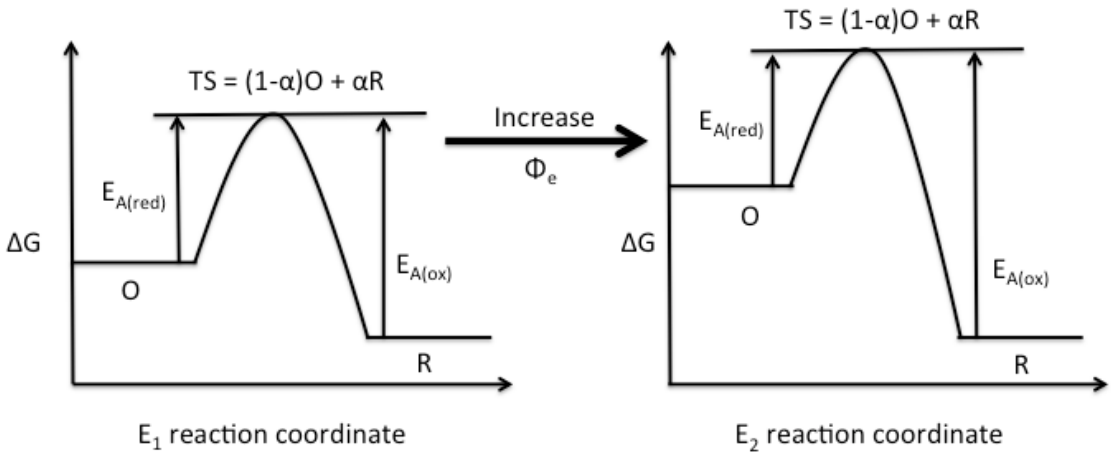


**Figure 2.3** The effect of potential on the activation energy for an electrochemical reduction reaction.

Figure 2.3 illustrates by increasing the potential at the electrode ($\Phi_e$), the energy level of the reactant (O) is increased (by 1 unit) through the transfer of the electron from the

electrode at which the potential was increased and the energy of the transition state is also increased (but not to the same extent as the electrode, by a unit of (1- α)). The product energy remains unchanged which results in a reduction of the $E_{A(red)}$ and increase in the $E_{A(ox)}$, clearly showing that the rate of electrolysis can be changed by varying the applied potential. In order to overcome the activation barrier, an overpotential is applied ($\eta = E - E^o$), see equation (2.17) and (2.18).

$$k_{red} = k^o_{red} \exp \frac{-\alpha F \eta}{RT} \tag{2.17}$$

$$k_{ox} = k^o_{ox} \exp \frac{(1-\alpha) F \eta}{RT} \tag{2.18}$$

The parameter α is the transfer coefficient, typically a value of 0.5, and gives an indication to the way the transition state is influenced by the voltage. A value of half means that the transition state behaves midway between the reactants and products response to the applied voltage.

Equation (2.17) and (2.18) can be related to the net current density when the system is not at equilibrium, $i = i_{ox} - i_{red}$, and the Butler-Volmer expression is obtained which describes the steady-state voltammetry when the electron transfer is the rate limiting step, Equation (2.19).

$$i = i_o \left( \exp \frac{(1-\alpha) F \eta}{RT} - \exp \frac{-\alpha F \eta}{RT} \right) \tag{2.19}$$

The Butler-Volmer equation predicts how the observed current varies as a function of the overpotential, η, and the transfer coefficient, α. From the equation, it can be deduced that for large deviations from the equilibrium potential, a high overpotential is needed to drive the reaction. Therefore, for large positive values of η, $i_{ox}$ tends towards i and a large negative value of η is needed for $i_{red}$ to tend towards i.

## 2.5 Electrochemical Equipment

To conduct a wide range of voltammetric experiments a common three-electrode set-up is used, involving a working electrode (WE), reference electrode (RE) and counter electrode (CE), see Figure 2.4.

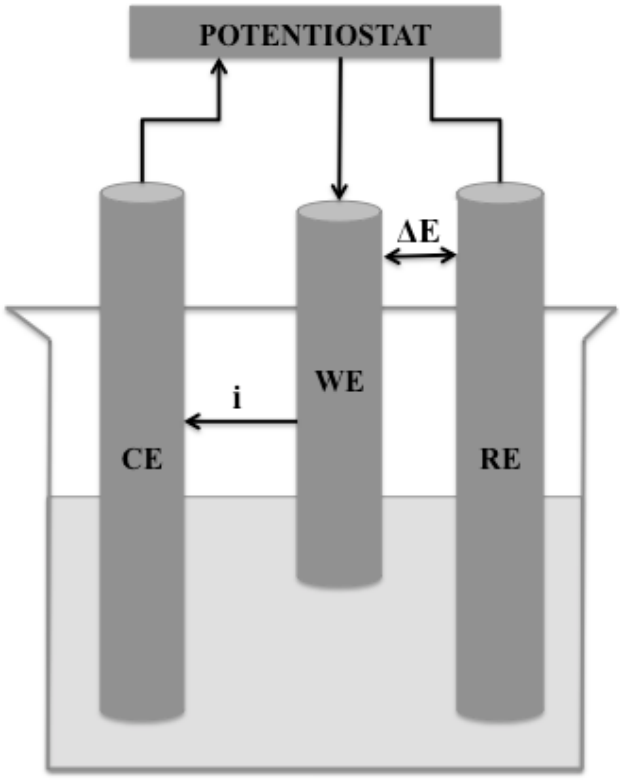


**Figure 2.4** A common three-electrode set-up involving a working (WE), reference (RE) and counter (CE) electrodes with a potentiostat to deliver applied potential. ΔE is the potential difference and i is the current.

The working electrode is used to measure the response from the analyte of interest and is generally small in size to provide a high current density at the electrode surface [5]. The reference electrode has a fixed and stable potential, and the working electrode potential is held relative to this. This enables the potential drop between the solution and the electrode ($\phi_m$ - $\phi_s$) to be measured upon the application of a voltage. Finally, the counter electrode (usually made of an inert material such as platinum) is used to complete the circuit and control the potential applied to the working electrode. To ensure that the flow of current is only passed through the WE and CE and not through the RE, a potentiostat is used by fixing the potential, *E*, between the WE and RE.

## 2.6 Voltammetric Techniques

### 2.6.1 Voltammetry

Voltammetry is the term used for electroanalytical techniques that measure the electrode current as a function of the voltage applied to the electrochemical cell, providing information on the mechanism of the cell reaction [1, 5]. An electrochemical process can provide information regarding the mechanism or kinetics of the reaction. The displayed current is observed from the oxidation or reduction of the redox analyte and is known as the Faradaic current; the magnitude of which can be explained by Equation 2.20.

$$i = nAFj \tag{2.20}$$

Where i is the current density, n is the number of electrons, A is the electrode area ($cm^2$), F is the Faraday constant (96485 C $mol^{-1}$) and j is the flux (amount of material undergoing electrochemical reaction per unit area within a unit time).

### 2.6.2 Cyclic Voltammetry

Cyclic voltammetry is one of the most important techniques in electrochemistry, used to characterise the electrochemical processes at the electrode surface – solution interface [6]. As mentioned previously, the current flow through the working electrode is recorded as a function of the applied potential, generating a voltammogram (plot of Current vs. Potential) [2]. It is conducted in a stationary solution and as a result the transport of material to the surface of the electrode relies solely on diffusion.

At the start of the experiment, a chosen potential (E2) is applied to the working electrode to ensure that the chemical species of interest do not undergo any redox processes. This potential is then increased (in a linear manner), to a value where electron transfer is rapid (E1), after which the sweep is reversed and the electrode potential is scanned back to its original value, (E2). The value for (E1) is chosen such that the potential interval (E1 – E2) involves the oxidation or reduction process of interest [2]. This potential cycle can be illustrated as a triangular waveform, Figure 2.5.

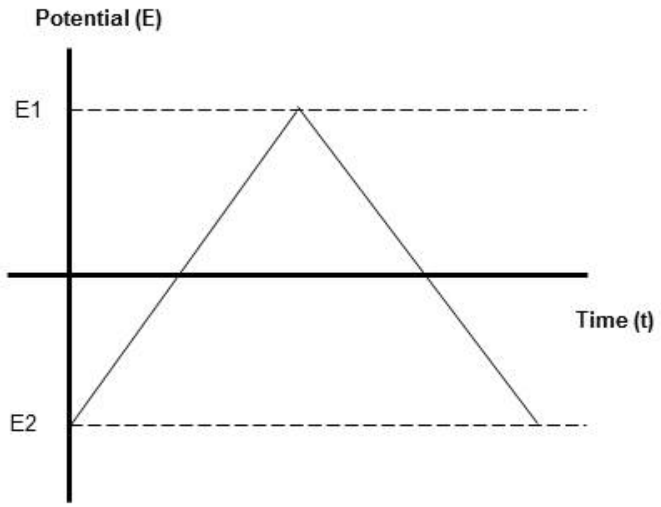


**Figure 2.5** Cyclic Voltammetry waveform to show potential as a function of time.

A lot of information can be gathered from investigating the shape of the cyclic voltammogram. Initially no current is passed as the potential is set to a value where electron transfer is not favourable. But as the potential is scanned to more reducing values (more negative), a potential is reached where current starts to pass and the reduction at the electrode surface commences. Eventually a maximum is reached, known as the peak current, as there is no longer an excess of material at the electrode surface, which is dependent on the diffusion of material from the bulk solution. Once the potential is switched and the reverse scan begins, a similar shape emerges in the voltammogram for the oxidation of the species.

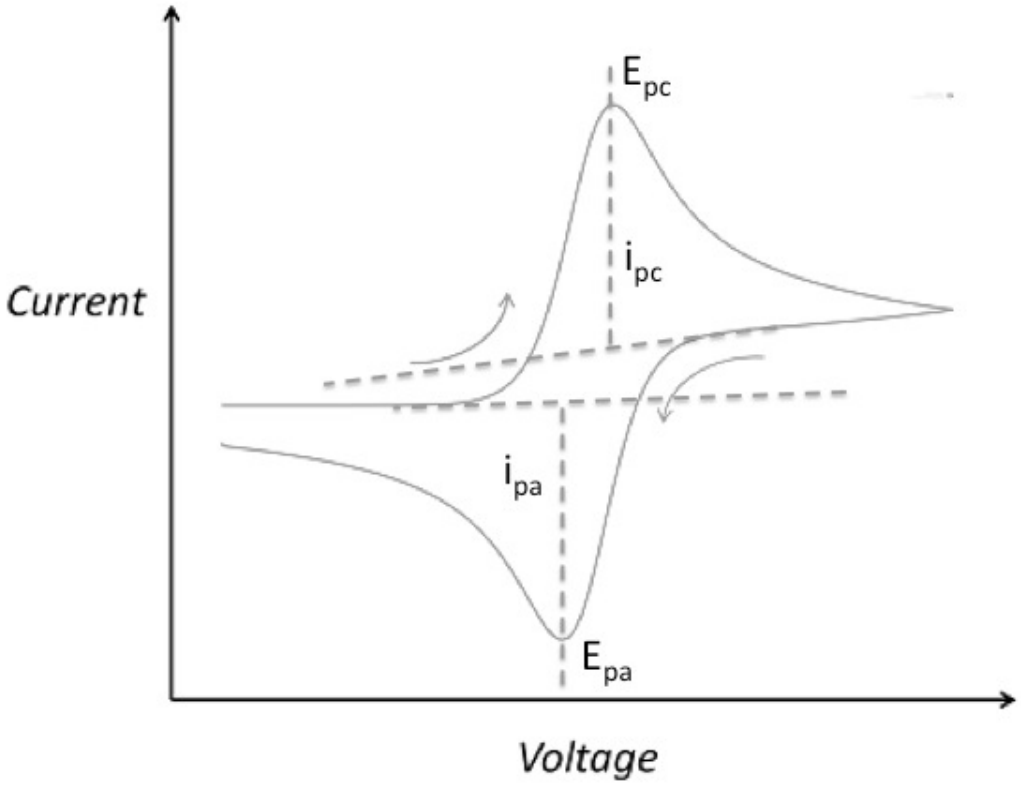


**Figure 2.6** Cyclic voltammogram for a reversible electron transfer reaction where: $E_{pc}$ is the cathodic peak potential, $E_{pa}$ is the anodic peak potential and $i_{pc}$ and $i_{pa}$ are the cathodic and anodic peak currents respectively.

Cyclic voltammograms can be categorised into three types: reversible, irreversible and quasi-reversible (intermediate) and are apparent from their voltammetric shapes. A reversible system is referred to as fast electrode kinetics as the mass transport conditions are slow compared to the electron transfer conditions. The opposite is therefore true for an irreversible electrochemical system (slow electron kinetics). A reversible process obeys the Nernst equation (2.9), which tells us that a half-cell potential will change by 59 mV per 10-fold change in the concentration for a species undergoing a one-electron oxidation or reduction, corresponding to a specific peak separation ($E_p^{ox} – E_p^{red}$) of ~59 mV. This can be seen when the Nernst equation is rewritten in the form of log10, Equation (2.21) and at standard temperature, where T = 298K, Equation (2.22).

$$E = E° - \frac{2.303RT}{nF} \log \frac{[ox]}{[red]} \quad (2.21)$$

$$E = E° - \frac{0.059}{n} \log \frac{[ox]}{[red]} \quad (2.22)$$

### 2.6.3 Square Wave Voltammetry

Another important voltammetric analysis technique is Square Wave Voltammetry and its introduction saw advances in sensitivity, allowing for the detection of small concentrations of electroactive species [2]. Developed by Baker and Jenkins in 1952 [7], this potential step technique takes the original potential staircase sweep and superimposes a square wave, shown in Figure 2.7.

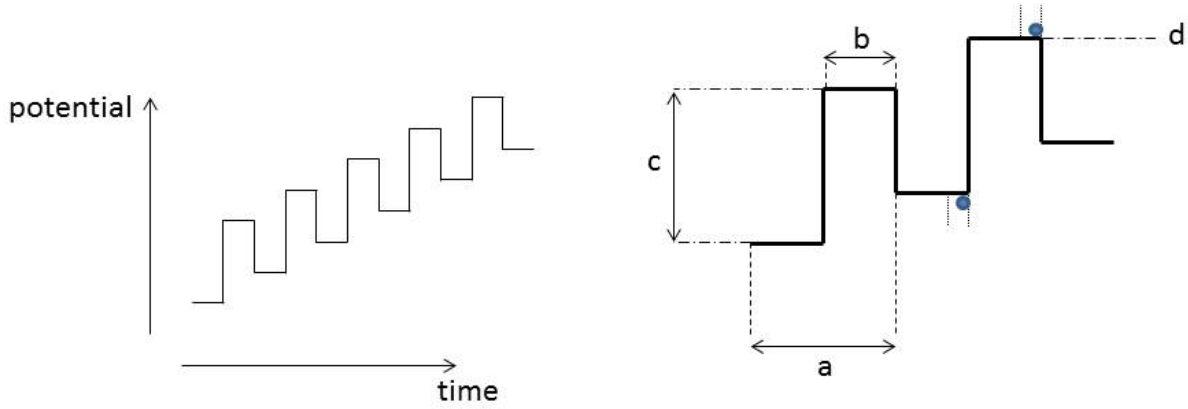


**Figure 2.7** Diagram depicting the waveform for Square Wave Voltammetry where a is the pulse period, b is the pulse width, c is the pulse amplitude, d is the step potential and the circles represent the sample period.

Each square wave cycle exists as one staircase period; the current is measured at the end of each pulse (potential change) and just before the start of the next pulse (Figure 2.7). The difference between these two measurements is taken and recorded resulting in a peaked response, seen in Figure 2.8. The charging current is therefore partially eliminated due to the subtraction of the measurements taken during two successive half cycles [8].

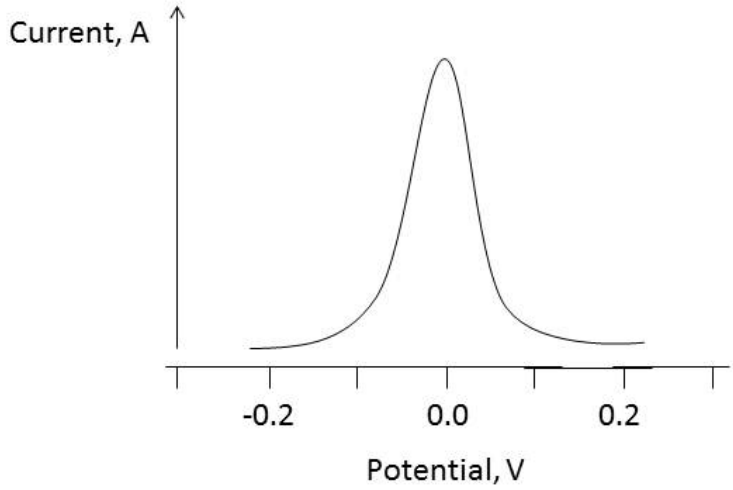


**Figure 2.8** Peaked response for square wave voltammetry.

## 2.7 Generator – Collector Electrodes (bipotentiostatic)

A generator – collector electrode setup, uses the common three-electrode system in addition to another working electrode. During an electrochemical experiment of this nature, the analyte of interest is oxidised or reduced at the generator electrode (working electrode 1), after which it is transported (diffuses) across a small inter-electrode gap to the collector electrode (working electrode 2). The collector electrode is held at a fixed potential (unlike the generator electrode which is scanning the potential window), to

convert the newly generated species back to the starting material or to another species, in turn creating a redox feedback loop [9], see Figure 2.9. This results in enhanced sensitivity due to the potential increase in current, allowing for the measurement of very low concentrations and the possibility of detecting intermediates due to faster reaction kinetics.

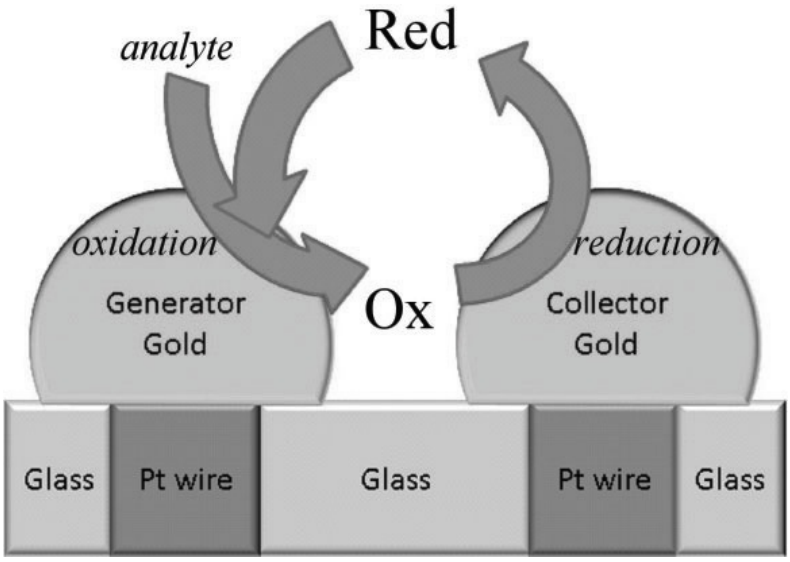


**Figure 2.9** Generator-collector feedback loop

To achieve more accurate and sensitive results in a generator – collector electrode system, a high collection efficiency value, N, should be achieved, (Equation 2.23). This is solved by calculating the ratio of the collector current, to the current at the generator electrode, where: $N$ is the collection efficiency, $I_{col}$ is the collector current and $I_{gen}$ is the generator current.

$$N = -\frac{I_{col}}{I_{gen}} \tag{2.23}$$

The main approach to improving the collection efficiency is to prevent the escape of analyte to the bulk solution. This can be accomplished by; i) generating a small inter-electrode gap, in-turn providing a short diffusion pathway between the two working electrodes, ii) directing the flow of current to the electrode via convection methods, or iii) having a collector electrode that completely encases the generator. These parameters can be achieved through the use of different electrode geometries, as seen in section 2.7.1 and onwards.

### 2.7.1 Rotating Ring-Disc Electrodes

Developed in the 1950s, the rotating ring-disc electrodes (RRDE) consists of a rotating central disc separated by an insulating material from the outer ring electrode [10]. The system rotates to induce radial convective flow from the bulk solution towards the disc (generator) electrode and then across the ring (collector) electrode. The resulting currents are dependant upon the rotation speed and size, spacing and potential of the two electrodes. The collection efficiency on such a system is defined as the proportion of material produced electrochemically on the disc electrode, which reaches the ring electrode [11]. This efficiency is improved as the insulating gap size decreases and area of the collector electrode increases.

The fabrication of rotating ring-disc electrodes involves more complex methods than other generator-collector electrodes, such as chemical vapour deposition [12], and lithography [13]. They have been widely used to study reaction kinetics, the oxygen reduction mechanism [14] and mass transport effects (Scanning Electrochemical Microscopy) [15, 16].

A progression from the RRDE is the wall jet ring-disc electrode (WJRDE) [17, 18], which has a similar geometry, except the convective flow is generated from a nozzle that ejects an analyte solution over the disc electrode. Its applications include the detection of contaminants in drinking water [19] and reaction mechanisms [20].

### 2.7.2 Double Channel Flow Electrodes

Another generator – collector system that uses forced convection is the double channel flow electrode (DCFE) [21, 22]. Two working electrodes are held in series (collector downstream of the generator) within an insulating channel, where a continual flow of electrolyte is passed over the electrodes. They offer some advantages over the previously mentioned disc electrodes; namely they are easier to fabricate [23], tolerate a wider range of flow rates and have less interference from contaminants as fresh solution is continually flowed through the system. They have been widely applied to study complex mechanisms [24, 25], oxidative dissolution of metals [26, 27] and paired with mass spectrometry to study the mechanistic details with reference to fuel cells [28].

### 2.7.3 Interdigitated Array Electrodes

Interdigitated electrode arrays utilizes the idea of analyte transportation via diffusion only (eliminating the need for forced convection) by maintaining very small, μm, gaps between the working electrodes placed side-by-side [29], see Figure 2.10. The two interlocking ‘comb’ shaped electrodes are extensively used for the sensitive detection of electroactive species [30] due to having high collection efficiencies [31].

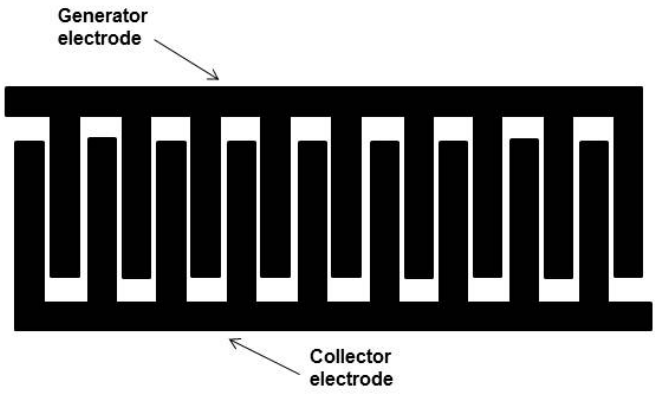


**Figure 2.10** Schematic diagram of an interdigitated electrode array

### 2.7.4 Dual Disc/Hemisphere Electrodes

The concept of having a short diffusion path in an attempt to enhance collection efficiencies has recently been demonstrated in the use of Dual disc/hemisphere electrodes [32, 33]. These are prepared by twisting together two platinum wires to close proximity, placing them into a glass capillary and back polishing to achieve the desired separation [33]. Modifications can be made to such a device, one example is the electro deposition of gold onto the surface of the discs to create dual-hemispheres [34], see Figure 2.11. The collection efficiency of these electrodes is very much dependant on the inter-electrode gap width; as the distance increases there is loss of analyte to the bulk solution, decreasing the efficiency.

The double hemisphere electrodes are widely used by the Marken group for the detection of various analytes by cyclic voltammetry [35], and examining ion transport across liquid/liquid interfaces [36] using a triple phase junction where a redox active oil

(organic) phase is placed between the two gold hemisphere electrodes and submerged into an aqueous solution [37].

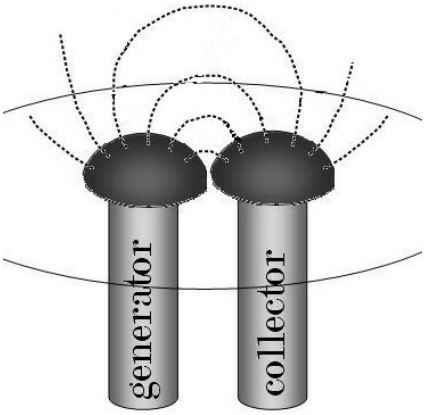


**Figure 2.11** Schematic diagram of a dual hemisphere electrode

### 2.7.5 Dual-Plate Electrodes

Pioneered by Anderson and Reilly [38, 39], dual band electrodes are designed to have two planar working electrodes placed in parallel and separated by a non-conductive spacer. Their close proximity enhances steady state currents, enabling the study of reaction kinetics. Lemay and co-workers further developed the design towards nano-gap electrochemical devices, which enable single molecule detection [40-42].

The Marken group has recently developed dual-plate microtrench electrodes [43, 44] where the spacer is etched to leave a trench. Using various electrode materials they have been employed for the electrochemical detection of cysteine/cystine [45] and nitrate/nitrite systems [46], for ion transport [37] and pH titrations [47]. Benefits of this geometry include easy and relatively fast fabrication, rapid diffusion of analyte to the trench, and fast diffusion within the trench generating faster redox cycling.

## 2.8 Conclusion

This thesis demonstrates a variety of electrochemical techniques for the sensitive detection of various analytes with well-known redox pathways. All voltammetric techniques are used in bipotentiostatic mode for signal enhancement due to redox cycling within the inter-electrode gap of the junction electrode. Square wave voltammetry is shown to distinguish between the fully reduced species and the intermediate species by varying the pH environment. Cyclic voltammetry is used for the detection of nitrobenzene and phosphate anion at a triple phase boundary. Finally, an electrochemical flow injection system is fabricated for the detection of hydroquinone using chronoamperonmetry.

## 2.9 References

1. Fisher, A., *Electrode Dynamics*. Oxford Chemistry Primers, ed. R. Compton. Vol. 34. 1996, United States: Oxford University Press, Chapter 1.

2. Compton, R., G and C. Banks, E, *Understanding Voltammetry*. second ed. 2011 Singapore: World Scientific Publishing, Chapter 1.

3. Rieger, P., *Electrochemistry*. 2 ed. 1994, New York: Chapman and Hall, Chapter 2.

4. Wang, J., *Analytical Electrochemistry* 3rd ed. 2006, New Jersey: John Wiley & Sons, Chapter 1.

5. Thomas, F. and G. Henze, *Introduction to Voltammetric Analysis: Theory and Practice*. 2001, Austrailia: CSIRO Publishing, p. 1-7.

6. Holze, R., *Experimental Electrochemistry*. 2009, Weinheim: John Wiley & Sons, p.77.

7. Barker, G.C. and I.L. Jenkins, *Square-wave polarography.* Analyst, 1952. **77**(920): p. 685-696.

8. Mirceski, V., S. Komorsky-Lovric, and M. Lovric, *Square Wave Voltammetry: Theory and Application*. 2007, Berlin: Springer.

9. Barnes, E.O., et al., *Generator-collector double electrode systems: A review.* Analyst, 2012. **137**(5): p.1068-1081.

10. Albery, W.J., *Ring-disc electrodes .1. A new approach to theory.* Transactions of the Faraday Society, 1966. **62**(523P): p. 1915-1919.

11. Albery, W.J. and Bruckens.S, *Ring-disc electrodes .2. Theoretical and experimental collection efficiences.* Transactions of the Faraday Society, 1966. **62**(523P): p. 1920-1931.

12. Zhao, G., D.M. Giolando, and J.R. Kirchhoff, *Chemical-vapour-deposition and characterization of silica-coated carbon-fiber ultramicroelectrodes.* Analytical Chemistry, 1995. **67**(15): p. 2592-2598.

13. Chen, Y. and A. Pepin, *Nanofabrication: Conventional and nonconventional methods.* Electrophoresis, 2001. **22**(2): p. 187-207.

14. Kramm, U.I., et al., *Effect of an Ammonia Treatment on Structure, Composition, and Oxygen Reduction Reaction Activity of Fe-N-C Catalysts.* Journal of Physical Chemistry C, 2011. **115**(47): p. 23417-23427.

15. Liljeroth, P., et al., *Disk-generation/ring-collection scanning electrochemical microscopy: Theory and application.* Analytical Chemistry, 2002. **74**(9): p. 1972-1978.

16. Liljeroth, P., et al., *Micro ring-disk electrode probes for scanning electrochemical microscopy.* Electrochemistry Communications, 2002. **4**(1): p. 67-71.

17. Albery, W.J. and C.M.A. Brett, *The wall-jet ring-disc electrode. 1. Theory.* Journal of Electroanalytical Chemistry, 1983. **148**(2): p. 201-210.

18. Albery, W.J. and C.M.A. Brett, *The wall-jet ring-disc electrode .2. Collection efficiency, titration curves and anodic stripping voltammetry.* Journal of Electroanalytical Chemistry, 1983. **148**(2): p. 211-220.

19. Sue, J.-W., et al., *Disposable screen-printed ring disk carbon electrode coupled with wall-jet electrogenerated iodine for flow injection analysis of arsenic(III).* Electrochemistry Communications, 2008. **10**(7): p. 987-990.

20. Compton, R.G., A.C. Fisher, and G.P. Tyley, *The wall-jet electrode and the study of electrode-reaction mechanisms - The EC (catalytic) mechanism.* Journal of Applied Electrochemistry, 1991. **21**(1): p. 2-5.

21. Fisher, A.C. and R.G. Compton, *Double-channel electrodes - Homogeneous kinetics and colletion efficiency measurememnts.* Journal of Applied Electrochemistry, 1991. **21**(3): p. 208-212.

22. Unwin, P.R., *The ECE-DISP1 problem - General resolution via double channel electrode collection efficiency measurements.* Journal of Electroanalytical Chemistry, 1991. **297**(1): p. 103-124.

23. Paixao, T., R.C. Matos, and M. Bertotti, *Design and characterisation of a thin-layered dual-band electrochemical cell.* Electrochimica Acta, 2003. **48**(6): p. 691-698.

24. Barnes, E.O., et al., *Voltammetry in the absence of excess supporting electrolyte - ECE-DISP1 reactions: The electrochemical reduction of 2-nitrobromobenzene in acetonitrile solvent.* Journal of Electroanalytical Chemistry, 2011. **659**(1): p. 25-35.

25. Compton, R.G., et al., *Mass-transport to channel and tubular electrodes - The SIngh and Dutt approxiamtion.* Journal of Electroanalytical Chemistry, 1987. **238**(1-2): p. 43-66.

26. Shrestha, B.R., et al., *Application of channel flow double electrode to the study on platinum dissolution during potential cycling in sulfuric acid solution.* Electrochimica Acta, 2011. **56**(27): p. 9714-9720.

27. Wang, Z., E. Tada, and A. Nishikata, *In-Situ Monitoring of Platinum Dissolution under Potential Cycling by a Channel Flow Double Electrode.* Journal of the Electrochemical Society, 2014. **161**(4): p. 380-385.

28. Wang, H., E. Rus, and H.D. Abruna, *New Double-Band-Electrode Channel Flow Differential Electrochemical Mass Spectrometry Cell: Application for Detecting Product Formation during Methanol Electrooxidation.* Analytical Chemistry, 2010. **82**(11): p. 4319-4324.

29. Tomcik, P., M. Krajcikova, and D. Bustin, *Determination of pharmaceutical dosage forms via diffusion layer titration at an interdigitated microelectrode array.* Talanta, 2001. **55**(6): p. 1065-1070.

30. Tomcik, P., D. Bustin, and V. Tvarozek, *Microelectrode arrays with interacting diffusion layers: Voltammetric applications.* Chemicke Listy, 1999. **93**(11): p. 678-682.

31. Odijk, M., et al., *Simulation of redox-cycling phenomena at interdigitated array (IDA) electrodes: Amplification and selectivity.* Electroanalysis, 2008. **20**(5): p. 463-468.

32. Matysik, F.M., *Voltammetric characterization of a dual-disc microelectrode in stationary solution.* Electrochimica Acta, 1997. **42**(20-22): p. 3113-3116.

33. Cutress, I.J., et al., *Dual-microdisk electrodes in and theory transient generator-collector mode: Experiment.* Journal of Electroanalytical Chemistry, 2011. **655**(2): p. 147-153.

34. Dale, S.E.C., et al., *Gold-Gold Junction Electrodes: The Disconnection Method.* Chemical Record, 2012. **12**(1): p. 143-148.

35. French, R.W., et al., *Paired gold junction electrodes with submicrometer gap.* Journal of Electroanalytical Chemistry, 2009. **632**(1-2): p. 206-210.

36. French, R.W., et al., *Liquid-liquid ion transport junctions based on paired gold electrodes in generator-col lector mode.* Electrophoresis, 2009. **30**(19): p. 3361-3365.

37. Dale, S.E.C., et al., *A gold-gold oil microtrench electrode for liquid-liquid anion transfer voltammetry.* Electrophoresis, 2013. **34**(14): p. 1979-1984.

38. Anderson, L.B. and C.N. Reilley, *Thin-layer electrochemistry - Steady-state methods of studying rate processes.* Journal of Electroanalytical Chemistry, 1965. **10**(4): p. 295-296.

39. Anderson, L.B. and C.N. Reilley, *Thin-layer electrochemistry - Use of twin working electrodes for study of chemical kinetics.* Journal of Electroanalytical Chemistry, 1965. **10**(5-6): p. 538-552.

40. Lemay, S.G., et al., *Single-Molecule Electrochemistry: Present Status and Outlook.* Accounts of Chemical Research, 2013. **46**(2): p. 369-377.

41. Singh, P.S., et al., *Stochasticity in Single-Molecule Nanoelectrochemistry: Origins, Consequences, and Solutions.* Acs Nano, 2012. **6**(11): p. 9662-9671.

42. Rassaei, L., P.S. Singh, and S.G. Lemay, *Lithography-Based Nanoelectrochemistry.* Analytical Chemistry, 2011. **83**(11): p. 3974-3980.

43. Dale, S.E.C., C.E. Hotchen, and F. Marken, *Generator-collector electroanalysis at tin-doped indium oxide-epoxy-tin-doped indium oxide junction electrodes.* Electrochimica Acta, 2013. **101**: p. 196-200.

44. Dale, S.E.C. and F. Marken, *Pulse electroanalysis at gold-gold micro-trench electrodes: Chemical signal filtering.* Faraday Discussions, 2013. **164**: p. 349-359.

45. Hammond, J.L., et al., *Cysteine-Cystine Redox Cycling in a Gold-Gold Dual-Plate Generator-Collector Microtrench Sensor.* Analytical Chemistry, 2014. **86**(14): p. 6748-6752.

46. Gross, A.J., et al., *Nitrite/nitrate detection in serum based on dual-plate generator-collector currents in a microtrench.* Talanta, 2015. **131**: p. 228-235.

47. Dale, S.E.C., et al., *Nano-Litre Proton/Hydrogen Titration in a Dual-Plate Platinum-Platinum Generator-Collector Electrode Micro-Trench.* Electrochimica Acta, 2014. **125**: p. 94-100.

# Chapter 3

# Square Wave Electroanalysis at Generator - Collector Gold - Gold Double Hemisphere Junctions

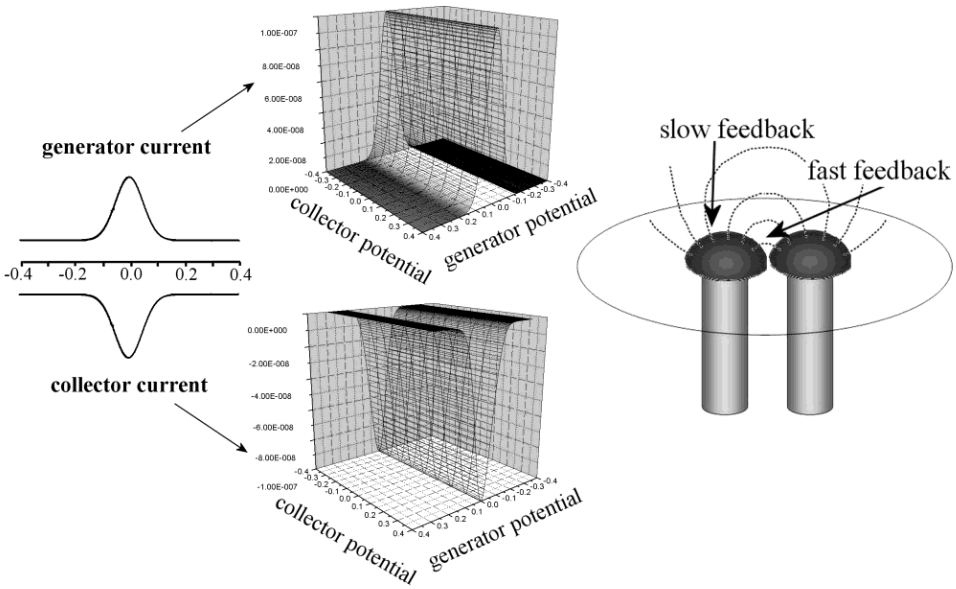


This work is published as "Square Wave Electroanalysis at Generator-Collector Gold-Gold Double Hemisphere Junctions" Lewis, G.E.M.; Dale, S.E.C.; Kasprzyk-Hordern, B.; Barnes, E.O.; Compton, R.G.; Marken, F., Electroanalysis 24 (2012) 1726-1731.

## Abstract

In this chapter, a paired gold double-hemisphere junction electrode is employed in generator-collector mode for square wave voltammetry. Small inter-electrode gaps are achieved using a disconnection method after gold electrodeposition. Electrochemical data are recorded as a function of both generator and collector potential to give three-dimensional response "maps". At sufficiently low frequencies, close-to-steady-state conditions for the collector response are achieved and peak responses complementary to those for the generator electrode are recorded. Due to localised inter-electrode gap diffusion (fast) as opposed to peripheral diffusion (slow), information about reaction products and intermediates can be obtained. Local pH gradient effects provide additional "fingerprint" information beneficial for future application in analytical detection.



## Acknowledgement

Support during electrode fabrication from Dr. Sara E.C. Dale is gratefully acknowledged.

# Contents

## 3.1 Introduction

The detection of emerging environmental pollutants is extremely important for maintaining water quality, and sees the demand for newer, portable technology that can provide faster on-site analysis and deliver the sensitivity and reliability of current techniques. Electrochemical methods offer a suitable alternative and the potential of generator-collector mode electrochemistry, particularly low cost systems [1], have been recognized for sensing applications. In this chapter a recently developed generator-collector electrode is discussed with the use of pulse voltammetry to investigate whether these electrode systems have the selectivity needed for environmental analysis.

Generator – collector electrochemical detectors, where each working electrode is independently controlled [2, 3] have been successfully employed for a wide number of analytical measurements. With their many and varied geometries [4-9], constant improvements are made towards lower detection limits by fabricating smaller inter-electrode gaps for faster inter diffusion; most recently involving nano-gap sensors reaching sub-pico-molar levels [10]. A recent development towards a low cost generator-collector electrode is the gold-gold dual hemisphere system with sub-micrometre gap [11]. The gold hemispheres are grown simultaneously via electro-deposition [12] onto two closely spaced platinum wires - a simple lab-bench fabrication. To control the gap size and growth of the hemispheres, an optimal potential is chosen. These electrodes have been proposed for NO sensing where detection limits of 10 μM were reached [13], and tested for chloramphenicol where the rate of diffusion and collection efficiency was increased with increasing microwave power and that diffusion dominates convection (which suppress feedback mechanisms) within the electrode gap [14]. Low detection limits in the range of 0.2 μM – 200 μM were also reached when

studying a range of bio-molecules at gold paired electrodes due low levels of background current present [15]. With the success of this electrode geometry within the Marken group and the low concentration levels achieved, it was clear that the gold-gold dual hemisphere electrode was a good choice to study the selectivity these devices have to offer. This is vital for environmental analysis as many compounds present in the aqueous environment could interfere with the electrode and block the electrode surface or contaminants of similar structure could exhibit the same redox activity enhancing the true concentration level of the target analyte.

Pulse methods are commonly employed in electrochemistry for sensitive detection as appropriate time-domains can be selected and there are minimal contributions from non-Faradaic currents [16]. New generator-collector pulse methods have been suggested, for example using "hydroxide pulses" for the detection of glucose at gold electrodes [17]. Square wave voltammetry in generator-collector mode has been employed to characterize diffusional interactions between adjacent microelectrodes [18] and computer simulation [19, 20] has been compared to analytical theory [21, 22]. This particular pulse method under close to steady-state diffusion conditions [23, 24] can deliver quicker analysis, with "simple" peak-shaped responses, by operating scan rates of up to 1 V/sec, much faster than normal voltammetric techniques.

This chapter features a gold-gold dual-hemisphere electrode employed in generator-collector mode square wave voltammetry and offers improved sensitivity and potentially improved selectivity; key parameters for the development of environmental electrochemical sensors. Square wave voltammetric "mapping" (discussed in Chapter 3.2) provides data for both the reduced and oxidized form of the redox species and

allows an electrochemical "fingerprint" to be obtained. Two redox systems are explored in this chapter, a well studied one-electron reduction of $Ru(NH_3)_6^{3+}$ and a more complex reduction of Indigo Carmine.

## 3.2 Theory

Figure 3.1A illustrates zones of fast (localized intra-gap) and slow (peripheral) diffusion fields at double hemisphere geometry, corresponding to areas of fast and slow reaction kinetics that can be investigated. As a result, varying the conditions of the generator and collector electrodes enables information to be gathered on either the reduced or oxidized form of the redox species. In Figure 3.1B, the generator electrode is scanned from a positive (oxidation) to a negative (reduction) potential and the collector electrode is set at a positive potential. Initially the solution redox species is in the oxidized form and as the experiment proceeds, the reduced from builds up on the generator and the collector process is dominated by the oxidation response, providing information about the reduced form of the molecule. To obtain data for the oxidized form, the generator is scanned in a positive direction and the collector is held at a negative potential and the reduction response now dominates the collector process.

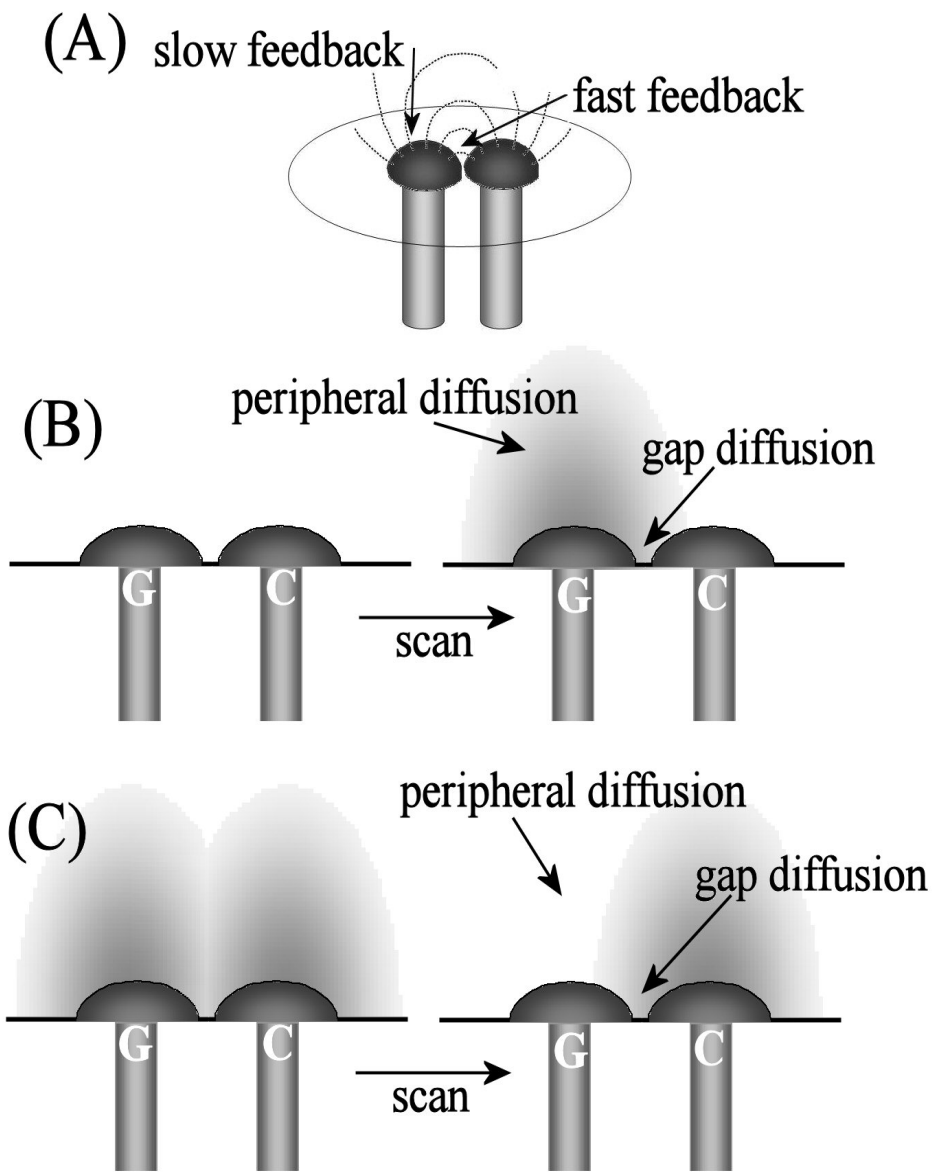


**Figure 3.1** (A) Schematic drawing of two adjacent electrodes with small inter-electrode gap (ca. 1 μm, fast feedback via diffusion) and a diameter of ca. 120 μm (slow feedback via diffusion). (B) Schematic drawing indicating the case of both electrodes, generator and collector, initially positive (solution redox system in oxidised form, reduced form indicated as grey) with a negative potential scan applied to the generator electrode. (C) Schematic drawing as before, but with both generator and collector electrodes initially with negative potential applied.

Square wave voltammetry is a powerful analytical tool and Figure 3.2 demonstrates schematically how it can be used in a generator-collector mode experiment. Working electrode W1 has a conventional square wave pulse sequence applied [25], as described in Chapter 2.5.3, and W2 is held at a constant fixed potential. During forward (F) and backward (B) pulses, measurements are taken (indicated by the grey zones), and the difference in current between the two measurements is plotted against potential, resulting in peaked responses for the Faradaic process. The currents at both electrodes are recorded simultaneously and a similar but inverted peak response is expected from the close-to-steady-state conditions of the inter-electrode diffusion. (Note that under close-to-steady-state conditions, for example at microelectrodes [26], the square wave voltammetric response is consistent with a derivative of the staircase voltammetric response and therefore peaks indicate changes in redox state). To optimise the collector potential which is held at a fixed value, experiments can be repeated with the collector potential changing systematically along the potential window to construct a 3D-square wave voltammogram, shown here as a wire frame topography or contour plot, (see Figure 3.1). The simplistic nature of the schematic drawing demonstrates the expected responses for a simple redox system, where the generator and collector signals appear to be the same shape.

Various factors can influence the shape of the square wave response; (i) non-ideal geometry of the generator – collector electrode system, (ii) changes in the diffusion rate when comparing oxidised state and reduced state, (iii) changes in chemical reactivity for the oxidised state versus the reduced state, and (iv) compositional gradients within the inter-electrode gap e.g. pH gradients, all of which are discussed in this chapter.

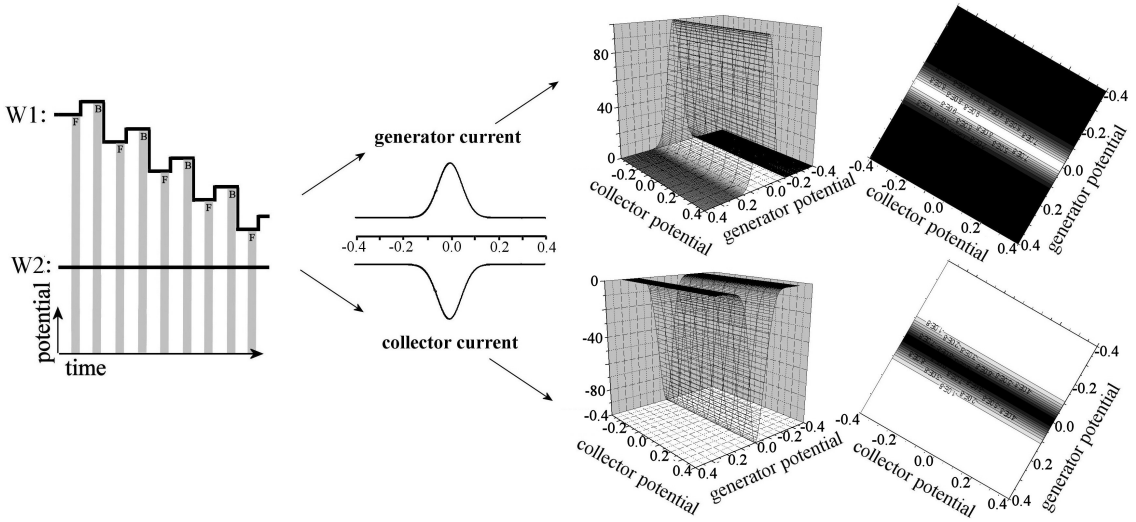


**Figure 3.2** Schematic drawing of the pulse sequence applied to working electrodes W1 and W2 for a gold–gold generator–collector system employing square wave voltammetric mapping.

## 3.3 Experimental Details

### 3.3.1 Chemical Reagents

Phosphate buffer solutions were prepared from $H_3PO_4$ and NaOH. $Ru(NH_3)_6Cl_3$ (Alfa Aesar) and indigo carmine (Aldrich) were used without further purification. Water was taken from a Thermo Scientific purification system (Barnstead Nanopure) with not less than 18 MOhm/cm resistivity. Argon (Pureshield, BOC) was used to de-aerate electrolyte solutions.

### 3.3.2 Instrumentation

A PGSTAT12 biopotentiostat system (Autolab, EcoChemie, The Netherlands) with GPES and NOVA software options was used for generator – collector electrochemical measurements. The NOVA software allows bipotentiostatic square wave voltammetry experiments to be designed for paired electrode systems with simultaneous current read out at both electrodes. A conventional four-electrode cell with platinum wire counter electrode and saturated calomel reference electrode (SCE, Radiometer, Copenhagen) and a gold – gold junction working electrode was employed. All experiments were conducted at 22 ± 2$^{o}$C.

### 3.3.3 Formation of Gold-Gold Double Hemisphere Junction Electrode

Gold – gold junction electrodes were electrodeposited using a literature method [27][28] onto a pair of platinum discs made from adjacent wires (100 μm diameter, ca. 45 μm apart) sealed into glass. The disc electrodes were carefully polished (wet 3 μm, 1 μm, and 0.3 μm alumina on Buehler microcloth) and rinsed before electrodeposition by Aurofab plating solution (Aurofab BP RTU II, Rohm and Haas electronic materials, used as received) at -0.4 V vs. SCE (50 $^{o}$C). The resulting short-circuited junction is then immersed into 0.5 M NaCl and a +0.95 V vs. SCE etching potential is applied until the point where the current suddenly drops (disconnection point [27]). The resulting junction electrodes are typically 120 μm in diameter with ca. 1 μm gap.

### 3.3.4 Voltammetry Conditions

Before progressing with square wave voltammetry, generator-collector cyclic voltammetry was carried out on the gold-gold dual-hemisphere electrode with a well-

known redox system, 1 mM $Ru(NH_3)_6^{3+}$ in 0.1 M KCl. The following parameters were used: scan rate 10, 20, 50 and 100 mVs-1 (only 10 mVs-1 is shown), start potential of 0.2 V vs. SCE, switch potential of -0.6 V vs., SCE and a collector potential of 0.1 V vs. SCE.

Square wave voltammetry uses a set step potential of 1 mV and a 20 mV amplitude throughout all the experiments. The frequency is changed from 8 Hz for the $Ru(NH_3)_6^{3+}$ experiments to 2 Hz for the indigo carmine experiments. A range of frequencies were investigated, and the lower frequency gave a more pronounced peak response due to the increase in "slow feedback" from the increased time domain for each step cycle. For each experiment the collector potential is varied across the potential window. Initially the collector potential is held at the start potential and after each scan it is changed to a more negative potential. The supporting electrolytes used are 0.1 M KCl and 0.1 M phosphate buffer solution at pH 12 and pH 7.

## 3.4 Results and Discussion

### 3.4.1 Square Wave Voltammetric Mapping of Junction Processes I: $Ru(NH_3)_6^{3+}$ Reduction in Aqueous 0.1 M KCl

Initially, a well known one electron redox system, the reduction of $Ru(NH_3)_6^{3+}$ in 0.1 M KCl is investigated (see Equation 3.1). This system has recently been studied also at adjacent generator – collector microdisc electrodes [27].

$$Ru(NH_3)_6^{3+}\ (aq) + e^- \leftrightharpoons Ru(NH_3)_6^{2+}\ (aq) \qquad (3.1)$$

A reversible voltammogram is observed (see Figure 2.3A) with a midpoint potential of ca. $E_{mid}$ = ½ ($E_{ox}$ + $E_{red}$) = -0.19 V vs. SCE (see dashed line) which is consistent with literature reports [28]. The collector response has close to steady state characteristics with a small hysteresis effect and a collection efficiency of ca. $I_{collector}/I_{generator}$ = 50 %. When the experiment is repeated in square wave voltammetry mode (with a sufficiently low frequency), and for a fixed collector potential setting from +0.2 to -0.6 V vs. SCE, a set of similar responses is obtained (see Figure 3B) with a slight shift in peak potential of ca. ½ amplitude (due to the instrument using the forward potential). The square wave voltammetry current collection efficiency under these conditions (8 Hz frequency) is only approximately 5 % due to the shorter time domain during pulse measurements compared to cyclic voltammetry measurements. Decreasing the frequency to 2 Hz increases the collection efficiency to ca. 15%.

In the square wave voltammetry experiment the generator current response appears positive and the collector current response negative (see Figure 3.3C and 3.3D respectively) due to the chosen scan direction from negative to positive potentials. In contrast to the cartoon case in Figure 3.2, there are indications of more complicated characteristics. Although generator responses are essentially independent of the applied collector potential, the collector responses show some variation. In the contour plot (Figure 3.3F) a “shoulder effect” occurs with more positive collector potential settings causing a trailing current at more negative generator potentials (and vice versa). The effect becomes more pronounced at lower frequencies (not shown) and the proposed reason is an increase in “slow feedback” current from outside the gap (see Figure 3.2A) as opposed to the fast gap feedback current responsible for the peak response.

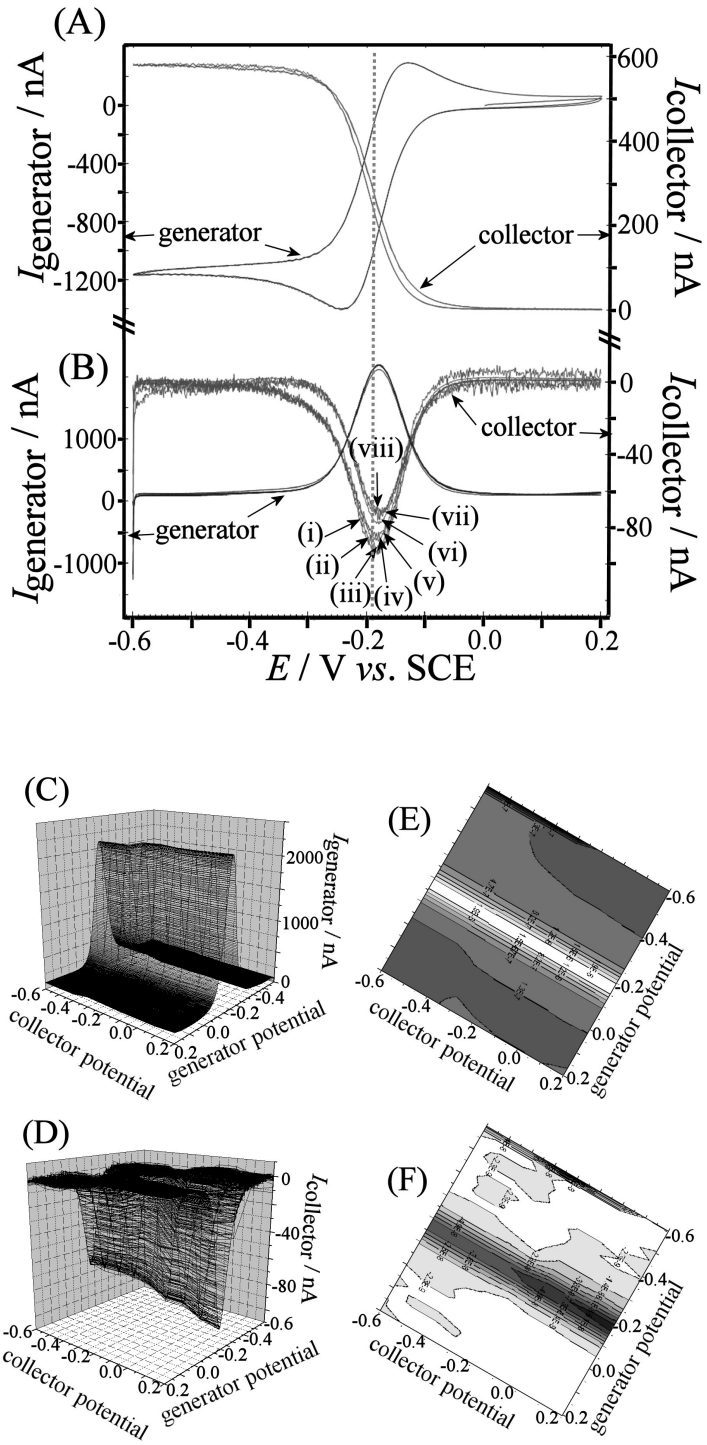


**Figure 3.3** (A) Cyclic voltammograms (generator and collector current shown, scan rate 10 $mVs^{-1}$, $E_{collector}$ = 0.1 V vs. SCE) for the reduction of 1 mM $Ru(NH_3)_6^{3+}$ in 0.1 M KCl at a gold-gold junction in generator collector mode. (B) Square wave voltammetric signal (generator and collector current shown, 8 Hz, 20 mV amplitude, 1 mV step potential) for $E_{collector}$ = (i) 0.1, (ii) 0.0, (iii) -0.1, (iv) -0.2, (v) -0.3, (vi) -0.4, (vii) -0.5, and (viii) -0.6 V vs. SCE. Also shown are (C) generator current topography plot, (D) collector current topography plot, (E) generator current contour plot, and (F) collector current contour plot.

When inspecting the topography plot of the collector current (Figure 3.3D) a decrease in the peak response is also observed. The collector peak current decreases from 94 nA ($E_{collector}$ = 0.1 V vs. SCE) to 72 nA ($E_{collector}$ = -0.6 V vs. SCE) corresponding to a 25 % drop. This observation is in good agreement with the effect of the reported diffusion coefficients of $D_{(Ru(NH3)63+)} = 0.84 \times 10^{-9}$ $m^2s^{-1}$ and $D_{(Ru(NH3)62+)} = 1.18 \times 10^{-9}$ $m^2s^{-1}$ measured under similar conditions [29]. For more positive applied collector potentials the collector peak response is dominated by diffusion of the reduced form of the metal complex and vice versa.

### 3.4.2 Square Wave Voltammetric Mapping of Junction Processes II: Indigo Carmine Reduction in Phosphate Buffer pH 12

Next, the reduction of indigo carmine was investigated under generator – collector junction conditions. A 2-electron reduction accompanied by 2-proton association (Equation 3.2) or 1-proton association at pH > 8 (Equation 3.3) has been reported [30, 31].

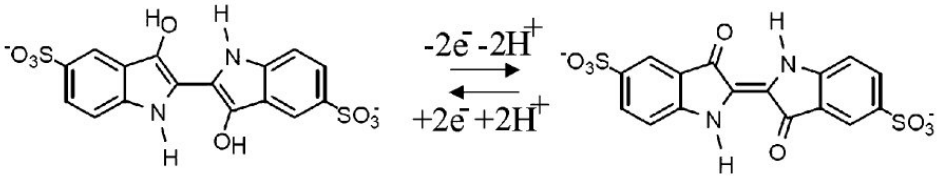


(3.2)

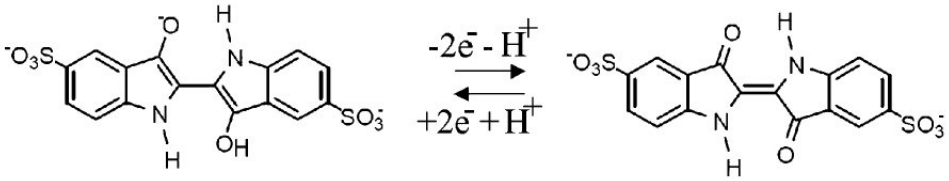


(3.3)

When working in solution more acidic than the $pK_a$ value of the redox analyte, protons in solution compensate for the gain of electrons through the reduction process. However in solutions with a more alkaline pH, the first electron transfer sees a proton consumed but the second electron transfer does not. The $pK_a$ value of the reduced indigo carmine (leuco-indigo carmine) has a value of ca. 8, hence at pH 7 (see section 3.4.3) a 2-electron, 2-proton process is observed but at pH 12 the 2-electron 1-proton process is seen.

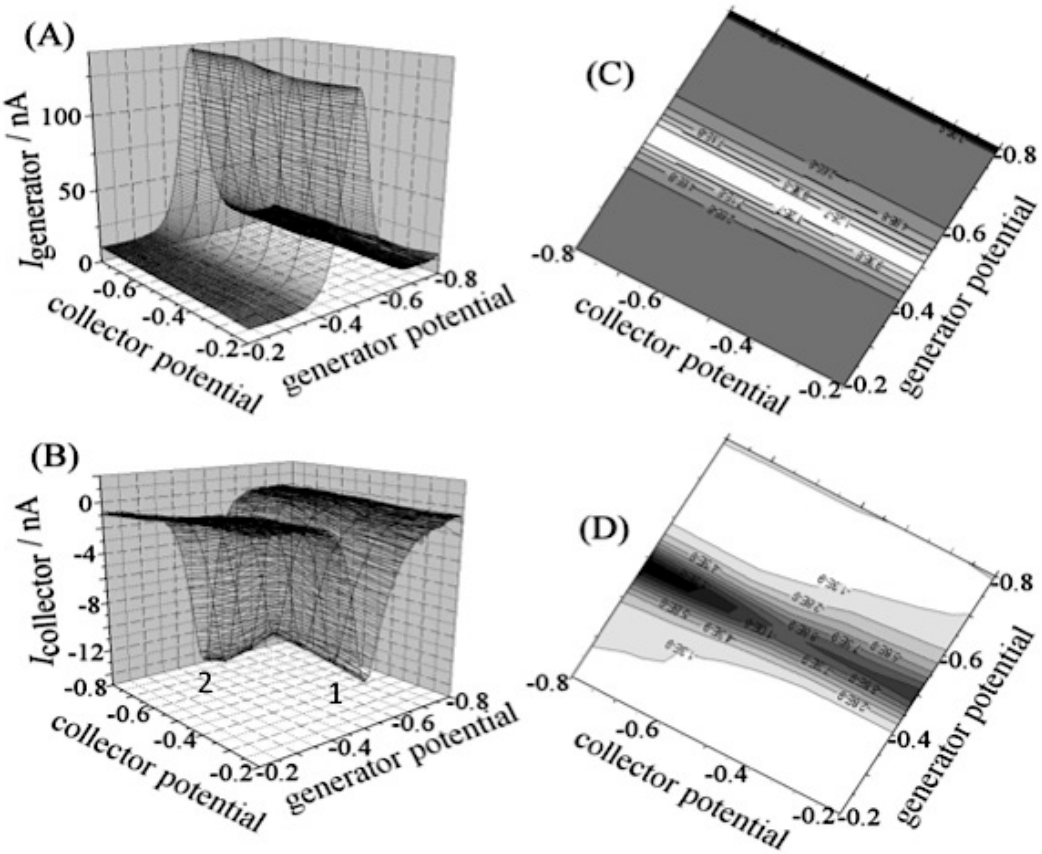


**Figure 3.4** (A) Square wave voltammetric signal (generator current topography plot shown, 2 Hz, 20 mV amplitude, 1 mV step potential) for 1 mM indigo carmine in 0.1 M phosphate buffer pH 12. (B) Collector current topography plot. (C) Generator current contour plot. (D) Collector current contour plot.

Under argon and in phosphate buffer pH 12, highly consistent generator responses are observed at -0.5 V vs. SCE (see Figure 3.4A) consistent with the expected position for the 2 electron – 1 proton reduction of indigo carmine [30]. Figure 3.4B and 3.4D shows the square wave voltammetric collector current peak occurs at the same potential (peak 1) with a "shoulder effect" (peak 2) probably due to peripheral diffusion contributions.

Contour plots are used to graphically show the 3D topography model in 2-dimension, with the lightest shaded area depicting the most positive peak current value of the square wave response and the darkest area being the most negative peak current value. Hence the peaks illustrated on the contour plots are the light and dark shaded areas for the generator and collector responses respectively. It is graphically easier to see the potentials at which the redox activity (oxidation or reduction) of the target species occurs.

The overall reaction sequence can be summarised into an extended scheme of squares (see Equation 3.4) where the reduction and the oxidation (here at the collector electrode) are linked via a single fast reversible protonation step. Therefore, both reduction and oxidation processes at the collector electrode (under the chosen time domain conditions) appear at the same potential.

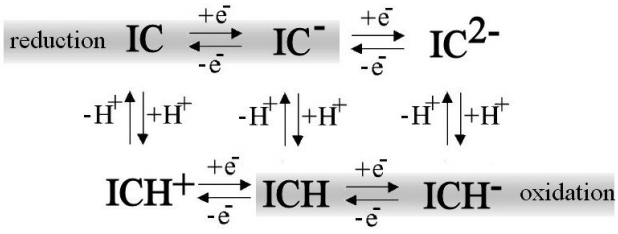


(3.4)

The scheme of squares is network of heterogeneous electron transfer and homogeneous (proton) transfer and is a standard guide when determining a reaction mechanism. Due to the complex nature of the generator-collector responses in this chapter, the scheme of squares aid in understanding the relatively unknown processes that are involved. The areas that are highlighted in grey indicate the pathway that best describes the reaction mechanism from the voltammetric responses seen in the topography and contour plots. Here it looks as though an EC mechanism is responsible for the signal as there is a full diffusion controlled peak compared to a CE mechanism where you would observe a small step with a fraction of the current seen in the EC mechanism. The EC mechanism is an electron transfer step followed by a chemical reaction, hence the areas highlighted are associated with such a mechanism.

### 3.4.3 Square Wave Voltammetric Mapping of Junction Processes III: Indigo Carmine Reduction in Phosphate Buffer pH 7

When working in phosphate buffer pH 7, new types of processes are observed. The generator signal with positive collector shows a peak at ca. -0.5 V vs. SCE (peak 1 in Figure 3.5A) now consistent with a 2 electron – 2 proton indigo carmine reduction peak but more negative when compared to the expected signal at ca. -0.4 V vs. SCE [30]. However, as the collector potential is approaching -0.4 V vs. SCE this peak is fading and a new peak emerges at -0.2 V vs. SCE (peak 2 in Figure 3.5A). A very similar (but clearer) trend is observed for the collector current responses. The equilibrium potential expected for pH 7 is approximately -0.4 V vs. SCE [30] which seems consistent with the mixed potential half way between both processes.

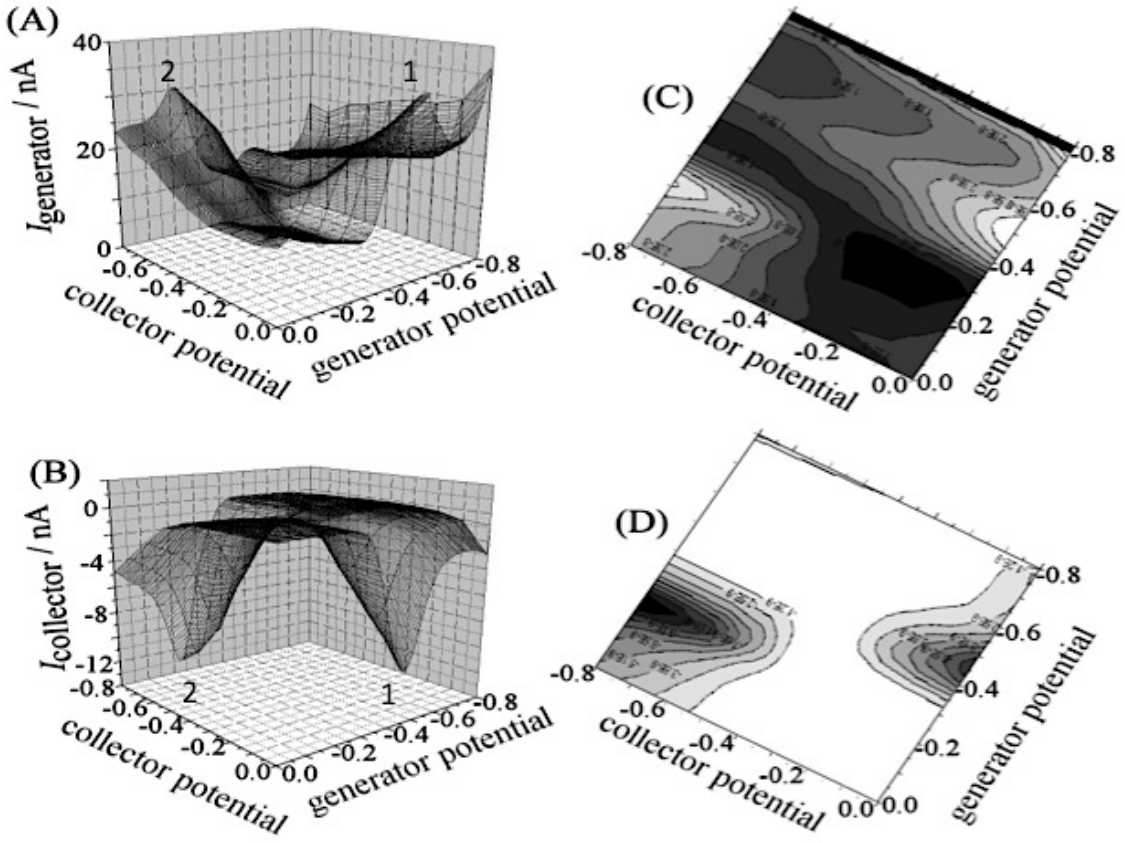


**Figure 3.5** (A) Square wave voltammetric signal (generator current topography plot shown, 2 Hz, 20 mV amplitude, 1 mV step potential) for 1 mM indigo carmine in 0.1 M phosphate buffer pH 7. (B) Collector current topography plot. (C) Generator current contour plot. (D) Collector current contour plot.

The collector current responses are much better defined and can be discussed in terms of the appropriate extended square reaction scheme for the coupled electron/proton transfer process (see Equation 3.5). With the collector fixed at more negative potentials and the generator in the more positive range, the reduction at the collector electrode is "switched on" and the corresponding peak has moved more positive at pH 7 (peak 2 in Figure 3.5B) when compared to that at pH 12 (peak 2 in Figure 3.4B). In contrast, with the collector fixed at more positive potentials and the generator potential scanning negative, the oxidation at the collector is "switched on" (peak 2 in Figure 3.5B). A separate peak response for reduction of indigo carmine (peak 2) and for oxidation of

leuco-indigo carmine (peak 1) is observed here probably due to a multi-step protonation with a less fast equilibration of intermediates. Both oxidation and reduction mechanism are summarised in Equation 3.5.

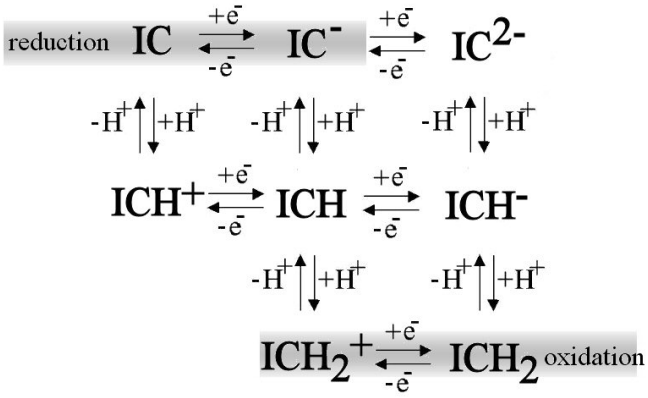


(3.5)

### 3.4.4 Square Wave Voltammetric Mapping of Junction Processes IV: Indigo Carmine Reduction in KCl

In the absence of buffer, voltammetric responses become affected by additional pH gradients between generator and collector electrode. In this case new additional phenomena are observed such as a mismatch between the appearance of the generator and collector square wave voltammetry contour features. Figure 3.6 shows topography and contour plots for the reduction of 1 mM indigo carmine at the gold – gold junction electrode. The square wave voltammetric response at the generator electrode is dominated by the peak at -0.45 V vs. SCE (peak 1 in Figure 3.6A) which is consistent with a locally generated proton activity of ca. pH 11 due to the $pK_a$ of the leuco-indigo carmine product [30] and the corresponding consumption of ca. 1 mM protons locally at the generator electrode surface.

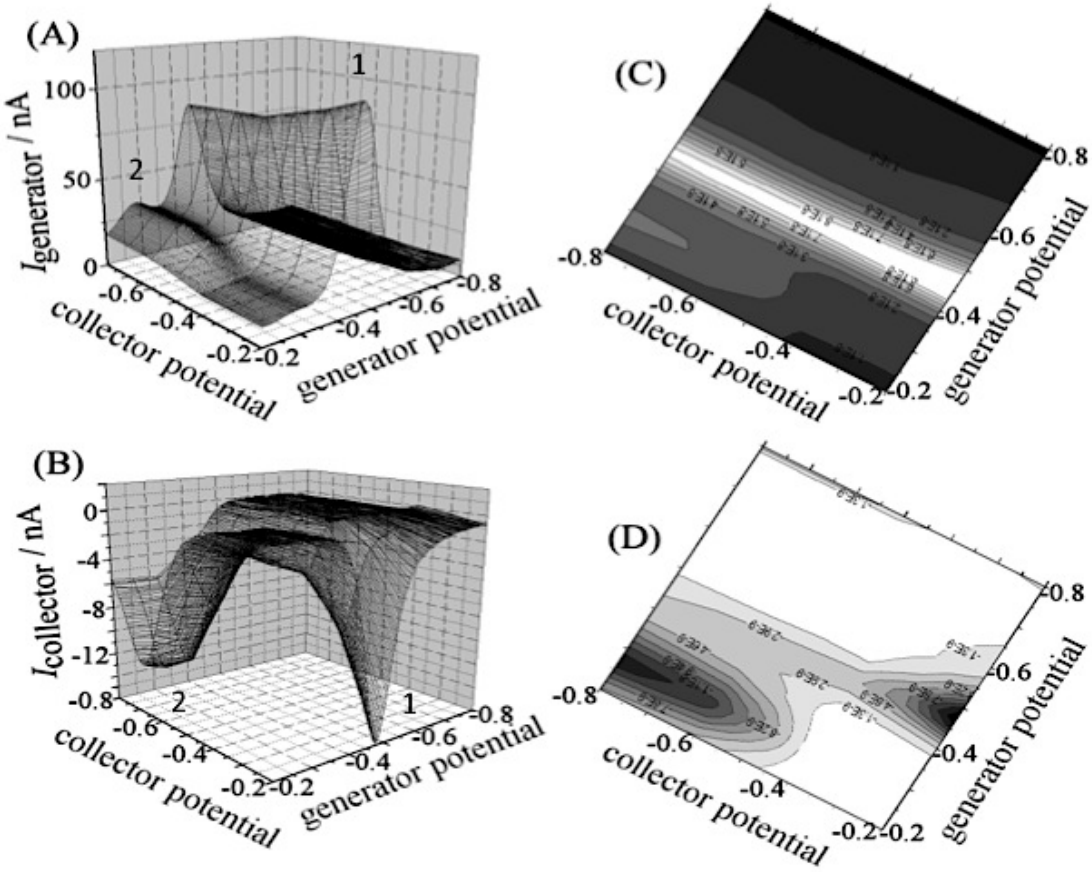


**Figure 3.6** (A) Square wave voltammetric signal (generator current topography plot shown, 2 Hz, 20 mV amplitude, 1 mV step potential) for 1 mM indigo carmine in 0.1 M KCl. (B) Collector current topography plot. (C) Generator current contour plot. (D) Collector current contour plot.

Perhaps surprisingly, when the collector potential is fixed at more negative potentials the collector response (see Figure 3.6D) shows similarity to that observed previously at pH 7 (see Figure 3.5D) with a strong peak at ca. -0.28 V vs. SCE (peak 2). It is possible that the transport of protons (associated with reduced indigo carmine) generates a local pH gradient in KCl solution with conditions at the collector electrode creating a slightly more acidic environment.

## 3.5 Summary and Conclusion

Environmental detection of pollutants requires selective and sensitive analysis using reliable sensing devices. This chapter studied square wave voltammetry at gold-gold hemisphere generator-collector electrodes, using compounds with well-known reduction pathways, in order to evaluate the electrochemical method and electrode geometry as potential alternatives to current techniques.

The paired gold hemisphere electrode provides important qualitative information for the reactivity of indigo carmine using square wave voltammetry mapping in generator-collector mode. This voltammetric method enables the specific detection of either the intermediate species or the fully reduced species by simply varying buffer conditions. The resulting data from the 3D "maps" and topography plots give more information compared to a conventional cyclic voltammogram, and allows the possibility to explore short-lived reaction intermediates due to the fast response times of this method. In un-buffered media, more complex data arises due to the changing pH gradients across the potential window, resulting in disagreements between the generator and collector signals.

Despite its complexitiy, this data is beneficial when detecting the "fingerprint" region of complex analytes compared to single voltammetric signals that cannot provide the depth of detail needed for their identification. This is an important aspect for electrochemical sensor applications as many contaminants have similar redox behaviour to other environmental compounds. They are also present in many forms, as the unaltered parent compound, metabolite or conjugate, so a device that is able to be more selective is advantageous and more comparable to the current analytical techniques that can

distinguish between the different forms present. Some forms may only be present in the aqueous environment for a short time, possibly due to degradation, further metabolism processes and adhesion to solid particles, so the fast analysis time of square wave voltammetry and the ability to conduct real-time measurements would enable the detection of these analytes; an advantage over techniques such as LC-MS where the time between sample collection and sample analysis is longer than the lifetime of these compounds.

Although these results are promising, the electro-deposition fabrication for this electrode is problematic. Low symmetry of the hemispherical growth makes numerical simulation more complicated, and the small active area, zone of fast diffusion, gives low collection efficiencies, less than 30%. Improvements to the geometry could enhance the electrochemical data and subsequent chapters show electrodes where the active area is much greater compared to these dual-hemispheres.

## 3.6 References

1. Rajantie, H. and D.E. Williams, *Potentiometric titrations using dual microband electrodes.* Analyst, 2001. **126**(11): p. 1882-1887.

2. Barnes, E.O., G.E.M. Lewis, S.E.C. Dale, F. Marken, and R.G. Compton, *Generator-collector double electrode systems: A review.* Analyst, 2012. **137**(5): p. 1068-1081

3. Postlethwaite, T.A., J.E. Hutchison, R. Murray, B. Fosset, and C. Amatore, *Interdigitated array electrode as an alternative to the rotated ring-disk electrode for determination of the reaction products of dioxygen reduction.* Analytical Chemistry, 1996. **68**(17): p. 2951-2958.

4. Vagin, M.Y., A.A. Karyakin, A. Vuorema, M. Sillanpaa, H. Meadows, F.J. Del Campo, M. Cortina-Puig, P.C.B. Page, Y.H. Chan, and F. Marken, *Coupled triple phase boundary processes: Liquid-liquid generator-collector electrodes.* Electrochemistry Communications, 2010. **12**(3): p. 455-458.

5. Tomcik, P., D. Bustin, and V. Tvarozek, *Microelectrode arrays with interacting diffusion layers: Voltammetric applications.* Chemicke Listy, 1999. **93**(11): p. 678-682.

6. Amatore, C., N. Da Mota, C. Sella, and L. Thouin, *Theory and Experiments of Transport at Channel Microband Electrodes Under Laminar Flow. 3. Electrochemical Detection at Electrode Arrays under Steady State.* Analytical Chemistry, 2010. **82**(6): p. 2434-2440.

7. Bard, A.J., F.R.F. Fan, J. Kwak, and O. Lev, *Scanning electrochemical micopscopy - introduction and principles.* Analytical Chemistry, 1989. **61**(2): p. 132-138.

8. Schulte, A., M. Nebel, and W. Schuhmann, *Scanning Electrochemical Microscopy in Neuroscience.* Annual Review of Analytical Chemistry, Vol 3, 2010. **3**: p. 299-318.

9. Albery, W.J. and M.L. Hitchman, *Ring-Disc Electrodes*. 1971, Oxford: Clarendon Press.

10. Rassaei, L., P.S. Singh, and S.G. Lemay, *Lithography-Based Nanoelectrochemistry.* Analytical Chemistry, 2011. **83**(11): p. 3974-3980.

11. French, R.W., S.N. Gordeev, P.R. Raithby, and F. Marken, *Paired gold junction electrodes with submicrometer gap.* Journal of Electroanalytical Chemistry, 2009. **632**(1-2): p. 206-210.

12. Dale, S.E.C., A. Vuorema, E.M.Y. Ashmore, B. Kasprzyk-Horden, M. Sillanpaa, G. Denuault, and F. Marken, *Gold-Gold Junction Electrodes: The Disconnection Method.* Chemical Record, 2012. **12**(1): p. 143-148

13. French, R.W., A.M. Collins, and F. Marken, *Growth and Application of Paired Gold Electrode Junctions: Evidence for Nitrosonium Phosphate During Nitric Oxide Oxidation.* Electroanalysis, 2008. **20**(22): p. 2403-2409.

14. Rassaei, L., R.W. French, R.G. Compton, and F. Marken, *Microwave-enhanced electroanalytical processes: generator-collector voltammetry at paired gold electrode junctions.* Analyst, 2009. **134**(5): p. 887-892.

15. French, R.W. and F. Marken, *Growth and characterisation of diffusion junctions between paired gold electrodes: diffusion effects in generator-collector mode.* Journal of Solid State Electrochemistry, 2009. **13**(4): p. 609-617.

16. Wang, J., *Analytical Electrochemistry*. 3rd ed. 2006, New Jersey: John Wiley & Sons, Chapter 3.

17. Rassaei, L. and F. Marken, *Pulse-Voltammetric Glucose Detection at Gold Junction Electrodes.* Analytical Chemistry, 2010. **82**(17): p. 7063-7067.

18. Mirceski, V., S. Komorsky-Lovric, and M. Lovric, *Square Wave Voltammetry: Theory and Application*. 2007, Berlin: Springer, Chapter 2.

19. Brookes, B.A., J.C. Ball, and R.G. Compton, *Simulation of square wave voltammetry: Reversible electrode processes.* Journal of Physical Chemistry B, 1999. **103**(25): p. 5289-5295.

20. Brookes, B.A., G. Macfie, and R.G. Compton, *Simulation of square wave voltammetry at hemispherical electrodes: Electrochemically reversible, irreversible and quasi-reversible processes.* Journal of Physical Chemistry B, 2000. **104**(24): p. 5784-5789.

21. Baur, J.E. and P.N. Motsegood, *Diffusional interactions at dual disk microelectrodes: comparison of experiment with three-dimensional random walk simulations.* Journal of Electroanalytical Chemistry, 2004. **572**(1): p. 29-40.

22. Osteryoung, J. and J.J. Odea, *Square-wave voltammetry.* Electroanalytical Chemistry, 1986. **14**: p. 209-308.

23. Enright, P., J. Cassidy, and A. Betts, *Evaluation of a naive model for square wave voltammetry at a microdisk electrode.* Journal of Electroanalytical Chemistry, 2008. **619**: p. 206-208.

24. Bragato, C., S. Daniele, and M.A. Baldo, *Low frequency square-wave voltammetry of weak acids at platinum Microelectrodes.* Electroanalysis, 2005. **17**(15-16): p. 1370-1378.

25. Barker, G.C. and A.W. Gardner, *40 years of square-wave polarography.* Analyst, 1992. **117**(12): p. 1811-1828.

26. Suwatchara, D., N.V. Rees, M.C. Henstridge, E. Laborda, and R.G. Compton, *Experimental comparison of the Butler-Volmer and Marcus-Hush-Chidsey formalisms of electrode kinetics: The reduction of cyclooctatetraene at mercury hemispherical electrodes via cyclic and square wave voltammetries.* Journal of Electroanalytical Chemistry, 2012. **665**: p. 38-44.

27. Cutress, I.J., Y. Wang, J.G. Limon-Petersen, S.E.C. Dale, L. Rassaei, F. Marken, and R.G. Compton, *Dual-microdisk electrodes in and theory transient generator-collector mode: Experiment.* Journal of Electroanalytical Chemistry, 2011. **655**(2): p. 147-153.

28. Marken, F., R.P. Akkermans, and R.G. Compton, *Voltammetry in the presence of ultrasound: The limit of acoustic streaming induced diffusion layer thinning and the effect of solvent viscosity.* Journal of Electroanalytical Chemistry, 1996. **415**(1-2): p. 55-63.

29. Wang, Y., J.G. Limon-Petersen, and R.G. Compton, *Measurement of the diffusion coefficients of Ru(NH3)(6) (3+) and Ru(NH3)(6) (2+) in aqueous*

*solution using microelectrode double potential step chronoamperometry.* Journal of Electroanalytical Chemistry, 2011. **652**(1-2): p. 13-17.

30. Diaz-Gonzalez, M., C. Fernandez-Sanchez, and A. Costa-Garcia, *Comparative voltammetric behavior of indigo carmine at screen-printed carbon electrodes.* Electroanalysis, 2002. **14**(10): p. 665-670.

31. Watkins, J.D., R. Lawrence, J.E. Taylor, S.D. Bull, G.W. Nelson, J.S. Foord, D. Wolverson, L. Rassaei, N.D.M. Evans, S.A. Gascon, and F. Marken, *Carbon nanoparticle surface functionalisation: converting negatively charged sulfonate to positively charged sulfonamide.* Physical Chemistry Chemical Physics, 2010. **12**(18): p. 4872-4878.

# Chapter 4

# Cavity Transport Effects in Generator - Collector Electrochemical Analysis of Nitrobenzene

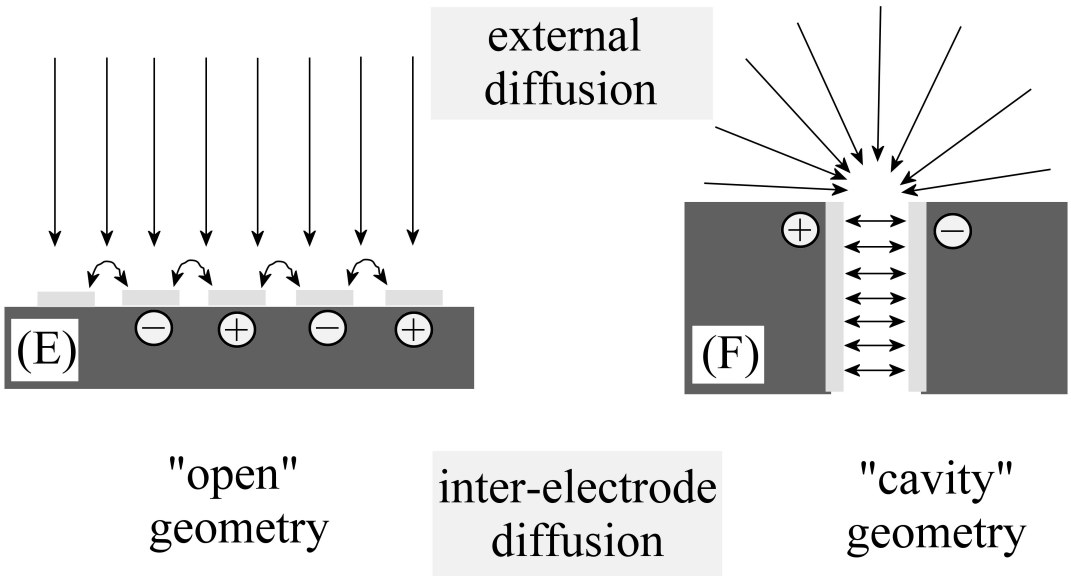


This work is published as "Cavity transport effects in generator-collector electrochemical analysis of nitrobenzene" Lewis, G.E.M.; Dale, S.E.C; Kasprzyk-Hordern, B.; Lubben, A.T.; Barnes, E.O.; Compton, R.G.; Marken, F., *Physical Chemistry Chemical Physics* 16 (2014) 18966-18973

# Abstract

The geometry of the generator-collector electrode is of vital importance in electroanalysis, especially in complex media. A comparison is made between two types of junction electrodes (i) a gold interdigitated microband array (commercially available) and (ii) a gold-gold dual-plate microtrench (made in the laboratory) to investigate the reduction of nitrobenzene in aerated aqueous 0.1 M NaOH. The presence of ambient levels of oxygen is challenging when accessing the analytical signal presented by the generator-collector feedback steady state currents.

The cavity-like microtrench electrode provided a more stable and readily detectable current for nitrobenzene reduction at 1 mM concentration, compared to the interdigitated array electrode with a more openly accessible geometry, where a signal drift and less-defined response was observed. Both types of electrode show oxygen-enhanced low concentration collector current responses due to additional feedback via reaction intermediates.

The responses are interpreted using the cavity transport coefficient, demonstrating that the dual-plate microtrench supresses the oxygen interference effects and the analytical signal is amplified and stabilised.

# Contents

## 4.1 Introduction

The previous chapter illustrated the use of gold-gold hemisphere electrodes, for three-dimensional square wave voltammetric mapping, to obtain information about reaction products and short-live intermediates [1]. Despite the promising results, these electrodes are of limited use in electroanalysis due to their small active area, demonstrating the importance of electrode geometry for enhanced currents from faster feedback.

With that in mind, two generator-collector electrode geometries are compared; (i) a dual-plate micro-trench electrode where cavity transport effects allow fast inter-electrode diffusion with limited access to the open solution, and (ii) a commercially produced interdigitated band array where the sensor surface is openly accessible for all solution components.

The interdigitated electrode array, fabricated using lithographic [2] techniques, consists of two interlocking "comb-like" arrays of microelectrodes with the integration of reference and counter electrodes in the same device. They benefit from being low cost with high sensitivity and have been extensively used for electroanalysis, flow systems and biosensors. Figure 4.1E illustrates the open geometry of the interdigitated electrode offering semi-infinite planar diffusion access for the bulk solution.

The dual-plate generator-collector electrode was pioneered by Anderson and Reilley [3-5] and successfully exploited within the Marken group for electroanalysis [6, 7], pH titration [8], liquid-liquid anion transfer [9], as well as the detection of cysteine/cystine [10] and nitrite/nitrate [11] systems. The trench-like feature, produced by etching the spacer between the two working electrodes, provides a cavity for "internal" feedback of

the redox species under investigation. They offer many advantages including rapid diffusion of analyte into the trench, simple laboratory assembly and the ability to discriminate the reversible redox analyte from irreversible interferences. This geometry can therefore be considered as a cavity case (see Figure 4.1F) to explore the transport effects within the trench where the relative transport rates of bulk solution differ from the redox cycle components. A more recent study employing the dual-plate microtrench electrode system addressed the effect of suppressed oxygen signal due to the irreversible removal of $O_2$ diffusing into the "mouth" of the dual-plate electrode [12]. A similar effect is investigated here for the reduction of nitrobenzene.

Nitrobenzene may be regarded as a model system for nitro-aromatic analytes [13], many of which are in the class of explosives [14], and known environmental pollutants. It is used to manufacture aniline for the production of polyurethane, to produce lubricating oils and to manufacture dyes, drugs, pesticides and synthetic rubber. The reduction of nitrobenzene follows a multi-step pathway but a distinct "redox-cyclable" one-electron transfer is observed in alkaline solution [15], and will be used to evaluate the performance of (i) a gold interdigitated band array (gold bands 10 μm wide, 10 μm separation, Figure 4.1A,B) and (ii) gold-gold dual-plate electrode (micro-trench with 5 mm length, 300 μm depth, 45 μm width, Figure 4.1C,D). It is predicted that both the open and cavity systems will give comparable steady state generator-collector current responses due to diffusional increase in the detector current and similar electrode dimensions. However, secondary issues that strongly affect the detection of nitrobenzene in aqueous 0.1 M NaOH solution (required to partially stabilise the nitrobenzene radical anion [16]), indicate that the micro-trench electrode is much better suited for this type of analytical problem.

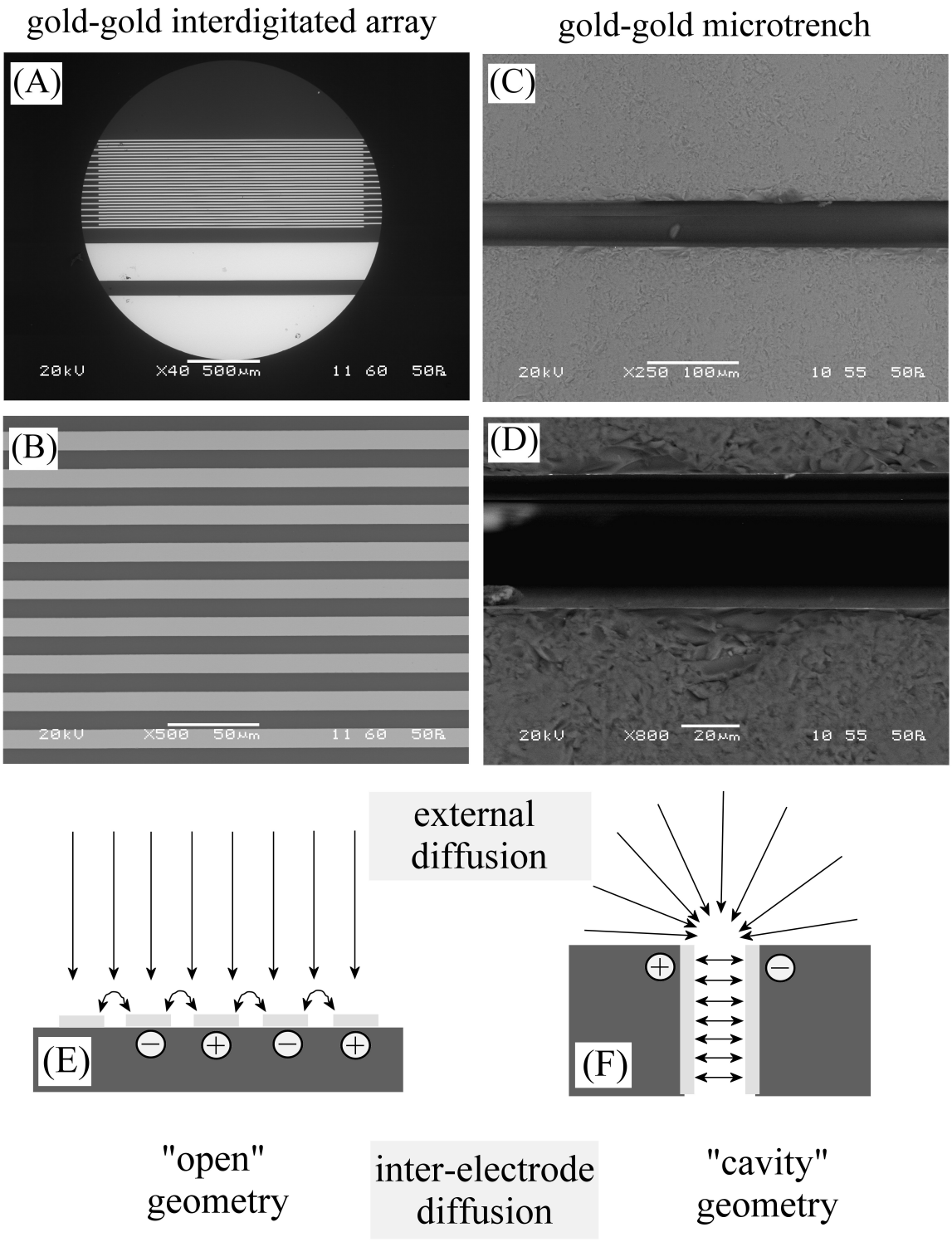


**Figure 4.1** (A,B) SEM images of a gold-gold interdigitated array electrode (Micrux ED-IDA1-Au) with two sets of 15 bands (interdigitated) of length 1.8 mm, width 10 µm, separation 10 µm, and thickness 150 nm. (C,D) SEM images of a gold-gold dual-plate microtrench electrode with 5 mm length, 45 µm width, 300 µm depth (see text), and 100 nm gold film thickness. (E,F) Schematic drawing of open and cavity generator-collector electrode systems.

## 4.2 Theory

To quantify the relative rates of mass transport within the redox cycle feedback and from the outside bulk solution, the cavity transport coefficient is introduced (see Equation 4.1).

$$\Phi_{cavity} = \frac{\text{flux due to inter-electrode diffusion}}{\text{flux due to external diffusion}} \tag{4.1}$$

This is expressed as a function of time for two components: for (i) the internal reversible redox cycle responsible for the generator-collector feedback current, and for (ii) the diffusion of bulk components to the dual-electrode followed by irreversible transformation.

For the dual-plate microtrench an approximate expression can be derived by dividing (i) the reversible Nernstian dual-plate diffusion current expression (ignoring time-dependent terms, Equation 4.2) [17] by (ii) the diffusional current for a microband "inlet" (with time-dependent term, Equation 4.3) [18, 19] to give approximate Equation 4.4 (see Figure 4.2).

$$I_{internal} = \frac{n_{internal}\, F D_{internal}\, l \times d \times c_{internal}}{\delta} \tag{4.2}$$

$$I_{external} = n_{external} F D_{external} l \times c_{external} \times \left[ \frac{\pi e^{-2.5\sqrt{\frac{\pi D_{external} t}{\delta^2}}}}{4\sqrt{\frac{\pi D_{external} t}{\delta^2}}} + \frac{\pi}{\ln\left(\left[\frac{64 e^{-0.577} D_{external} t}{\delta^2}\right]^{1/2} + e^{5/3}\right)} \right]^{-1} \quad (4.3)$$

$$\Phi_{microtrench} = \frac{I_{internal}}{I_{external}} = \frac{n_{internal}}{n_{external}} \times \frac{D_{internal}}{D_{external}} \times \frac{c_{internal}}{c_{external}} \times \frac{d}{\delta} \times \left[ \frac{\pi e^{-2.5\sqrt{\frac{\pi D_{external} t}{\delta^2}}}}{4\sqrt{\frac{\pi D_{external} t}{\delta^2}}} + \frac{\pi}{\ln\left(\left[\frac{64 e^{-0.577} D_{external} t}{\delta^2}\right]^{1/2} + e^{5/3}\right)} \right]^{-1} \quad (4.4)$$

In these expressions $n$ denotes the number of electrons transferred per molecule diffusing to the electrode, $F$ is the Faraday constant, $c$ is the concentration (with $c_{internal} = c_{ox} + c_{red}$ [8] to take into account the two components of the redox cycle), and the length $l$, the depth $d$, and the inter-electrode gap $\delta$ are geometric parameters. A plot of the cavity coefficient as a function of time $t$ is shown in Figure 4.2C.

For the interdigitated microband array electrode system a similar approach can be employed to define the cavity transport coefficient, $\Phi_{IDE,}$ based on the steady state feedback current for the microband array (ignoring time-dependent terms and inserting band width = gap-width, equation 4.5 [20-22] and the Cottrell equation (semi-infinite, time-dependent, see equation 4.6) ignoring edge terms.

$$I_{internal} = 0.49 \times N_{gap} \times n_{internal}\, FD_{internal}\, c_{internal}\, l \tag{4.5}$$

$$I_{external} = \frac{n_{external}\, FA_{IDE} \sqrt{D_{external}}\, c_{external}}{\sqrt{\pi}\,\sqrt{t}} \tag{4.6}$$

$$\Phi_{IDE} = \frac{I_{internal}}{I_{external}} = \frac{n_{internal}}{n_{external}} \times \frac{D_{internal}}{\sqrt{D_{external}}} \times \frac{c_{internal}}{c_{external}} \times \frac{0.49 \times N_{gap} \times l \times \sqrt{\pi} \times \sqrt{t}}{A_{IDE}} \tag{4.7}$$

Here, $N_{gap}$ denotes the number of generator-collector gaps and $A_{IDE}$ is the total active area of the interdigitated array.

Both expressions for the cavity transport coefficient are time-dependent terms, which have a characteristic effect over a timescale of several seconds (see Figure 4.2C). Due to the strongly reduced diffusional access to the microtrench geometry, the cavity transport coefficient is twice as high. This suggests that the generator-collector redox process is "decoupled" from the diffusion of reactive molecules from the bulk solution, which has implications for the chemical processes within the gap compared to those on the IDE. Also, the relative change in $\Phi_{microtrench}$ is much lower compared to that in $\Phi_{IDE}$, which implies a more stable analytical signal.

The data for the plot in figure 4.2C was obtained using the cavity transport coefficients in equation (4.4) and equation (4.7) for the microtrench electrode and interdigitated array respectively. The diffusion coefficient of ferrocyanide was used and the geometric parameters were taken from the electrodes mentioned in this chapter.

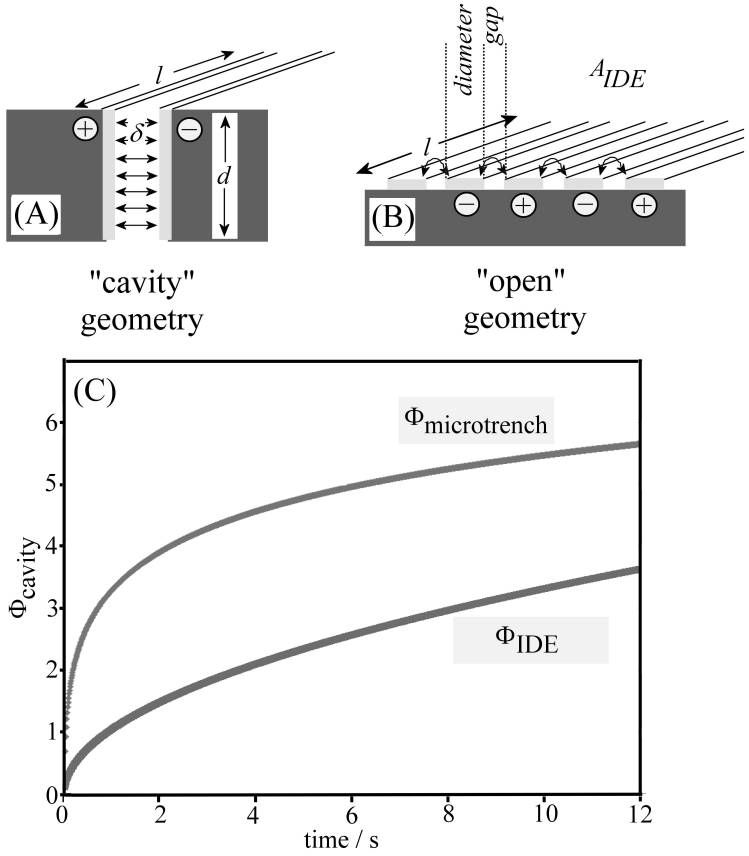


**Figure 4.2** Schematic drawings for (A) the microtrench geometry and (B) the interdigitated electrode geometry with key parameters. (C) Plot of the cavity transport coefficient $\Phi_{cavity}$ for microtrench and for interdigitated array for $D = 0.6 \times 10^{-9}$ $m^2s^{-1}$, $n = 1$, $c_{internal} = c_{external}$ and geometric parameters as given above.

## 4.3 Experimental Details

### 4.3.1 Chemical Reagents

Nitrobenzene, potassium ferrocyanide, and NaOH were purchased from Sigma-Aldrich UK. Chemical reagents were used as purchased, without further purification. Water was taken from a Thermo Scientific purification system (Barnstead Nanopure) with not less than 18.2 MOhm cm resistivity at 20 $^{o}$C.

### 4.3.2 Instrumentation

Generator-collector experiments were performed using an Autolab PGSTAT30 bipotentiostat (Metrohm, UK) in four-electrode configuration with a platinum gauze and saturated calomel (SCE, Radiometer) as the counter and reference electrode respectively. Two types of dual working electrodes were used: (i) a gold-gold dual-plate working electrode, and (ii) a commercial gold-gold interdigitated array electrode (ED-IDA1-Au, Micrux Technologies, Spain).

### 4.3.3 Production of Gold-Gold Dual-Plate Micro-Trench Electrodes

Gold-gold dual-plate microtrench electrodes were produced using a literature method [7] by cutting gold-coated microscope slides (Aldrich) into 1 cm × 3 cm strips using a diamond cutter (Buehler Isomet 1000 precision saw). The gold was then etched to leave a 5 mm strip down the middle of the slides and placed in a furnace at 500$^{o}$C for 30 minutes to oxidise the remaining titanium metal. Two gold slides were stuck together vis-à-vis using slow curing epoxy and cured at room temperature. Once cured, the end of the electrode was sliced off , polished flat and the epoxy was then etched for 5 minutes, forming a microtrench between the two gold electrodes with dimensions of 5 mm length, 45 μm width (as determined by SEM) and ca. 240 μm depth (estimated by voltammetry with the $Fe(CN)_6^{3-/4-}$ calibration redox system). All experiments were conducted at a temperature of 22 ± 2 $^{o}$C.

### 4.3.4 Voltammetry Conditions

The gold-gold dual-plate micro-trench electrode and the gold-gold interdigitated array electrode is calibrated by cyclic voltammetry using a solution of 2 mM ferrocyanide in

0.1 M KCl. To investigate the redox potential of the ferrocyanide solution, a typical 3-electrode cell set-up is used with a 1.6 mm gold disc electrode as the working electrode. The potential window is set as -0.1 V vs. SCE to 0.4 V vs. SCE with the forward scan scanning in a positive direction at scan rates of 10, 20, 50 and 100 $mVs^{-1}$ (with the 10 $mVs^{-1}$ scan shown in the results section). The same potential window and scan rates are used when employing the gold-gold dual-plate micro-trench electrode as the working electrode with the collector potential fixed at -0.1 V vs. SCE. The potential window is extended slightly to 0.5 V vs. SCE for the interdigitated electrode and the collector potential is held at 0.0 V vs. SCE.

To investigate the redox activity of nitrobenzene at the Au-Au microtrench electrode and the Au-Au interdigitated array electrode, 0.1 M NaOH is used as the supporting electrolyte and scan rates of 10, 20, 50 and 100 $mVs^{-1}$ are applied. Cyclic voltammetry without generator-collector mode applied is carried out on the Au-Au microtrench electrode, by having both of the working electrodes scanning the potential window, to study the reduction processes of nitrobenzene. The potential window for the these experiments is set at -0.1 V vs. SCE to -1.0 V vs. SCE. When the generator-collector mode is switched on, the same conditions are applied but the potential window is changed to -0.2 V vs. SCE to -0.9 V vs. SCE and the collector electrode is now held at a fixed potential of -0.2 V vs. SCE.

When studying the effect of nitrobenzene concentration using generator-collector cyclic voltammetry, the applied scan rate is 10 $mVs^{-1}$, the collector potential is fixed at -0.2 V vs. SCE, with the generator electrode scanning in a negative direction on the forward scan and the potential window is set from -0.2 V vs. SCE to -0.9 V vs. SCE.

## 4.4 Results and Discussion

### 4.4.1 Gold-Gold Dual-Plate Generator-Collector Electrode: Ferrocyanide Calibration

The oxidation of ferrocyanide (Equation 4.8), a well-known redox system, is used to calibrate the trench depth of the Au-Au dual-plate electrode (see Figure 4.3).

$$Fe(CN)_6^{4-}\ (aq) \leftrightharpoons Fe(CN)_6^{3-}\ (aq) + e^- \qquad (4.8)$$

Figure 4.3A shows a typical cyclic voltammogram obtained at a 3 mm diameter gold disc electrode with a quasi-reversible oxidation and back-reduction centred at the reversible potential of 0.193 V vs. SCE. When investigated in an Au-Au dual-plate microtrench electrode (Figure 4.3B), the oxidation at the generator electrode is accompanied with the back-reduction of $Fe(CN)_6^{3-}$ at the collector electrode. Some capacitive charging can be seen at the generator current signal with only some diffusion of analyte towards the cavity, compared to a well-defined collector signal with a clear mass transport controlled limiting current.

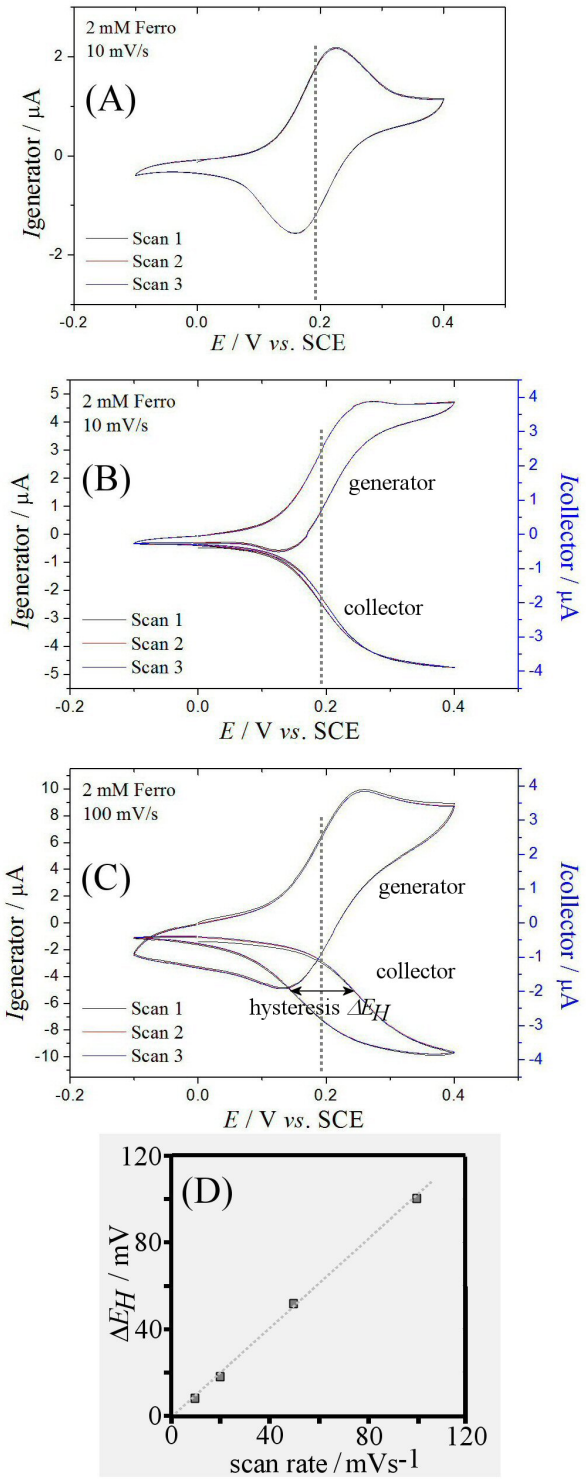


**Figure 4.3** Cyclic voltammograms for the oxidation of 2 mM $Fe(CN)_6^{4-}$ in 0.1 M KCl (A) at a 1.6 mm diameter gold disc electrode (scan rate 10 mV $s^{-1}$) and (B) at a dual-plate Au-Au microtrench generator-collector electrode for the generator scanning and the collector fixed at -0.1 V vs. SCE (scan rate 10 mV $s^{-1}$), and (C) for the generator scanning and the collector potential fixed at -0.1 V vs. SCE (scan rate 100 mV $s^{-1}$). (D) Plot of the collector current hysteresis versus scan rate.

The magnitude of the collector limiting current, $I_{collector}$, for the dual-plate geometry can be written as in Equation 4.9 (compare Equation 4.2).

$$I_{collector} = \frac{nFD_{Fe(CN)_6^{4-}} A c_{Fe(CN)_6^{4-}}}{\delta} \tag{4.9}$$

In this equation $n$ is the number of electrons transferred per molecule reacting at the electrode surface, $F$ is the Faraday constant, $D_{Fe(CN)_6^{4-}}$, is the diffusion coefficient for $Fe(CN)_6^{4-}$ (additional effects from the slight difference in diffusion coefficients for $Fe(CN)_6^{4-}$ and $Fe(CN)_6^{3-}$ [17] are here assumed to be insignificant), $A$ is the plate area, $c_{Fe(CN)_6^{4-}}$ is the bulk concentration of $Fe(CN)_6^{4-}$, and $\delta$ = 45 μm is the inter-electrode gap.

The hysteresis effect, $\Delta E_H$, in the collector current (see Figure 4.3C) can be used to obtain an estimate for the diffusion coefficient (see Equation 4.10 [23]).

$$D_{Fe(CN)_6^{4-}} = \frac{0.0071F\delta^2}{\Delta E_H RT} \tag{4.10}$$

In this equation a linear trend is predicted for $\Delta E_H$ versus the scan rate $v$ (see Figure 4.3D) and with the gas constant $R$ and the absolute temperature $T$, the diffusion coefficient can be estimated as $D_{Fe(CN)_6^{4-}} = 0.6 \times 10^{-9}$ $m^2s^{-1}$. This value is in good agreement with literature [24] and therefore used throughout this study. Finally, the trench depth is obtained by rearranging Equation 4.9 into Equation 4.11.

$$\text{Trench depth} = \frac{I_{collector} \times \delta}{nFDwc} = 300\ \mu m \qquad (4.11)$$

In this equation $w$ = 5 mm is the width of the microtrench and $I_{collector}$ is 3.6 μA (see Figure 4.3B). The average trench depth of 300 μm is consistent with an aspect ratio of between 6 to 7.

### 4.4.2 Gold-Gold Dual-Plate Generator-Collector Electrode: Reduction of Nitrobenzene

In alkaline media the reduction of nitrobenzene follows a multi-step pathway [25, 26], with an initial one-electron reduction to the unstable radical anion (see Figure 4.4A, P1, Equation 4.12) followed by the transfer of another three electrons to give a mixture of products (see Figure 4.4A, P2).

$$C_6H_5NO_2\ (aq) + e^- \leftrightharpoons C_6H_5NO_2^{\cdot -}\ (aq) \qquad (4.12)$$

The focus of this study is the one-electron reduction, P1, which occurs at a midpoint potential of -0.7 V vs. SCE (Figure 4.4A). When studying this process on the Au-Au microtrench electrode (with only one 'active' working electrode), a third process is seen, P3, when the potential is scanned in the positive direction, (Figure 4.4B). The additional signal can be associated with surface immobilised redox active products which further complicate the behaviour of the electrode (Figure 4.4C).

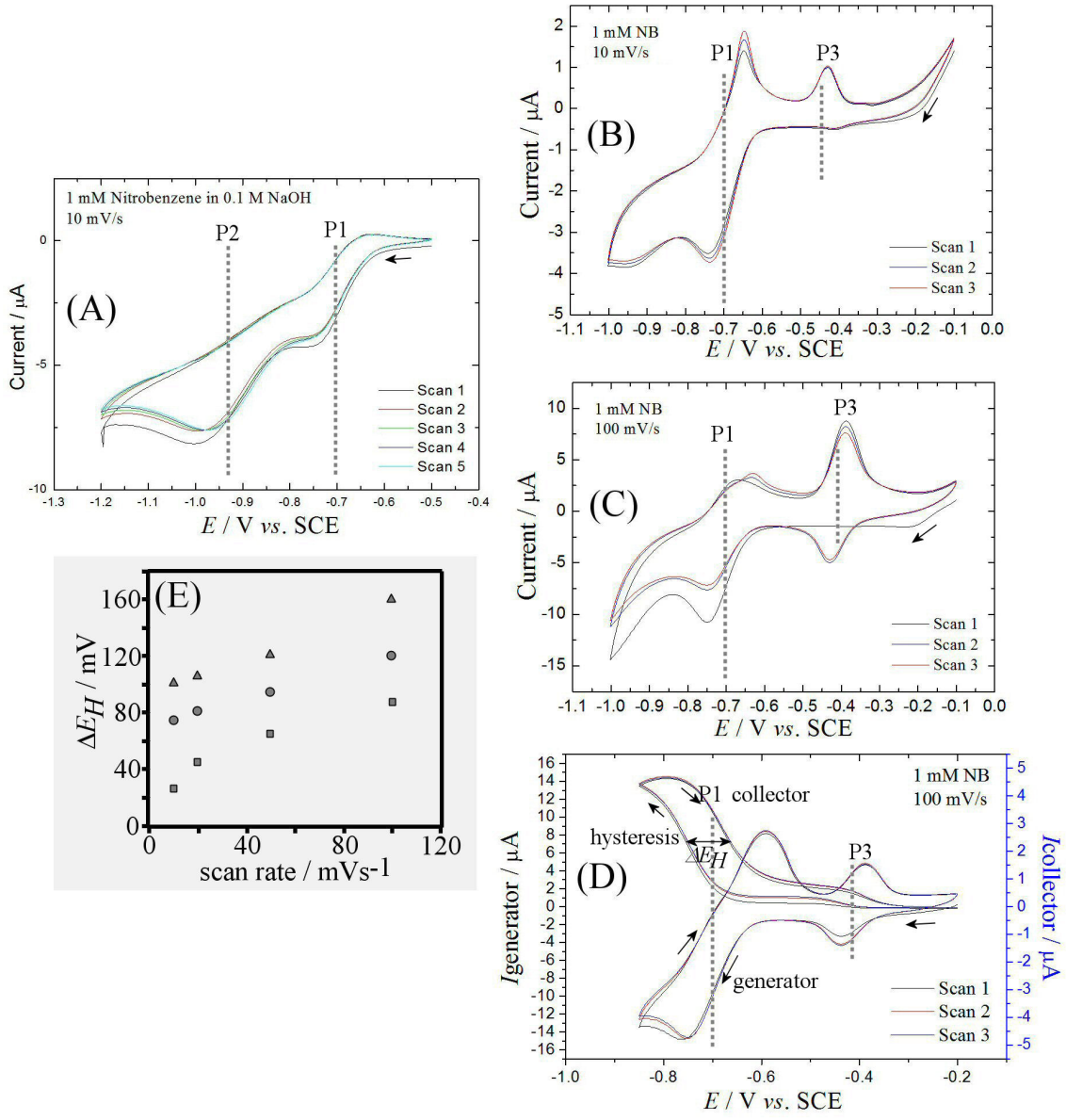


**Figure 4.4** (A) Reduction of 1 mM nitrobenzene in 0.1 M NaOH (scan rate 10 mV $s^{-1}$) at a 3 mm diameter gold disc electrode. (B) Reduction of 1 mM nitrobenzene in 0.1 M NaOH (scan rate 10 mV $s^{-1}$) at Au-Au microtrench electrode with both electrodes scanning. (C) As before but with scan rate 100 mV $s^{-1}$. (D) Reduction of 1 mM nitrobenzene in 0.1 M NaOH at Au-Au microtrench with the generator electrode scanning and the collector potential fixed at -0.2 V vs. SCE. (E) Plot of the collector current hysteresis for the nitrobenzene reduction as a function of scan rate (square: 1 mM, circle: 0.1 mM, and triangle: 0.01 mM nitrobenzene concentration).

When working in generator-collector mode, two well-defined processes, P1 and P3, are observed for the collector signal where a fixed potential of -0.2 V vs. SCE is applied (Figure 4.4D). At a more positive potential, a minor reduction signal consistent with process P3 is most likely due to oxygen reduction (all measurements were performed in the presence of ambient levels of dissolved oxygen). The second reduction signal is consistent with process P1 (see Equation 4.12) and likely to be a one-electron feedback process.

When analysing the mass transport limited collector current, $I_{collector}$ = ca. 3.3 μA, based on equation 4.9 and assuming a one-electron process, the nitrobenzene diffusion coefficient $D_{NB}$ can be estimated (equation 4.13) in good agreement with literature values [26].

$$D_{NB} = \frac{I_{collector} \times \delta}{nFAc_{NB}} \approx 1.0\times10^{-9} m^2 s^{-1} \qquad (4.13)$$

Figure 4.4E, a plot of the hysteresis parameter $\Delta E_H$ versus scan rate, shows non-linear characteristics with non-zero intercept and concentration dependent values. This could be due to the effects of deposited material and side reactions, possibly with $H_2O_2$ produced during oxygen reduction.

Further experiments were performed to investigate the low concentration feedback current for potential analytical applications. Process P1 gives well-defined collector current responses down to 1 μM nitrobenzene, with a fixed potential of -0.2 V vs. SCE and in the presence of ambient levels of oxygen, (see Figure 4.5). Interestingly, the feedback current for the nitrobenzene oxidation at the collector electrode is substantially

higher than expected (see double logarithmic plot in Figure 4.5E), as is the generator current (see line for linear behaviour). To explain this effect the presence of oxygen has to be taken into consideration as has been demonstrated recently for the reduction of $Ru(NH_3)_6^{3+}$ [6].

Compared to the generator current, the collector current signal is less sensitive to the presence of oxygen and could provide useful concentration data probably down to micromolar levels. To investigate the benefits of the Au-Au dual-plate microtrench electrode in this process, a comparison is now made to conventional interdigitated Au-Au band array electrodes.

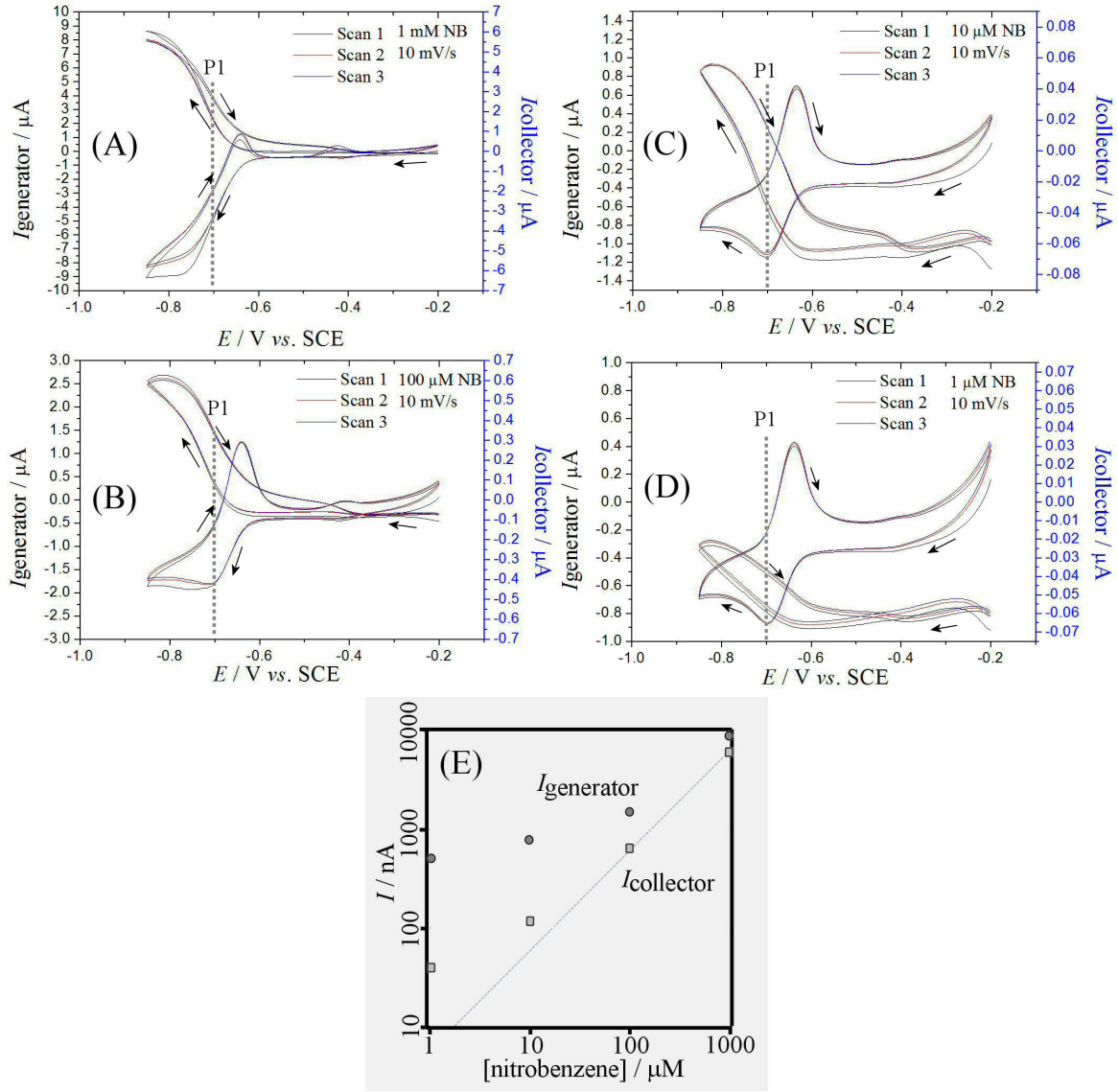


**Figure 4.5** Cyclic voltammograms for the reduction of (A) 1 mM, (B) 0.1 mM, (C) 0.01 mM, (D) 0.001 mM nitrobenzene in 0.1 M NaOH (scan rate 10 mV $s^{-1}$) at Au-Au microtrench electrode with collector potential fixed at -0.2 V vs. SCE. (E) Double logarithmic plot of generator and collector current (mass transport controlled feedback currents) as a function of nitrobenzene concentration. Line indicates linear behaviour.

### 4.4.3 Gold-Gold Interdigitated Array Generator-Collector Electrode: Oxidation of Ferrocyanide

Voltammetric current responses in generator – collector mode for the oxidation and re-reduction of 2 mM $Fe(CN)_6^{4-}$ in 0.1 M KCl are shown in Figure 4.6. Steady state limiting currents of several μA similar to those observed at the microtrench are detected with good collection efficiency.

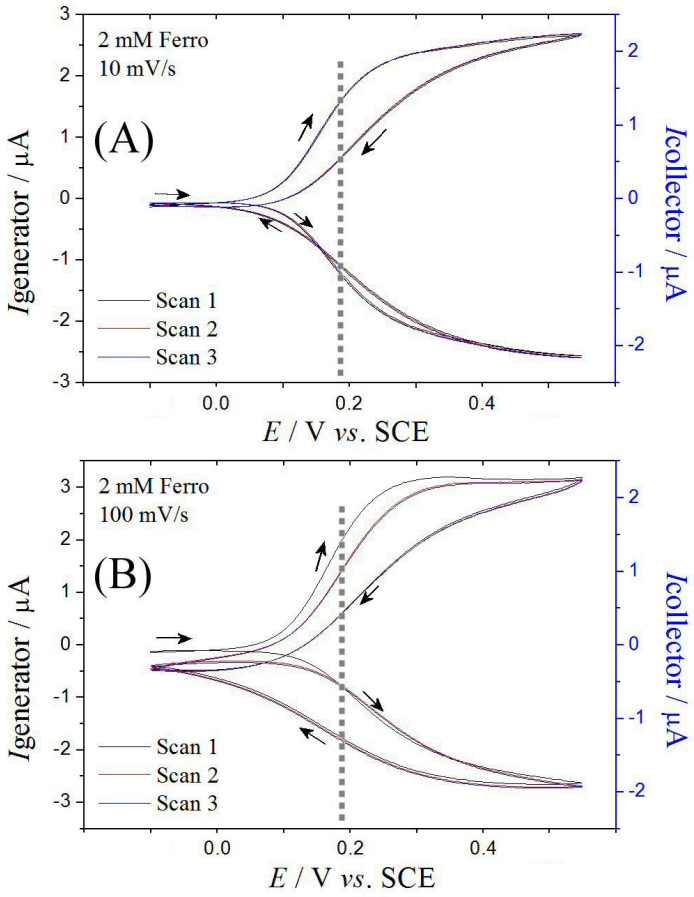


**Figure 4.6** Cyclic voltammograms for the oxidation of 2 mM $Fe(CN)_6^{4-}$ in 0.1 M KCl (scan rate (A) 10 mV $s^{-1}$ and (B) 100 mV $s^{-1}$) at an interdigitated array of Au band electrodes with collector potential -0.0 V vs. SCE.

The limiting currents at the generator and collector electrodes are almost independent of scan rate and determined here as 2.7 and -2.2 μA, respectively. This compares to the theoretically predicted collector current of 2.9 μA based on Equation 4.4.

### 4.4.4 Gold-Gold Interdigitated Array Generator-Collector Electrode: Reduction of Nitrobenzene

When investigating the generator-collector current responses for the reduction of nitrobenzene in 0.1 M NaOH at the interdigitated array electrode, the process P1 at -0.7 V vs. SCE is clearly identified (Figure 4.7A). Both generator and collector signal are well-defined. However, when lowering the nitrobenzene concentration to 100 μM and 10 μM a drift in the collector signal is apparent. At a nitrobenezene concentration of 1 μM the generator current response is no longer observed and the collector current response appears broadened. A double-logarithmic plot of collector current response versus nitrobenzene concentration (Figure 4.7E) shows a non-linear dependence more distorted compared to that for the microtrench electrode in Figure 4.5E. The reason for the non-linearity again is likely to be due to oxygen in the bulk solution and the increase in deviation from linearity here is likely to be linked to the lower cavity transport coefficient (see Figure 4.2C, oxygen can diffuse into the reaction zone at relatively higher rate).

All results in this chapter are of preliminary and exploratory nature to investigate the possibility of detecting nitro-based explosives using bipotentiostatically controlled generator-collector electrodes and comparing the redox behaviour at two electrodes with different geometries. The results shown were not repeated hence the absence of error bars for the plots of collector current hysteresis as a function of scan rate and the double logarithmic plots of collector current as a function of nitrobenzene concentration.

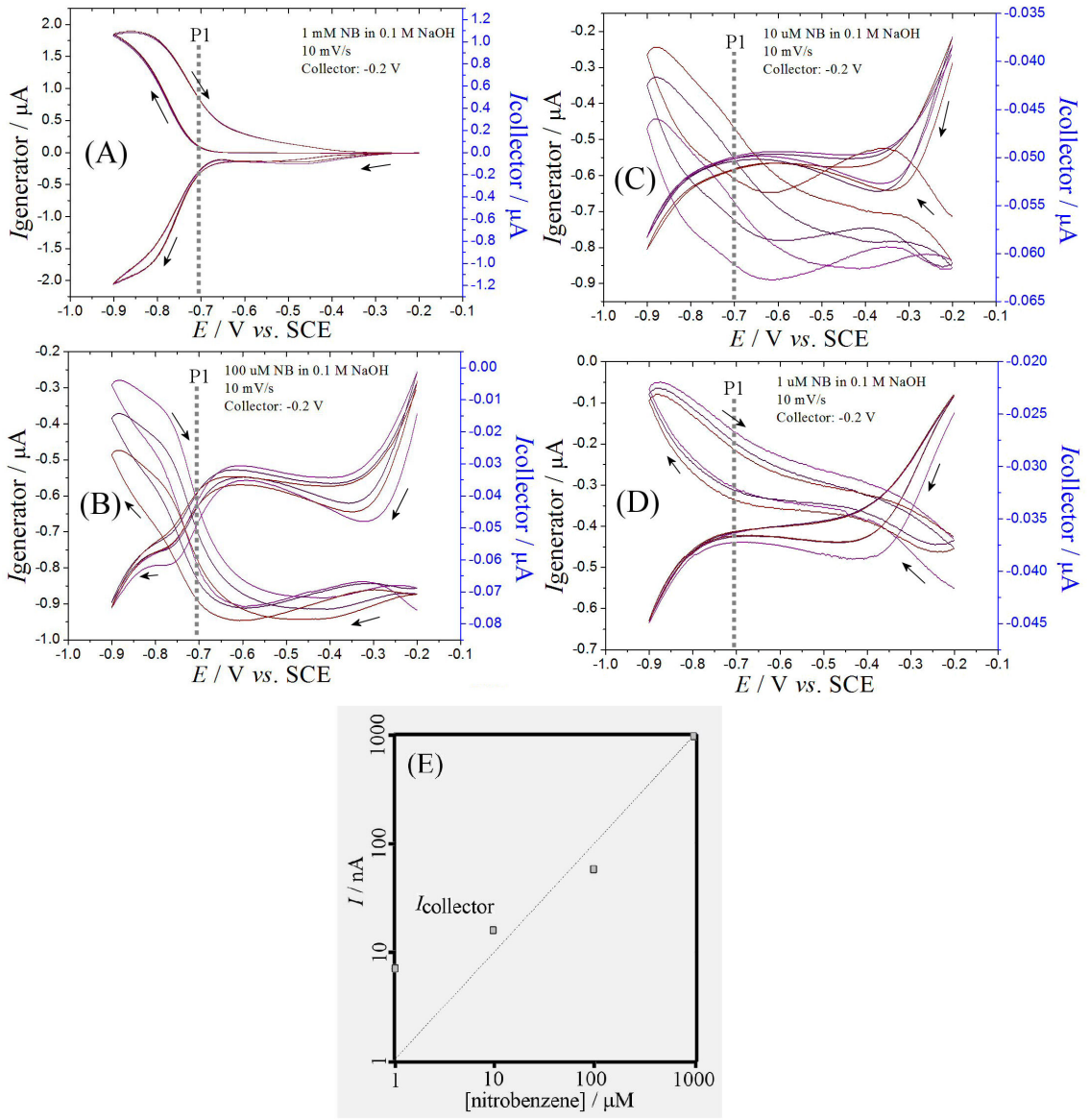


**Figure 4.7** Cyclic voltammetry (scan rate 10 mV $s^{-1}$) for the reduction of (A) 1 mM, (B) 0.1 mM, (C) 0.01 mM and (D) 0.001 mM nitrobenzene in 0.1 M NaOH at an interdigitated Au band array electrode. (E) Double logarithmic plot of collector current (mass transport controlled feedback currents) as a function of nitrobenzene concentration. Line indicates linear behaviour.

## 4.5 Summary and Conclusion

The previous chapter highlighted the importance of electrode geometry when designing electrochemical methods that have the potential to become sensitive detection devices for environmental pollutants. Here a comparison in the electroanalytical performance of a dual-plate microtrench electrode and an interdigitated array electrode has been investigated. The oxidation of $Fe(CN)_6^{4-}$ confirmed theoretical predictions that both types of electrodes give similar steady state voltammetric responses in a simple redox media. However, in more complex media under less ideal conditions, their behaviour differs. The complex reduction of nitrobenzene, studied in aerated solution, exhibited greater drifts in signal with less tolerance towards oxygen at the interdigitated array electrode compared to the microtrench electrode. This was further supported by the cavity transport coefficient $\Phi_{cavity}$, which was higher and more stable for the dual-plate electrode.

The dual-plate micro-trench electrode benefits from (i) more stable current responses, (ii) less interference from reagents (e.g. oxygen) diffusing in from the bulk, and (iii) less sensitivity to convection in the bulk. These are all desirable features for an environmental electrochemical sensor, however improvements to the electrode geometry, such as a deeper trench and shorter inter-electrode distance (moving towards nano-trench level dimensions), could further enhance the sensitivity and $\Phi_{cavity}$, providing a novel and powerful analytical tool.

Nitrobenzene was the chosen redox analyte as it can be used as a model system for nitro-based explosives. As the electrode device mentioned in this chapter is under continuous development, it is important to choose an analyte of similar structure with a

more simple and well-known redox reaction mechanism to be analysed before moving onto the desired environmental targets. To progress into analysing explosives in the aquatic environment, further improvements need to me made to reach detection levels in the low parts per million to parts per billion range and meet the standard of current analytical techniques.

From the results in this chapter, and after improvement in electrode geometry to reach the desired detection limits, interferences must be considered. Although the dual-plate micro-trench electrode had less tolerance towards oxygen in the aerated solutions (desirable for environmental analysis where oxygen is largely present), explosive compounds have very similar structures and could therefore interfere if detecting for a specific explosive compound. In view of environmental sensing, the technology could be used to detect for a group of compounds, say the nitro-based explosives, once improvements had been made to meet the desired detection limits. Although this does not eliminate subsequent analysis, it still lowers some of the financial and time demands faced with environmental analysis, as samples would only need to be collected and analysed once the level of explosive concentration in the aquatic environment reaches a hazardous level.

## 4.6 References

1. Lewis, G.E.M., S.E.C. Dale, B. Kasprzyk-Hordern, E.O. Barnes, R.G. Compton, and F. Marken, *Square Wave Electroanalysis at Generator-Collector Gold-Gold Double Hemisphere Junctions.* Electroanalysis, 2012. **24**(8): p. 1726-1731.

2. Streeter, I., N. Fietkau, J. del Campo, R. Mas, F.X. Munoz, and R.G. Compton, *Voltammetry at regular microband electrode arrays: Theory and experiment.* Journal of Physical Chemistry C, 2007. **111**(32): p. 12058-12066.

3. Anderson, L.B. and C.N. Reilley, *Thin layer electrochemistry - use of twin working electrodes for study of chemical kinetics.* Journal of Electroanalytical Chemistry, 1965. **10**(5-6): p. 538-552.

4. McDuffie, B., L.B. Anderson, and C.N. Reilley, *Twin-electrode thin-layer electrochemistry - determination of chemical reaction rates by decay of steady-state current.* Analytical Chemistry, 1966. **38**(7): p. 883-890.

5. Reilley, C.N., *Electrochemistry using thin-layer cells.* Reviews of Pure and Applied Chemistry, 1968. **18**(JUN): p. 137.

6. Dale, S.E.C., C.E. Hotchen, and F. Marken, *Generator-collector electroanalysis at tin-doped indium oxide-epoxy-tin-doped indium oxide junction electrodes.* Electrochimica Acta, 2013. **101**: p. 196-200.

7. Dale, S.E.C. and F. Marken, *Pulse electroanalysis at gold-gold micro-trench electrodes: Chemical signal filtering.* Faraday Discussions, 2013. **164**: p. 349-359.

8. Dale, S.E.C., A. Vuorema, M. Sillanpaa, J. Weber, A.J. Wain, E.O. Barnes, R.G. Compton, and F. Marken, *Nano-Litre Proton/Hydrogen Titration in a Dual-Plate Platinum-Platinum Generator-Collector Electrode Micro-Trench.* Electrochimica Acta, 2014. **125**: p. 94-100.

9. Dale, S.E.C., Y. Chan, P.C.B. Page, E.O. Barnes, R.G. Compton, and F. Marken, *A gold-gold oil microtrench electrode for liquid-liquid anion transfer voltammetry.* Electrophoresis, 2013. **34**(14): p. 1979-1984.

10. Hammond, J.L., A.J. Gross, P. Estrela, J. Iniesta, S.J. Green, C.P. Winlove, P.G. Winyard, N. Benjamin, and F. Marken, *Cysteine-Cystine Redox Cycling in a Gold-Gold Dual-Plate Generator-Collector Microtrench Sensor.* Analytical Chemistry, 2014. **86**(14): p. 6748-6752.

11. Gross, A.J., S. Holmes, S.E.C. Dale, M.J. Smallwood, S.J. Green, C.P. Winlove, N. Benjamin, P.G. Winyard, and F. Marken, *Nitrite/nitrate detection in serum based on dual-plate generator-collector currents in a microtrench.* Talanta, 2015. **131**: p. 228-235.

12. Hasnat, M.A., A.J. Gross, S.E.C. Dale, E.O. Barnes, R.G. Compton, and F. Marken, *A dual-plate ITO-ITO generator-collector microtrench sensor: surface activation, spatial separation and suppression of irreversible oxygen and ascorbate interference.* Analyst, 2014. **139**(3): p. 569-575.

13. Chua, C.K. and M. Pumera, *Influence of Methyl Substituent Position on Redox Properties of Nitroaromatics Related to 2,4,6-Trinitrotoluene.* Electroanalysis, 2011. **23**(10): p. 2350-2356.

14. Ceto, X., A.M. O' Mahony, J. Wang, and M. del Valle, *Simultaneous identification and quantification of nitro-containing explosives by advanced chemometric data treatment of cyclic voltammetry at screen-printed electrodes.* Talanta, 2013. **107**: p. 270-276.

15. Marken, F., S. Kumbhat, G.H.W. Sanders, and R.G. Compton, *Voltammetry in the presence of ultrasound: Surface and solution processes in the sonovoltammetric reduction of nitrobenzene at glassy carbon and gold electrodes.* Journal of Electroanalytical Chemistry, 1996. **414**(2): p. 95-105.

16. Kastenin.B and S. Vavricka, *Dismutation kinetics of Nitrobenzene anion.* Berichte Der Bunsen-Gesellschaft Fur Physikalische Chemie, 1968. **72**(1): p. 27.

17. Compton, R., G and C. Banks, E, *Understanding Voltammetry*. first ed. 2007, London: World Scientific Publishing, p. 95.

18. Szabo, A., D.K. Cope, D.E. Tallman, P.M. Kovach, and R.M. Wightman, *Chronoamperometric current at hemicylinder and band microelectrodes - theory and experiment.* Journal of Electroanalytical Chemistry, 1987. **217**(2): p. 417-423.

19. Amatore, C. and L. Rubinstein, *Physical Electrochemistry*. 1995 New York: Marcel Dekker, p. 155.

20. Aoki, K., M. Morita, O. Niwa, and H. Tabei, *Quantitative analysis of reversible diffusion-controlled currents of redox soluble species at interdigitated array electrodes under steady-state conditions.* Journal of Electroanalytical Chemistry, 1988. **256**(2): p. 269-282.

21. Aoki, K. and M. Tanaka, *Time dependance of diffusion-controlled currents of a soluble redox couple at interdigitated microarray electrodes.* Journal of Electroanalytical Chemistry, 1989. **266**(1): p. 11-20.

22. Barnes, E.O., G.E.M. Lewis, S.E.C. Dale, F. Marken, and R.G. Compton, *Generator-collector double electrode systems: A review.* Analyst, 2012. **137**(5): p. 1068-1081.

23. Vuorema, A., H. Meadows, N. Bin Ibrahim, J. Del Campo, M. Cortina-Puig, M.Y. Vagin, A.A. Karyakin, M. Sillanpaa, and F. Marken, *Ion Transport Across Liquid vertical bar Liquid Interfacial Boundaries Monitored at Generator-Collector Electrodes.* Electroanalysis, 2010. **22**(24): p. 2889-2896.

24. Adams, R.N., *Electrochemistry at Solid Electrodes*. 1969, New York: Marcel Dekker, p. 220.

25. Rubinstein, I., *Voltammetric study of Nitrobenzene and related-compounds on solid electrodes in aqueous solution.* Journal of Electroanalytical Chemistry, 1985. **183**(1-2): p. 379-386.

26. Zuman, P., Z. Fijalek, D. Dumanovic, and D. Suznjevic, *Polarographic and electrochemical studies of some aromatic and hetrocyclic nitro-compounds, .1. General mechanistic aspects.* Electroanalysis, 1992. **4**(8): p. 783-794.

# Chapter 5

# Generator – Collector Detection of Phosphate in Water

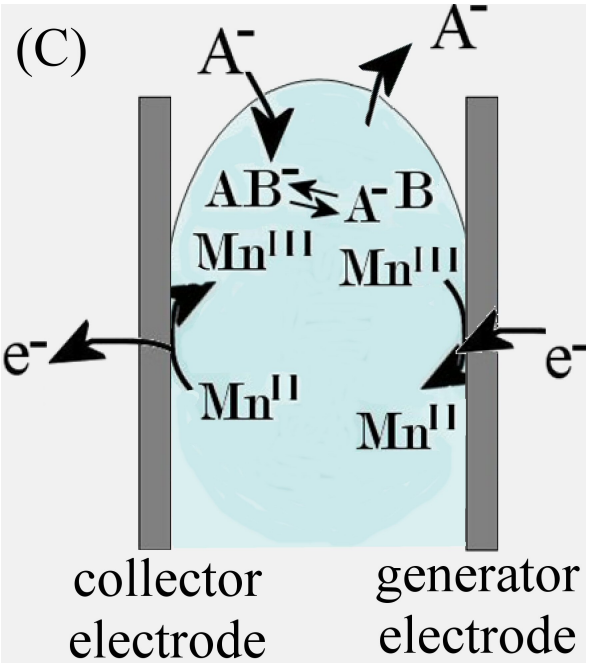


This work is published as "Oil | Water Interfacial Phosphate Transfer Facilitated by Boronic Acid: Observation of Unusually Fast Oil | Water Lateral Charge Transport" Li, M.; Lewis, G.E.M.; James, T.D.; Long, Y.T.; Kasprzyk-Hordern, B.; Mitchels, J.M.; Marken, F., *ChemElectroChem* 1 (2014) 1640-1646

# Abstract

Phosphates are important analytical targets for water quality monitoring, and have been extensively detected using electrochemical methods. This chapter explores bipotentiostatically controlled anion transfer across a liquid | liquid interface for future sensing applications. Electrochemically driven anion transfer, by the tetraphenylporphyrinato manganese(II/III) (or TPPMn) redox system, for highly hydrophilic phosphate anions and hydroxide anions into a water-immiscible organic phase, 3-(4-phenylpropyl)-pyridine (or PPP), with a hydrophobic oil-based boronic acid facilitator ((3-(1,3-dioxo-6-propylamino-1H-benzo[de]isoquinolin-2(3H)-yl)phenyl) boronic acid) is described. Experiments carried out with micro-droplet deposits on graphite (transient) show that phosphate transfer is boronic acid facilitated with a switch in mechanism at pH 7.5 from phosphate transfer (acidic pH) to hydroxide transfer (alkaline pH). This is further confirmed at the gold-gold dual-plate oil filled micro-trench electrode, where close to steady state currents are observed.



# Acknowledgment

The work illustrated in this chapter was a research project by fellow PhD student Meng Li, where I was asked to conduct the generator-collector experiments and analyse the results. I would like to thank Meng Li for the opportunity of this exciting collaboration.

# Contents

## 5.1 Introduction

Phosphates are prevalent in surface waters with surplus levels leading to excessive algae growth and a reduction in water quality [1]. Fertilisers are the main source of phosphates in the environment, as phosphorus is an essential nutrient for living cells, but they can also be introduced through detergents and pesticides. As an important analytical target for water quality monitoring [1], reliable and sensitive detection of phosphates in real-time is fundamental. Current methods involve colorimetric probes [2] (current laboratory standard), luminescence probes [3-5], fluorescence lifetime analysis [6], poly-amino-phenolic zinc receptors [7], or gravimetric probes [8]. Electrochemical techniques have been investigated and reviewed by Villalba [9] and Engbolm [10] but seen to suffer from poor selectivity and durability. Phosphate is particularly difficult to detect, as it is electrochemically inert and highly hydrophilic, but recent methods based on polymer-ferrocene derivatives [11], at zirconia modified screen printed electrodes [12], with molybdate-based sensor films [13], and by voltammetric ion-channel measurements [14] have been reported.

The transfer of ions at liquid|liquid interfaces using electrochemical methods is well known and has been studied for many years [15], including the transfer of phosphates with calixarene derivatives [16] or hexamolybdate heteropolyanion facilitators [17]. A more recent experimental approach for electrochemically driven ion transfer is the triple phase boundary [18], organic liquid | aqueous electrolyte | electrode, based on micro-droplet deposits [19, 20], and has been applied for the detection of highly hydrophilic anions such as chromate [21], carbonate [22], and fluoride [23]. It is most commonly assembled from a redox active micro-droplet deposit (water-immiscible liquid), such as

N,N,N',N'-tetrahexyl-phenelyne-diamine [20] and 4-(3-phenylprophyl)-pyridine [24] placed on a suitable electrode surface and immersed into aqueous electrolyte [25].

Figure 5.1A illustrates the anion A- transfer across a liquid | liquid interface to maintain charge neutrality upon the oxidation of Mn(II) to $Mn(III)^{+}$. In order to detect a selected anion (Figure 5.1B), a facilitator is required to aid anion transfer, such as a highly hydrophobic boronic acid (Figure 5.1C).

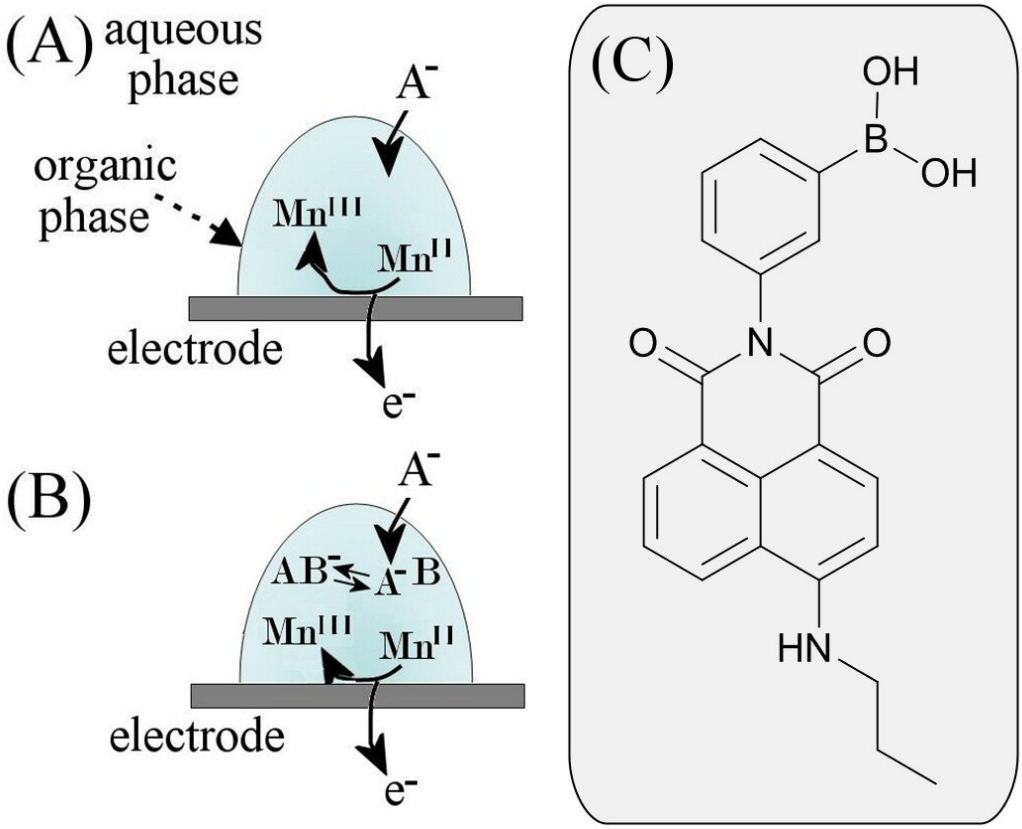


**Figure 5.1** Schematic representation of (A) an oil microdroplet with Mn(III/II) redox system allows anion transfer to be driven by oxidation. (B) In the presence of the facilitator B a complex $AB^{-}$ is formed to aid anion transfer. (C) Molecular structure of the hydrophobic boronic acid ((3-(1,3-dioxo-6-propylamino-1H-benzo[de]-isoquinolin-2(3H)-yl)phenyl)boronic acid).

As demonstrated in previous chapters, the use of a second sensor probe (in generator-collector mode) provides enhanced sensor current responses and introduces steady state characteristics. Liquid | liquid interfaces with bipotentiostatically controlled ion transfer is still a fairly new technique, where the water immiscible redox liquid is placed into the gap between two electrodes [26-28]. Following on from the success of the dual-plate electrode, the oil micro-trench methodology has been introduced [26].

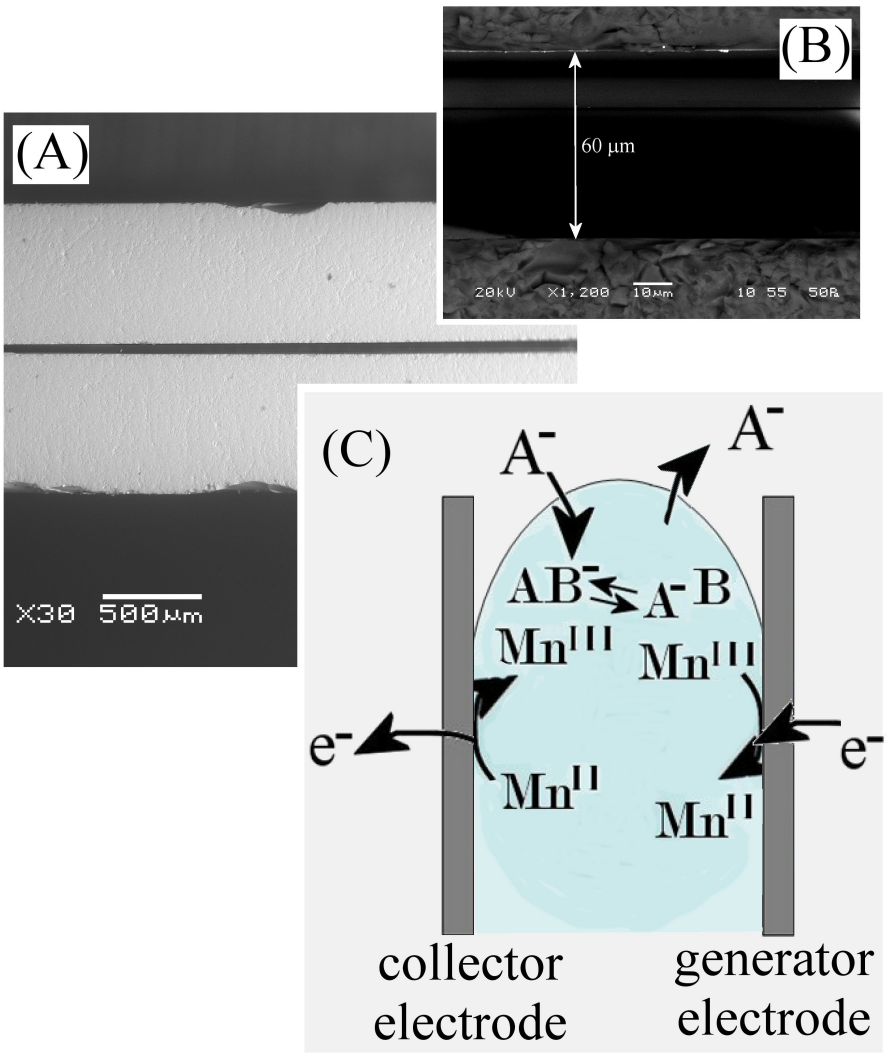


**Figure 5.2** (A) SEM image of the gold-gold dual-plate microtrench electrode. (B) SEM image showing the trench width. (C) Schematic representation of the coupled anode and cathode reaction in generator-collector mode.

The oil micro-droplet is placed into the trench (width 60 μm, length 5 mm, and trench depth 300 μm, see Figure 5.2A and 5.2B), and the corresponding triple phase boundary reaction zones are shown schematically in Figure 5.2C. Oxidation at the collector electrode will result in a positive charge upon the organic phase and the simultaneous transfer of anions from the aqueous phase into the organic phase. Rapid transport of the ions across the inter-electrode gap will then drive the reduction at the generator electrode and the corresponding anion expulsion back into the aqueous phase. This movement of ions between the two electrodes (feedback mechanism) generates an increase in current that can subsequently be measured.

For a homogeneous redox system the magnitude of the generator-collector signal, $I_{lim}$, is inversely proportional to the inter-electrode gap, δ, and proportional to the apparent diffusion coefficient, $D_{app}$, and concentration, $c_0$, (equation 5.1).

$$I_{lim} = \frac{FD_{app}Ac_0}{\delta} \qquad (5.1)$$

In this equation $F$ is the Faraday constant, $A$ is the electrode area, and $D_{app}$ is a composite parameter containing contributions from both oxidised and reduced states of the redox system [29] as well as possible contributions from Dahms-Ruff "hopping" of charges [30] at higher concentrations of the redox system.

In this chapter the gold-gold dual-plate micro-trench electrode (as seen in chapter 4) is used for electrochemically driven phosphate transfer at a triple phase boundary using a boronic acid facilitator.

## 5.2 Experimental Details

### 5.2.1 Chemical Reagents

5,10,15,20-tetraphenyl-21H,23H-porphine manganese(III) chloride (TPPMn(III)Cl), 4-(3-phenylpropyl)-pyridine, $NaClO_4$, and NaOH were purchased from Sigma Aldrich UK, and used without further purification. The boronic acid (see Figure 1C) was synthesized following literature methods [31, 32]. Demineralised and filtered water was taken from a Vivendi water purification system with not less than 18 MΩ cm resistivity at 22 $^oC$.

### 5.2.2 Instrumentation

Generator – collector voltammetric measurements were performed using an Autolab PGSTAT30 bipotentiostat with GPES software. The GPES software allows bipotentiostatic cyclic voltammetry experiments to be designed for paired electrode systems with simultaneous current read out at both electrodes. A conventional four-electrode cell with a saturated calomel (SCE, Radiometer) reference electrode, platinum gauze counter electrode and a gold-gold dual-plate micro-trench working electrode was used. All experiments were conducted at 22 ± 2$^oC$ and solutions were de-aerated with argon (BOC). Scanning electron microscopy (SEM) images were obtained on a JEOL SEM6480LV and atomic force microscopy (AFM) was performed with a Veeco Multimode Nanoscope III.

The micro-trench electrode was produced fabricated using a literature method where two gold-coated glass slides were assembled vis-à-vis using epoxy, with dimensions of 5 mm length, 60 μm width (SEM), and ca. 300 μm depth (measured by voltammetry with the $Fe(CN)_6^{3-/4-}$ calibration redox system [33]).

### 5.2.3 Formation of Micro-droplet Coatings and Fillings

Solutions of 4-(3-phenylpropyl)-pyridine (PPP) in acetonitrile with either (i) tetraphenylporphinato manganese(III) chloride MnTPPCl or (ii) boronic acid were prepared with 4 mg MnTPPCl/boronic acid and 80 mg PPP in 10 mL of acetonitrile. The two solutions (i) and (ii) were mixed and a volume of 5-10 μL of was deposited onto the basal plane pyrolytic graphite surface. After evaporation of the acetonitrile, a micro-droplet of approximately 80 nL PPP containing MnTPPCl and boronic acid remained. Microtrench filling was achieved by repeated evaporation of acetonitrile solution and gently wiping off excess organic phase from the microtrench surface. For each experiment, the electrode is rinsed and the microdroplet is renewed.

### 5.2.4 Voltammetry Conditions

To investigate the effect of boronic acid for the transfer of phosphate anions, cyclic voltammetry is used with a conventional 3-electrode cell set-up, where the working electrode is a graphite electrode and the supporting electrolyte is phosphate buffer solution at various concentration and pH 3 different concentrations of phosphate buffer solution were used, 0.01 M, 0.1 M and 1 M, at pH values of 4.5, 7 and 9.5. All scans are carried out at 50 $mVs^{-1}$ (chosen from preliminary scan rate studies) as it gave a clear peak current signal and the potential window is scanned negatively from 0.5 V to -0.7 V vs. SCE on the forward scan and then positively back to 0.5 V vs. SCE on the reverse scan.

For generator-collector cyclic voltammetry a 4-electrode cell set-up is used with a gold-gold dual-plate micro-trench electrode where the collector potential is held at 0.5 V vs. SCE. The supporting electrolyte used is 0.1M phosphate buffer at pH 4.5 and 9.5 and

initial experiments show that 10 $mVs^{-1}$ gave a clear peak current signal, so further experiments were conducted at this scan rate. The potential window varied given the pH of the solution; at pH 4.5 the start potential is 0.5 V vs. SCE and the switch potential is -0.4 V vs. SCE, but at pH 9.5 the potential window is extended to -0.8 V vs. SCE.

## 5.3 Results and Discussion

### 5.3.1 The Effect of Boronic Acid on the Transfer of Phosphate Anions

#### I: Transient Voltammetry

A graphite electrode with a microdroplet deposit of MnTPP and PPP immersed into aqueous 0.1 M $NaH_2PO_4$ (pH 4.5), gave a strong reduction signal observed at ca. 0.13 V vs. SCE (Figure 5.3A(i)). The reduction process is reversible exhibiting a corresponding oxidation signal and a midpoint potential, $E_{mid} = \frac{E_p^{ox} + E_p^{red}}{2}$, of 0.11 V vs. SCE. This electrochemical activity can be associated with anions (probably $H_2PO_4^-$ in this case) transferring into the oil phase to maintain charge neutrality. At pH 4.5 it is expected that $H_2PO_4^-$ is the transferring anion in the solution of pH 4.5 from the $pk_a$ values for each phosphate anion.

| Phosphate anion | $pK_a$ value |
|---|---|
| $H_2PO_4^-$ | 2.12 |
| $HPO_4^{2-}$ | 7.21 |
| $PO_4^{3-}$ | 12.67 |

**Table 5.1** $pK_a$ values of each phosphate anion.

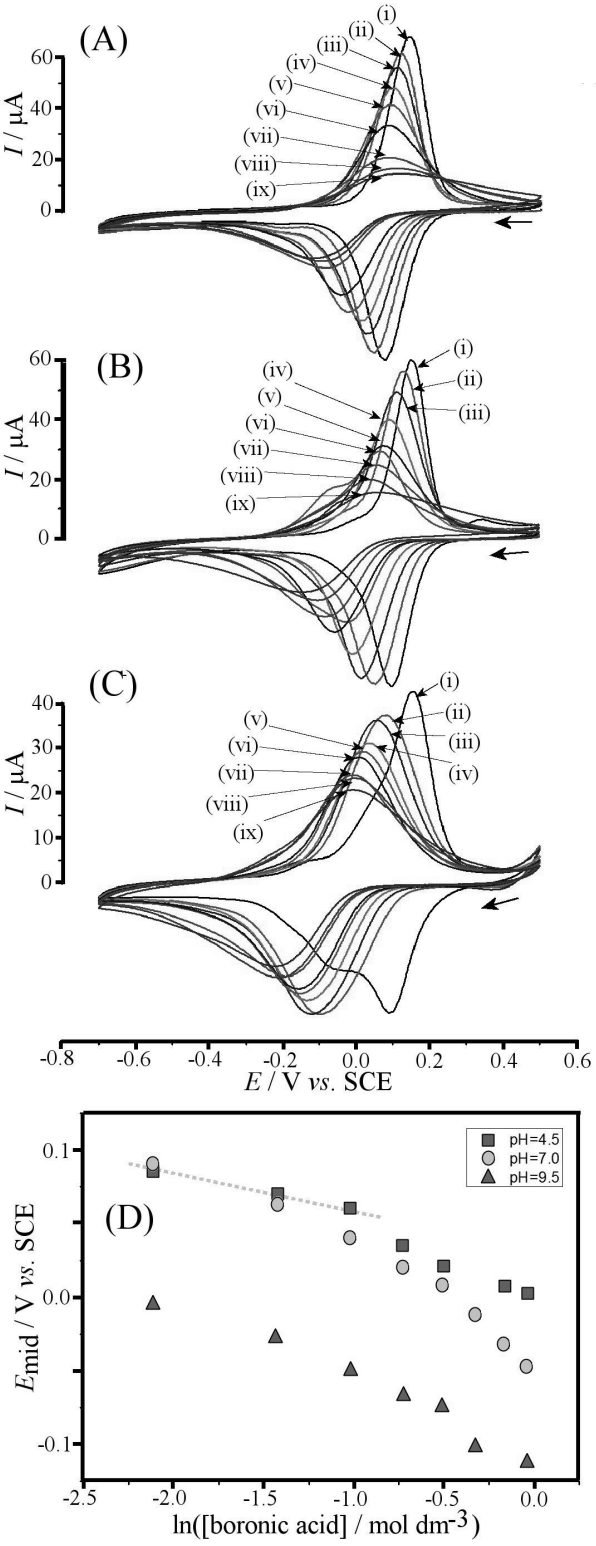


**Figure 5.3** (A) Cyclic voltammograms (scan rate 50 mV $s^{-1}$) for 56 mM TPPMn in PPP on graphite immersed in 0.1 M $NaH_2PO_4$ pH 4.5 with (i) 0.0, (ii) 0.12, (iii) 0.24, (iv) 0.36, (v) 0.48, (vi) 0.60, (vii) 0.72, (viii) 0.84, (ix) 0.96 M boronic acid. (B) As above, but at pH 7.0. (C) As above, but in 0.1 M $Na_2HPO_4$ pH 9.5. (D) Plot of $E_{mid}$ potentials versus boronic acid concentrations for pH= 4.5, 7.0, 9.5. The dashed line indicates the theoretical trend for a binding constant $K$ = 20 $mol^{-1}$ $dm^3$.

The use of boronic acid as a facilitator for anion transfer was investigated next, with figure 5.3A displaying voltammetric responses for 0.12 M additions of boronic acid. As the concentration is increased, the reduction and oxidation peak currents decrease and appear to be broadening, shifting the mid-point potential, $E_{mid}$, to more negative values. This shift in $E_{mid}$ is indicative of an easier oxidation/anion transfer attributed to the boronic acid complexing the anion in the organic phase, (figure 5.3D), assumed to be a 1:1 phosphate:boronic acid complex (equation 5.2). The nature of this complex is covalent bonding between the electrophilic boronic acid and the phosphate nucleophile.

$$Mn\ (II)_{(oil)} + B_{(oil)} + A^-_{(aq)} \rightleftharpoons Mn\ (III)^+_{(oil)} + AB^-_{(oil)} \qquad (5.2)$$

A paper by Katif *et. al* suggests an estimated binding constant of $K = \frac{[AB^-(oil)]}{[A^-(oil)][B(oil)]}$ = 20 $mol^{-1}$ $dm^3$ (see dashed line in Figure 5.3D) for this complex using a theoretical model [34] indicating relatively weak binding. However the trend in $E_{mid}$ values, (Figure 4D) observes stronger binding with increased boronic acid concentrations, proposing a 1:2 phosphate:boronic acid complex. The boronic acid facilitation effects and stronger binding at higher concentrations are also seen when the experiments are performed at pH 7 (see Figure 5.3B).

Experiments performed at pH 9.5, give similar voltammetric responses (Figure 5.3C) but show a slight deviation in the plot of $E_{mid}$ potentials (shifted more negative, see Figure 5.3D) compared to pH 4.5 and pH 7. To understand this effect, experiments with a fixed boronic acid concentration of 3.6 M but with varying pH were carried out, (Figure 5.4).

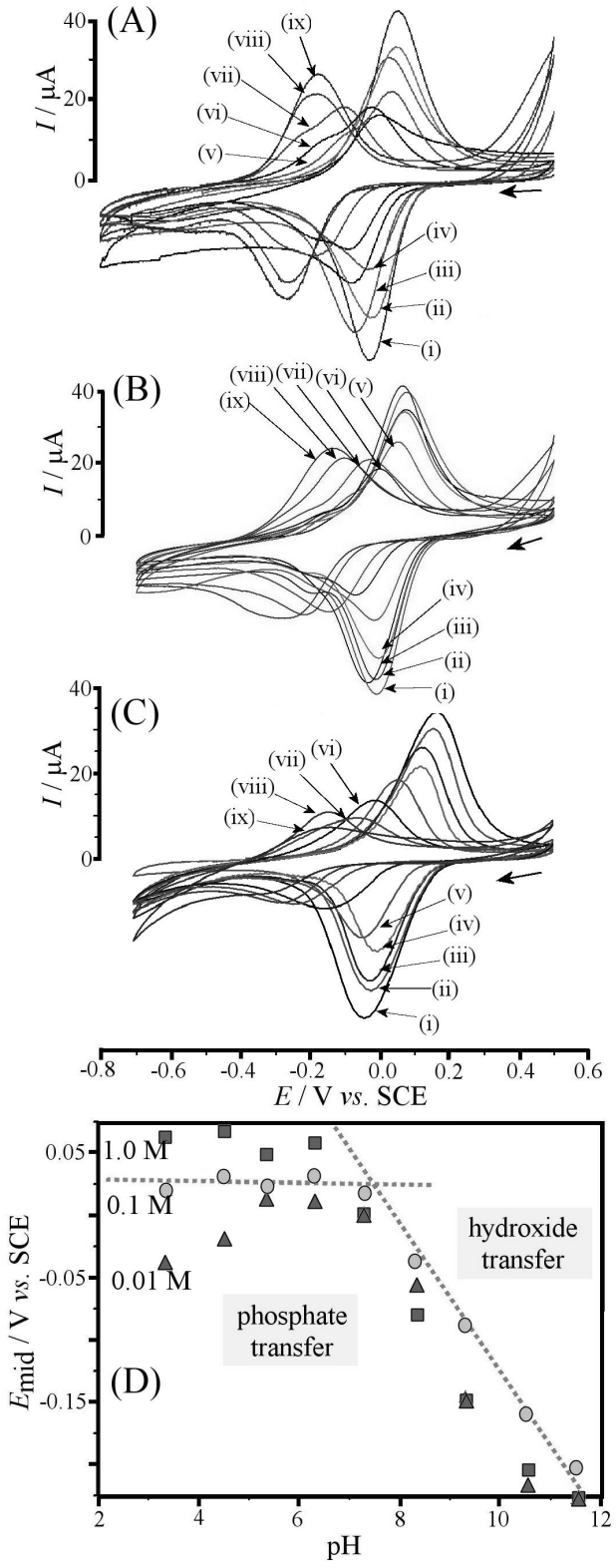


**Figure 5.4** (A) Cyclic voltammograms (scan rate 50 mV $s^{-1}$) for 64 mM TPPMn with 0.36 M boronic acid in PPP on graphite immersed in 1.0 M phosphate buffer at pH = (i) 3.4, (ii) 4.2, (iii) 5.3, (iv) 6.2, (v) 7.2, (vi) 8.3, (vii) 9.3, (viii) 10.5, (ix) 11.5. (B) As before for 0.1 M phosphate buffer. (C) As before for 0.01 M phosphate buffer. (D) Plot of $E_{mid}$ potentials *versus* pH.

Experiments conducted in 1.0 M phosphate buffer at varying pH give well-defined reversible reduction responses (figure 5.4A) and consistent midpoint potential values (plot of $E_{mid}$ values versus pH, Figure 5.4D) in the acidic pH range, characteristic of phosphate anion transfer (equation 5.2). However, in the alkaline pH range a smaller and slighter broader voltammetric peak is observed, and a switch in mechanism at pH 7.5 can also be seen in the plot of $E_{mid}$ values versus pH (Figure 5.4D), with a pH-dependent process in the alkaline pH region. This Nernstian slope of approximately -59 mV per pH unit suggests the transfer of either protons (expulsion) or hydroxide (uptake) during oxidation of MnTPP; tentatively assigned here to hydroxide uptake (equation 5.3).

$$Mn(II)_{(oil)} + B_{(oil)} + OH^-_{(aq)} \rightleftharpoons Mn(III)^+_{(oil)} + HOB^-_{(oil)} \quad (5.3)$$

Similar trends were observed for 0.1 M and 0.01 M phosphate buffer solutions, with an increase in peak-to-peak separation and decrease in peak current at lower supporting electrolyte.

### 5.3.2 The Effect of Boronic Acid on the Transfer of Phosphate Anions II: Steady State Voltammetry

A gold-gold dual-plate microtrench electrode (ca. 60 μm width, 5 mm length, and ca. 300 μm depth) is filled with oil phase (ca. 90 nL) and immersed into aqueous solution. Bipotentiostatically controlled experiments are conducted to further understand the phosphate transfer mechanism and steady state conditions for sensing.

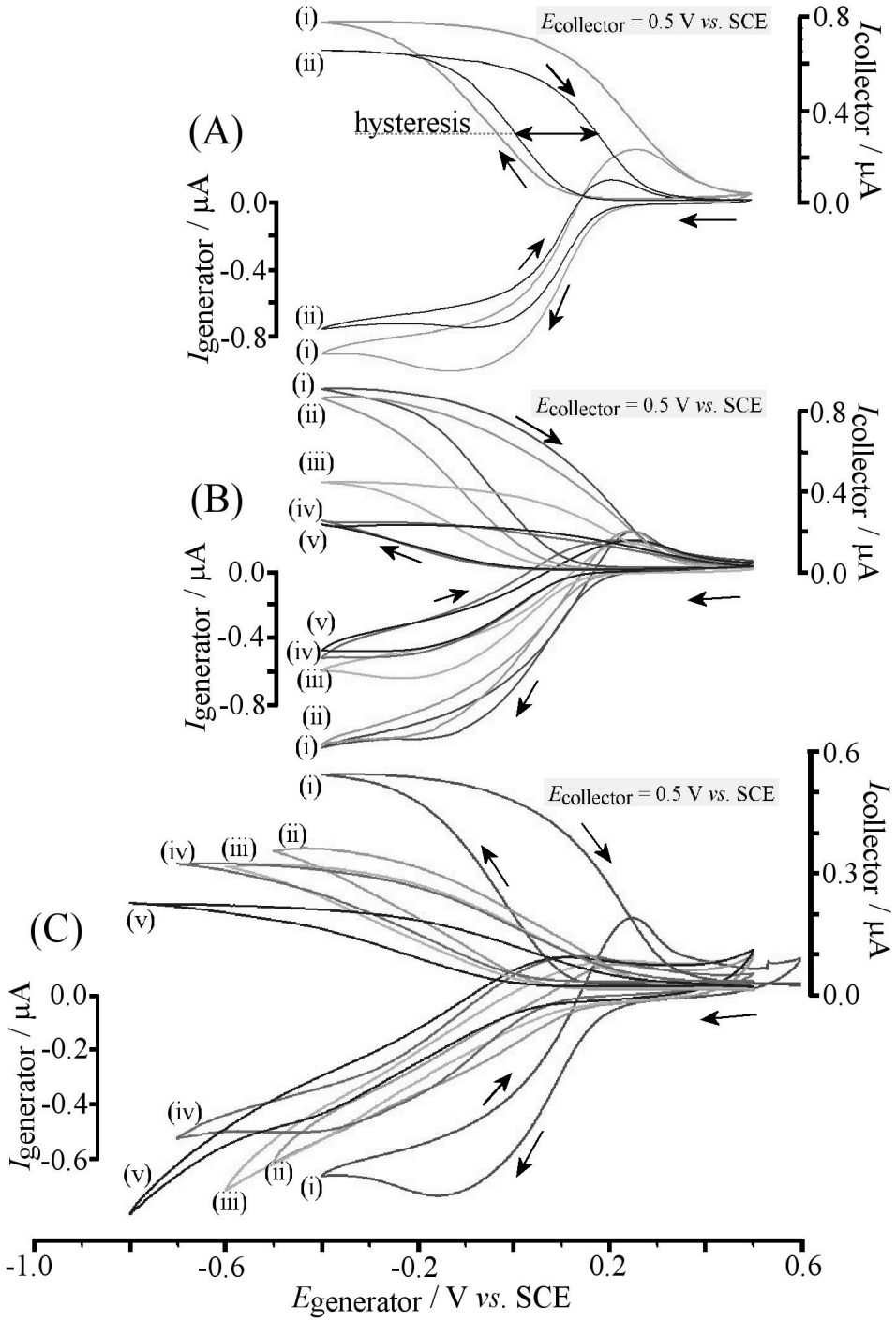


**Figure 5.5** (A) Generator and collector currents for cyclic voltammograms (scan rate (i) 20 mV $s^{-1}$ and (ii) 10 mV $s^{-1}$) for 65 mM TPPMn in PPP in a microtrench immersed in 0.1 M $NaH_2PO_4$ pH 4.5. The collector hysteresis effect is indicated. (B) Generator and collector currents for cyclic voltammograms (scan rate 10 mV $s^{-1}$) for 65 mM TPPMn in PPP immersed in 0.1 M $NaH_2PO_4$ pH 4.5 with (i) 0.0, (ii) 0.19, (iii) 0.37, (iv) 0.56, (v) 0.75 M boronic acid. (C) As before, but at pH 9.5.

Figure 5.5A shows a typical voltammogram with generator (reduction) and collector (oxidation) signals, coupled with anion uptake and expulsion. The collector electrode is held at a fixed potential, $E_{collector}$ of 0.5 V vs. SCE and the potential of the generator electrode, $E_{generato,r}$ is scanning, generating a mass transport controlled limiting current indicative of a rapid feedback process for Mn(III)/Mn(II). The apparent rate of diffusion can be assumed, given the hysteresis, $\Delta E_H$ of the collector current (indicated in Figure 5.5A), by equation 5.4 where $\Delta E_H$ is given by the scan rate $v$, the inter-electrode gap δ, the Faraday constant $F$, the apparent diffusion coefficient $D_{app}$, gas constant $R$, and absolute temperature $T$.

$$\Delta E_H = 0.0071 \times \frac{v\delta^2 F}{D_{app} RT} \qquad (5.4)$$

Figure 5.5A exhibits a $\Delta E_H$ of 0.1 V, resulting in an estimation of the apparent diffusion coefficient as $D_{app} = 10^{-10}$ m$^2$ s$^{-1}$. This value enables the calculation of the "active" trench depth (seen in chapter 4, equation 4.11), calculated at 13 μm. The $D_{app}$ value seems quite high given the viscous nature of the oil and size of molecular species involved, perhaps due to contributions from other transport mechanisms than the one under investigation. Also noteworthy is the small "active" trench depth, suggesting that only a thin layer of oil deposited at the top of the microtrench is "active" for the anion/electron transport, providing a shorter pathway for charge transfer.

Comparing data for pH 4.5 (Figure 5.5B) and pH 9.5 (Figure 5.5C) shows that phosphate transfer contributes a higher hysteresis (slower diffusion) compared to hydroxide transfer but both have similar limiting currents. Figure 5.5B (pH 4.5) also

shows a decrease in the collector limiting current with additions of boronic acid into the oil phase, which could be associated with the increase in viscosity when compared to the shape and peak current of the voltammogram in Figure 5.3A. The limiting current for hydroxide transfer (Figure 5.5C) also decreases with boronic acid additions yet the collector hysteresis remain constant, possibly due to a smaller change in $D_{app}$ and/or a change in reaction layer depth.

The focus of this chapter was to study the effect of boronic acid as a facilitator for phosphate anion transfer with an aim of applying the method to a generator-collector electrode. The results are promising but further work on reproducibility would need to be conducted. The reproducibility of the gold-gold dual-plate micro-trench electrode would need to be consider as well as the reproducibility between different micro-trench electrodes. Errors may occur if the electrodes exhibit a change in the inter-electrode gap size or the trench depth, quite possibly resulting in an increase or decrease in peak current and therefore sensitivity. Some imprecision error from the deposition of the microdroplet may have occurred in these experiments but with the extremely small volumes and high concentrations used, the errors would be negligible, but must be considered when working at lower concentrations.

## 5.4 Summary and Conclusion

The use of an oil filled gold-gold dual-plate microtrench electrode for the study of phosphate anion transfer, $H_2PO_4^-$, at the triple phase boundary reaction zone has been demonstrated. Boronic acid facilitator enables a more selective process, amplified in a steady state sensing configuration. The binding of boronic acid to phosphate after transfer from water to the oil phase is demonstrated to be weak concluded by observing a switch from phosphate transfer to hydroxide transfer. Information about electronic/ionic transport processes within the oil phase suggests unusually fast transport pathways based on viscosity and molecular diffusion. This preliminary data shows complex mechanistic and transport details, however phosphate ion transfer with steady state currents at high concentration and low pH (down to 4.5) has been achieved.

For further method development more insight should be gained about the effect of phosphate concentration on the anion transfer and transport in the microtrench, and effects of potential interferences. As a technology for environmental sensing of phosphates, experimental data with detection limits of low parts per millions to parts ber billion will need to be achieved to meet current analytical techniques. A boronic acid with a bi- or tri-dentate ligand would enable stronger binding to phosphate. The binding also needs to be selective towards phosphate and a multi-boronic acid fitting exactly around phosphate would be likely to work.

Improvements towards (i) stronger binding of the phosphate to the boronic acid, (ii) smaller inter-electrode distance (nano-gap) to increase the sensor current, and (iii) long-term water resistant oil phase for extended use would be greatly beneficial for development of robust sensor technology.

## 5.5 References

1. Warwick, C., A. Guerreiro, and A. Soares, *Sensing and analysis of soluble phosphates in environmental samples: A review.* Biosensors & Bioelectronics, 2013. **41**: p. 1-11.

2. Warwick, C., A. Guerreiro, A. Gomez-Caballero, E. Wood, J. Kitson, J. Robinson, and A. Soares, *Conductance based sensing and analysis of soluble phosphates in wastewater.* Biosensors & Bioelectronics, 2014. **52**: p. 173-179.

3. Bai, J.-M., L. Zhang, R.-P. Liang, and J.-D. Qiu, *Graphene Quantum Dots Combined with Europium Ions as Photoluminescent Probes for Phosphate Sensing.* Chemistry-a European Journal, 2013. **19**(12): p. 3822-3826.

4. Zheng, Z.-B., Y.-Q. Wu, K.-Z. Wang, and F. Li, *pH luminescence switching, dihydrogen phosphate sensing, and cellular uptake of a heterobimetallic ruthenium(II)-rhenium(I) complex.* Dalton Transactions, 2014. **43**(8): p. 3273-3284.

5. Massue, J., S.J. Quinn, and T. Gunnlaugsson, *Lanthanide luminescent displacement assays: The sensing of phosphate anions using Eu(III)-cyclen-conjugated gold nanoparticles in aqueous solution.* Journal of the American Chemical Society, 2008. **130**(22): p. 6900-6901.

6. Paredes, J.M., M.D. Giron, M.J. Ruedas-Rama, A. Orte, L. Crovetto, E.M. Talavera, R. Salto, and J.M. Alvarez-Pez, *Real-Time Phosphate Sensing in Living Cells using Fluorescence Lifetime Imaging Microscopy (FLIM).* Journal of Physical Chemistry B, 2013. **117**(27): p. 8143-8149.

7. Ambrosi, G., M. Formica, V. Fusi, L. Giorgi, A. Guerri, E. Macedi, M. Micheloni, P. Paoli, R. Pontellini, and P. Rossi, *Phosphates Sensing: Two Polyamino-Phenolic Zinc Receptors Able to Discriminate and Signal Phosphates in Water.* Inorganic Chemistry, 2009. **48**(13): p. 5901-5912.

8. Rodrigues, J.M.M., A.S.F. Farinha, P.V. Muteto, S.M. Woranovicz-Barreira, F.A. Almeida Paz, M.G.P.M.S. Neves, J.A.S. Cavaleiro, A.C. Tome, M.T.S.R. Gomes, J.L. Sessler, and J.P.C. Tome, *New porphyrin derivatives for phosphate anion sensing in both organic and aqueous media.* Chemical Communications, 2014. **50**(11): p. 1359-1361.

9. Villalba, M.M., K.J. McKeegan, D.H. Vaughan, M.F. Cardosi, and J. Davis, *Bioelectroanalytical determination of phosphate: A review.* Journal of Molecular Catalysis B-Enzymatic, 2009. **59**(1-3): p. 1-8.

10. Engblom, S.O., *The phosphate sensor.* Biosensors & Bioelectronics, 1998. **13**(9): p. 981-994.

11. Karagollu, O., M. Gorur, F. Gode, B. Sennik, and F. Yilmaz, *Phosphate ion sensors based on triazole connected ferrocene moieties.* Sensors and Actuators B-Chemical, 2014. **193**: p. 788-798.

12. Cheng, W.-L., J.-L. Chang, Y.-L. Su, and J.-M. Zen, *Facile Fabrication of Zirconia Modified Screen-Printed Carbon Electrodes for Electrochemical Sensing of Phosphate.* Electroanalysis, 2013. **25**(12): p. 2605-2612.

13. Aoki, H., K. Hasegawa, K. Tohda, and Y. Umezawa, *Voltammetric detection of inorganic phosphate using ion-channel sensing with self-assembled monolayers*

*of a hydrogen bond-forming receptor.* Biosensors & Bioelectronics, 2003. **18**(2-3): p. 261-267.

14. Girault, H.H.J. and D.J. Schiffrin, *Electrochemistry of liquid-liquid interfaces.* Electroanalytical Chemistry, 1989. **15**: p. 1-141.

15. Reymond, F., H.H. Girault, and R.A. Meyers, *Encyclopedia of Analytical Chemistry*, ed. R.A. Meyers. 2000: Wiley.

16. Kivlehan, F., W.J. Mace, H.A. Moynihan, and D.W.M. Arrigan, *Study of electrochemical phosphate sensing systems: Spectrometric, potentiometric and voltammetric evaluation.* Electrochimica Acta, 2009. **54**(7): p. 1919-1924.

17. Osakai, T., S. Himeno, A. Saito, and H. Katano, *A voltammetric phosphate sensor based on heteropolyanion formation at the Nitrobenzene water interface.* Electroanalysis, 1993. **5**(3): p. 215-219.

18. Banks, C.E., T.J. Davies, R.G. Evans, G. Hignett, A.J. Wain, N.S. Lawrence, J.D. Wadhawan, F. Marken, and R.G. Compton, *Electrochemistry of immobilised redox droplets: Concepts and applications.* Physical Chemistry Chemical Physics, 2003. **5**(19): p. 4053-4069.

19. Schroder, U., R.G. Compton, F. Marken, S.D. Bull, S.G. Davies, and S. Gilmour, *Electrochemically driven ion insertion processes across liquid/liquid boundaries: Neutral versus ionic redox liquids.* Journal of Physical Chemistry B, 2001. **105**(7): p. 1344-1350.

20. Marken, F., R.D. Webster, S.D. Bull, and S.G. Davies, *Redox processes in microdroplets studied by voltammetry, microscopy, and ESR spectroscopy:*

*oxidation of N,N,N ',N '-tetrahexylphenylene diamine deposited on solid electrode surfaces and immersed in aqueous electrolyte solution.* Journal of Electroanalytical Chemistry, 1997. **437**(1-2): p. 209-218.

21. Marken, F., C.M. Hayman, and P.C.B. Page, *Chromate and dichromate electro-insertion processes into a N,N,N ',N '-tetraoctylphenylenediamine redox liquid.* Electroanalysis, 2002. **14**(3): p. 172-176.

22. Collins, A.M., J.D. Watkins, N. Katif, Y.-J. Huang, Y.-B. Jiang, T.D. James, S.D. Bull, and F. Marken, *Liquid | liquid electrochemical bicarbonate and carbonate capture facilitated by boronic acids.* Chemical Communications, 2011. **47**(43): p. 12002-12004.

23. Collins, A.M., G.J. Blanchard, and F. Marken, *Spectroelectrochemical Investigation of TPPMn(III/II)-Driven Liquid Liquid | Electrode Triple Phase Boundary Anion Transfer into 4-(3-Phenylpropyl)-Pyridine: ClO4-, CO3H-, Cl-, and F.* Electroanalysis, 2012. **24**(2): p. 246-253.

24. Marken, F., K.J. McKenzie, G. Shul, and M. Opallo, *Ion transfer processes at 4-(3-phenylpropyl)-pyridine vertical bar aqueous electrolyte | electrode triple phase boundary systems supported by graphite and by mesoporous TiO2.* Faraday Discussions, 2005. **129**: p. 219-229.

25. Marken, F., J.D. Watkins, and A.M. Collins, *Ion-transfer- and photo-electrochemistry at liquid | liquid | solid electrode triple phase boundary junctions: perspectives.* Physical Chemistry Chemical Physics, 2011. **13**(21): p. 10036-10047.

26. Dale, S.E.C., Y. Chan, P.C.B. Page, E.O. Barnes, R.G. Compton, and F. Marken, *A gold-gold oil microtrench electrode for liquid-liquid anion transfer voltammetry.* Electrophoresis, 2013. **34**(14): p. 1979-1984.

27. French, R.W., Y.H. Chan, P.C. Bulman-Page, and F. Marken, *Liquid-liquid ion transport junctions based on paired gold electrodes in generator-col lector mode.* Electrophoresis, 2009. **30**(19): p. 3361-3365.

28. Vuorema, A., H. Meadows, N. Bin Ibrahim, J. Del Campo, M. Cortina-Puig, M.Y. Vagin, A.A. Karyakin, M. Sillanpaa, and F. Marken, *Ion Transport Across Liquid | Liquid Interfacial Boundaries Monitored at Generator-Collector Electrodes.* Electroanalysis, 2010. **22**(24): p. 2889-2896.

29. Dale, S.E.C., A. Vuorema, M. Sillanpaa, J. Weber, A.J. Wain, E.O. Barnes, R.G. Compton, and F. Marken, *Nano-Litre Proton/Hydrogen Titration in a Dual-Plate Platinum-Platinum Generator-Collector Electrode Micro-Trench.* Electrochimica Acta, 2014. **125**: p. 94-100.

30. Cummings, C.Y., J.D. Wadhawan, T. Nakabayashi, M.-a. Haga, L. Rassaei, S.E.C. Dale, S. Bending, M. Pumera, S.C. Parker, and F. Marken, *Electron hopping rate measurements in ITO junctions: Charge diffusion in a layer-by-layer deposited ruthenium(II)-bis(benzimidazolyl)pyridine-phosphonate-TiO2 film.* Journal of Electroanalytical Chemistry, 2011. **657**(1-2): p. 196-201.

31. Cao, H.S., D.I. Diaz, N. DiCesare, J.R. Lakowicz, and M.D. Heagy, *Monoboronic acid sensor that displays anomalous fluorescence sensitivity to glucose.* Organic Letters, 2002. **4**(9): p. 1503-1505.

32. Chen, Z., L. Wang, G. Zou, X. Cao, Y. Wu, and P. Hu, *A retrievable and highly selective fluorescent probe for monitoring dihydrogen phosphate ions based on a naphthalimide framework.* Spectrochimica Acta Part a-Molecular and Biomolecular Spectroscopy, 2013. **114**: p. 323-329.

33. Dale, S.E.C. and F. Marken, *Pulse electroanalysis at gold-gold micro-trench electrodes: Chemical signal filtering.* Faraday Discussions, 2013. **164**: p. 349-359.

34. Katif, N., R.A. Harries, A.M. Kelly, J.S. Fossey, T.D. James, and F. Marken, *Boronic acid-facilitated alpha-hydroxy-carboxylate anion transfer at liquid/liquid electrode systems: the EICrev mechanism.* Journal of Solid State Electrochemistry, 2009. **13**(10): p. 1475-1482.

# Chapter 6

# Feedback - Amplified Dual - Plate Boron - Doped Diamond Micro - Trench Detector for Electrochemical Flow Injection

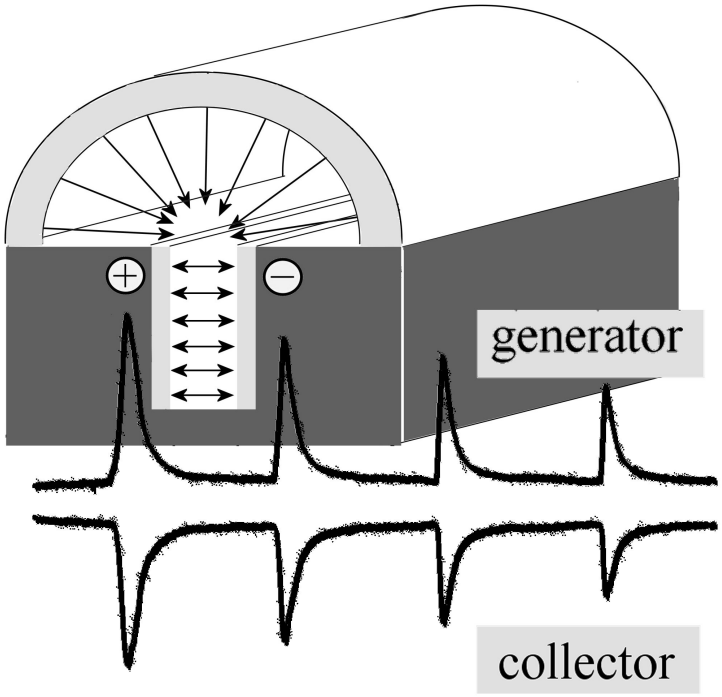


This work has been published in Electrophoresis as "Feedback-amplified electrochemical dual-plate boron-doped diamond micro-trench detector for flow injection analysis" Lewis, G.E.M.; Gross, A.J.; Kasprzyk-Hordern, B.; Lubben, A.T.; Marken, F., DOI: 10.1002/elps.201500017

# Abstract

A boron-doped diamond (BDD) dual-plate micro-trench electrode is used as a detector in a simple electrochemical flow injection cell design. The device is demonstrated by the flow injection electroanalysis of a simple redox system, hydroquinone in phosphate buffer pH 7, with the detector in generator-collector feedback mode and as a single working electrode. A key observation made is the improved sensitivity (by one order of magnitude) when using the generator-collector detector compared to the single working electrode detector. The diffusion process can be switched from an analyte consuming external process to an analyte regenerating internal process offering benefits in selectivity and sensitivity.



## Acknowledgment

I would like to thank Andrew Gross for the fabrication of the BDD-BDD dual-plate micro-trench electrodes that are used for the detector in the flow cell.

# Contents

## 6.1 Introduction

Previous chapters have shown the use of gold-gold dual-plate micro-trench electrodes for the analysis of nitrobenzene with comparison to a gold interdigitated electrode [1] and transfer of phosphate anions transfer facilitated by boronic acid in an oil filled trench [2]. These dual electrodes are readily produced with an open side to allow analyte diffusion into the inter-electrode gap, and enhance sensitivity with mass transport controlled steady state signals.

In this chapter a generator-collector detector, of the same electrode geometry, is used for flow injection analysis, but with improved production processes to generate a smaller gap between the two electrodes [3], and boron-doped diamond as the electrode material. It will be demonstrated for the electroanalysis of hydroquinone, which has a well-known oxidation pathway and is the metabolite of the environmental pollutants benzene and paracetamol. It can therefore be used as a model system for these compounds and others of similar structure.

BDD is most commonly used in the form of thin films on a silicon support, grown using chemical vapour deposition (CVD), and can be readily modified to carry out its desired function [4, 5]. It exhibits electrochemical properties valuable for the development of sensing devices in aqueous media. Its wide potential window in aqueous solutions [6] allows electrochemical measurements to be made at more positive potentials, with low background currents experienced across the potential range [7]. Analytes with high oxidation potentials can be studied as BDD offers low sensitivity to dissolved oxygen [8]. Its resistance to fouling due to weak absorption of polar substances to the surface, provides mechanical robustness for many applications [9], and gives the option to clean the electrode surface with aggressive reagents such as Piranha solution. BDD is a

material widely used for environmental applications [10-12] and BDD electrodes have been used for the analytical detection of pharmaceuticals [13] and determination of heavy metals [14].

Interest in generator-collector electrochemical flow systems, has arisen from the more common use of dual electrode detectors for liquid chromatography [15-18] and capillary electrophoresis [19-21]. Electrochemical detectors offer many advantages; they provide excellent selectivity, which is useful for more complex matrices, and have a high degree of sensitivity, with the added attraction of miniaturizing [22] the system without compromising the performance. Early designs of dual detectors for flow electrochemistry include the rotating ring-disc electrode (RRDE), extensively studied by Albery and co-workers [23, 24], closely followed by the wall jet ring-disc electrode (WJRDE) [25, 26] of similar geometry, and the double channel flow electrode [27-29] (all of which are mentioned in chapter 2).

Flow injection analysis is a common automated system where the sample analyte is injected into a stream of liquid carrier and transported to the detector, in this instance a generator-collector electrode. Micro-gap generator-collector flow-through analytical cells have been developed by Fenn and co-workers [30] and amplification effects in twin-electrode cells were investigated by many investigators including Anderson [31] and Yildiz [32]. Generator-collector flow analysis based on a dual-electrode device without amplification is also beneficial and powerful in analytical applications [33-35]. Figure 6.1 shows the BDD dual-plate micro-trench generator-collector detector in flow through mode (with reference electrode upstream and counter electrode downstream) for a simple flow injection system. The two BDD working electrodes are placed in parallel, separated by a 10 μm inter-electrode distance, with analyte flow over the top of the micro-trench. Key parameters for the operation of the detector are (i) the inter-

electrode distance δ, (ii) the trench length, and (iii) the trench depth. It is shown that all three have a direct effect on the detector sensitivity in generator-collector operational mode.

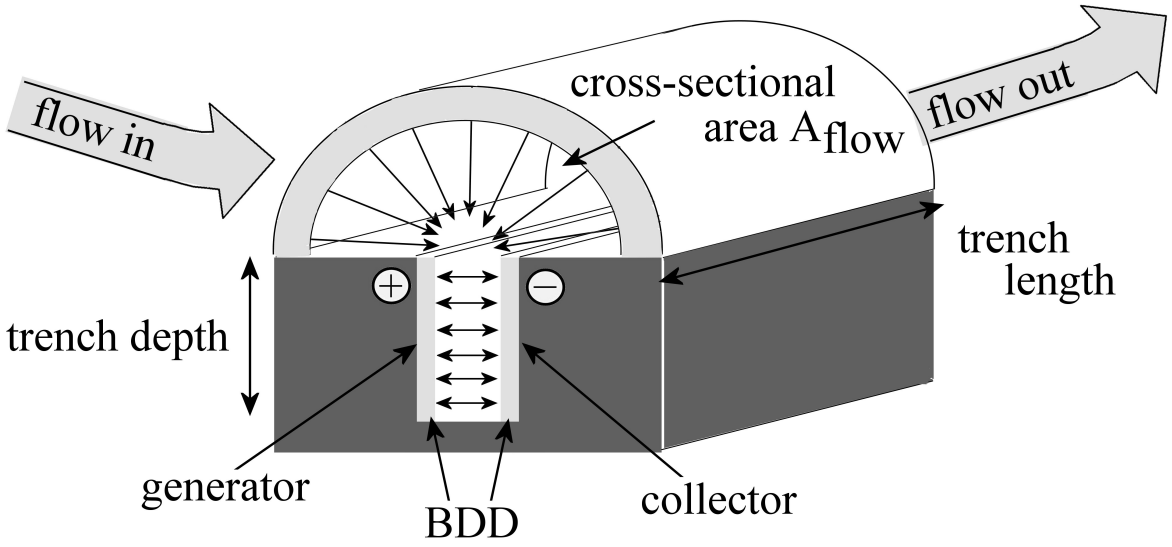


**Figure 6.1** Schematic drawing of the dual-plate BDD-BDD flow-cell trench detector with flow of analyte solution (with cross-sectional area $A_{flow}$) over the surface.

## 6.2 Experimental

### 6.2.1 Chemical Reagents

Phosphate buffer solutions were prepared from $H_3PO_4$ and NaOH. Hydroquinone, hydrogen peroxide (20 wt.% in water), sulphuric acid (≥ 95-99%) were obtained from Sigma Aldrich UK and used without further purification. Demineralised water was taken from a Thermo Scientific purification system (Barnstead Nanopure) with not less than 18 MOhm cm resistivity.

### 6.2.2 Instrumentation

A PGSTAT12 biopotentiostat system (Autolab, EcoChemie, The Netherlands) with GPES software was used for generator-collector electrochemical measurements. The GPES software allows bipotentiostatic cyclic voltammetry experiments to be designed for paired electrode systems with simultaneous current read out at both electrodes. A conventional four-electrode cell with a silver wire counter/reference electrode and a boron-doped diamond dual-plate micro-trench working electrode was utilised. All experiments were conducted at 22 ± 2$^{o}$C.

### 6.2.3 Production of BDD-BDD Dual-Plate Micro-Trench Electrodes

Boron-doped diamond dual-plate micro-trench electrodes were produced using a literature method [14]. In brief, a single layer of SU-8-2002 was spin coated onto two separate 5 mm x 20 mm BDD substrates (300 nm BDD, $SiO_2/Si_3N_4$ interlayer, 8000 ppm doping and resistivity = 10 μW cm, purchased from NeoCoat SA, Switzerland), at 500 rpm for 15s then 3000 rpm for 30s. The two electrodes were then

pushed together, vis-à-vis, and placed on a hot plate at 90°C (for 2 minutes) and ramped to 160°C for a further 5 minutes. After cooling to room temperature, the end of the dual-plate electrode was sliced off using a diamond cutter (Buehler, Isomet 1000 precision saw) and polished flat. Placing the electrode into Piranha solution (1:5 v/v $H_2O_2$:$H_2SO_4$) etched the photoresist to form a micro-trench electrode with dimensions of depth = 58 μm, length = 5 mm and inter-electrode gap, $\delta$ = 10 μm (see Figure 6.2). After etching, the micro-trench electrode was cleaned with demineralised water and conducting copper tape (RS) was applied to give two electrode contacts.

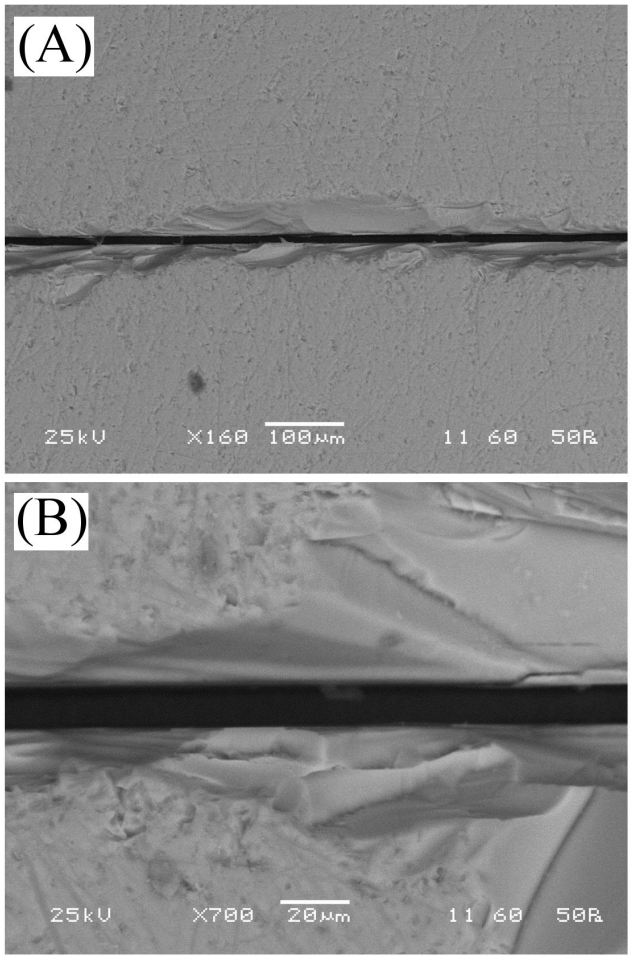


**Figure 6.2** Scanning electron micrographs with (A) lower and (B) higher magnification showing the BDD generator-collector trench with a width of typically δ = 10 μm.

### 6.2.4 Electrochemical Flow Analysis System

The electrochemical flow cell uses a 6-port 2-position switch valve to control the injection of the sample, and a syringe pump (KD Scientific Model 781100, USA) to maintain the flow of the supporting electrolyte. The injection volume was 20 μL. The BDD dual-plate detector electrode was placed between a reference electrode (upstream) and a counter electrode (downstream) with flow over the trench as shown in Figure 6.1.

### 6.2.5 Voltammetry Conditions

The BDD-BDD dual-plate micro-trench electrode is calibrated by cyclic voltammetry using a solution of 1 mM $Ru(NH_3)_6^{3+}$ in 0.1 M KCl. All voltammograms use a scan rate of 20 $mVs^{-1}$, and scan the potential window of 0.5 V to -0.6 V vs. SCE in a negative direction initially. When the biopotentiostat is set to generator-collector mode, the collector electrode is held at a potential of 0.4 V vs. SCE. To investigate the redox potential of hydroquinone at boron doped diamond electrodes, cyclic voltammograms are carried out using solutions containing different concentrations of hydroquinone and 0.1 M phosphate buffer at pH7. A range of scan rates is studied (20, 50, 100 and 200 $mVs^{-1}$) with a potential window of -0.6 V to 1.2 V vs. SCE, scanning initially in a positive direction. When the generator-collector mode is switched on, a solution of 1 mM hydroquinone in 0.1 M phosphate buffer at pH 7 is studied using a dual-plate BDD trench electrode at a scan rate of 20 $mVs^{-1}$ and collector potential of -0.4 V vs. SCE. All other conditions remain the same.

Chronoamperometry is the method of choice when studying the flow conditions with a BDD dual-plate micro-trench electrode. The applied potential is 1 V vs. SCE for all experiments and the supporting electrolyte used is 0.1 M phosphate buffer solution at

pH 7. Experiments without feedback (where only one working electrode is connected) study varying concentrations of hydroquinone (1, 0.1 and 0.01 mM) and use flow rates of 10 and 20 mL per hour. For the experiments with feedback, the collector potential is held at -0.4 V vs. SCE and the flow rate is varied from 10 to 25 mL per hour. The switch valve used for these experiments allows a constant flow of supporting electrolyte to flow through the electrode when in the "off" position. When turning the switch valve to the "on" position, a 20 μL injection of liquid containing the redox active compound is released into the flow of supporting electrolyte and a peak current is observed. After the peak current has reached it's maximum, the switch valve is turned back to the "off" position in preparation for the next injection. The next injection is made once the peak current has settled to its baseline current again.

## 6.3 Results and Discussion

### 6.3.1 Calibration of BDD-BDD Dual-Plate Micro-Trench Electrodes

A well known redox system, the reduction of 1 mM $Ru(NH_3)_6^{3+}$ in 0.1 M KCl, is employed to calibrate the depth of the trench after production (Figure 6.3). Cyclic voltammograms are obtained for each BDD working electrode by connecting just one electrode to the potentiostat at a time, see Figure 6.3A. The signals for each BDD electrode (i and ii) are similar suggesting a high quality symmetric dual-plate micro-trench electrode, and the small discrepancies in the shape are primarily due to imperfections at the edge of the trench. In generator-collector feedback mode (Figure 6.3B and 6.3C), where the collector is held at 0.4 V vs SCE, the voltammograms

obtained show the limiting current for mass transport controlled feedback to be approximately $I_{lim}$ = 2.5 μA.

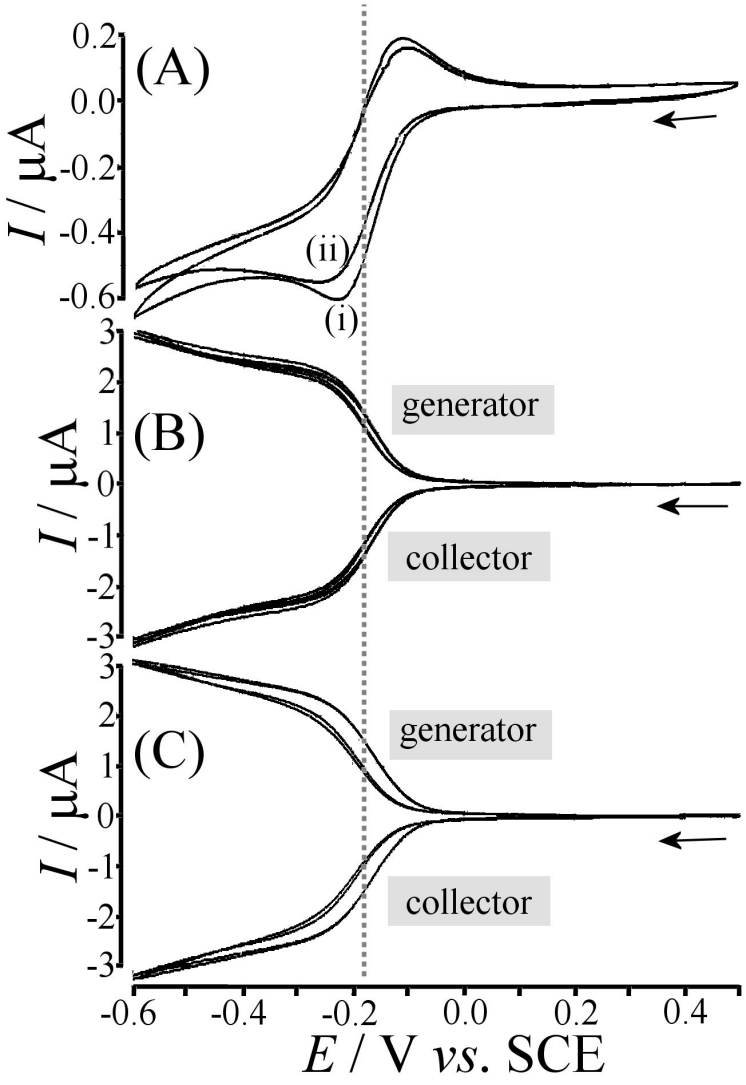


**Figure 6.3** (A) Cyclic voltammograms (scan rate 20 $mVs^{-1}$) for the reduction of 1 mM $Ru(NH_3)_6^{3+}$ in 0.1 M KCl at a dual-plate BDD electrode with only electrode 1 (i) or only electrode 2 (ii) active. Voltammograms in (B) and (C) are recorded under the same conditions with electrode 2 or electrode 1, respectively, held at 0.4 V vs. SCE in generator-collector mode.

To determine the trench depth, two assumptions must be made i) that the concentration profile is symmetrical (Nernstian [36]) and ii) the diffusion coefficients for the oxidised and reduced species are equivalent ($D_{ox} = D_{red} = D = 0.9 \times 10^{-9}$ m$^2$ s$^{-1}$, the diffusion coefficient) [37].

$$\text{depth} = \frac{I_{lim} \times \delta}{nFDc \times \text{length}} = 58\ \mu\text{m} \qquad (6.1)$$

In this equation $I_{lim}$ is the mass transport limited current, δ is the inter-electrode gap of the micro-trench as determined by electron microscopy, $D$ is the diffusion coefficient, $n$ is the number of electrons transferred per molecule diffusing to the electrode surface, $F$ is the Faraday constant, $c$ is the bulk concentration, and *length* is the overall length of the trench, 5 mm in this case. The estimated trench depth of 58 μm suggests an aspect ratio of ca. 6, which is consistent with previous reports for similar types of electrodes [38].

## 6.3.2 BDD-BDD Dual-Plate Generator-Collector Voltammetry: Hydroquinone Oxidation under Stagnant Conditions

The oxidation of hydroquinone (see equation 6.2) is used as a model redox system to explore the sensitivity of the BDD dual-plate micro-trench detector for a classical electrochemically irreversible (but chemically reversible) test system [39].

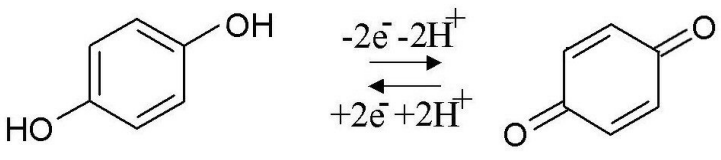


(6.2)

Figure 6.4A and 6.4B show cyclic voltammograms recorded at various scan rates at a single 5 mm × 5 mm BDD working electrode for 0.1 mM and 1.0 mM hydroquinone, respectively. The wide peak-to-peak separation highlights the relatively slow rate of electron transfer at the diamond electrode consistent with literature reports [40]. The peak currents scale with the square root of scan rate and with the hydroquinone concentration as anticipated for a diffusion-controlled peak. The midpoint potential $E_{mid}$ = ½ $E_{ox}$ + ½ $E_{red}$ is indicated by a dotted line at approximately 0.16 V vs. SCE (in phosphate buffer pH 7 [40]).

A clear generator-collector feedback voltammetric response for the oxidation of 1 mM hydroquinone (with the collector potential fixed at -0.4 V vs. SCE) is shown in Figure 6.4C. The slight increase in current can be attributed to the feedback response and the high degree of symmetry between the generated and collected currents suggests a well-defined redox process. A shift in mid-point potential is due to the irreversible nature of the electron transfer process.

To determine the diffusion coefficient, the mass transport controlled limiting current of approximately 2.8 μA, can be used (equation 6.3).

$$D = \frac{I_{lim} \times \delta}{nFc \times length \times depth} = 0.5 \times 10^{-9} m^2 s^{-1} \qquad (6.3)$$

This value is comparable to literature values for the hydroquinone diffusion coefficient [41] and confirms that the process observed here is mass transport limited and in agreement with a feedback-amplified process.

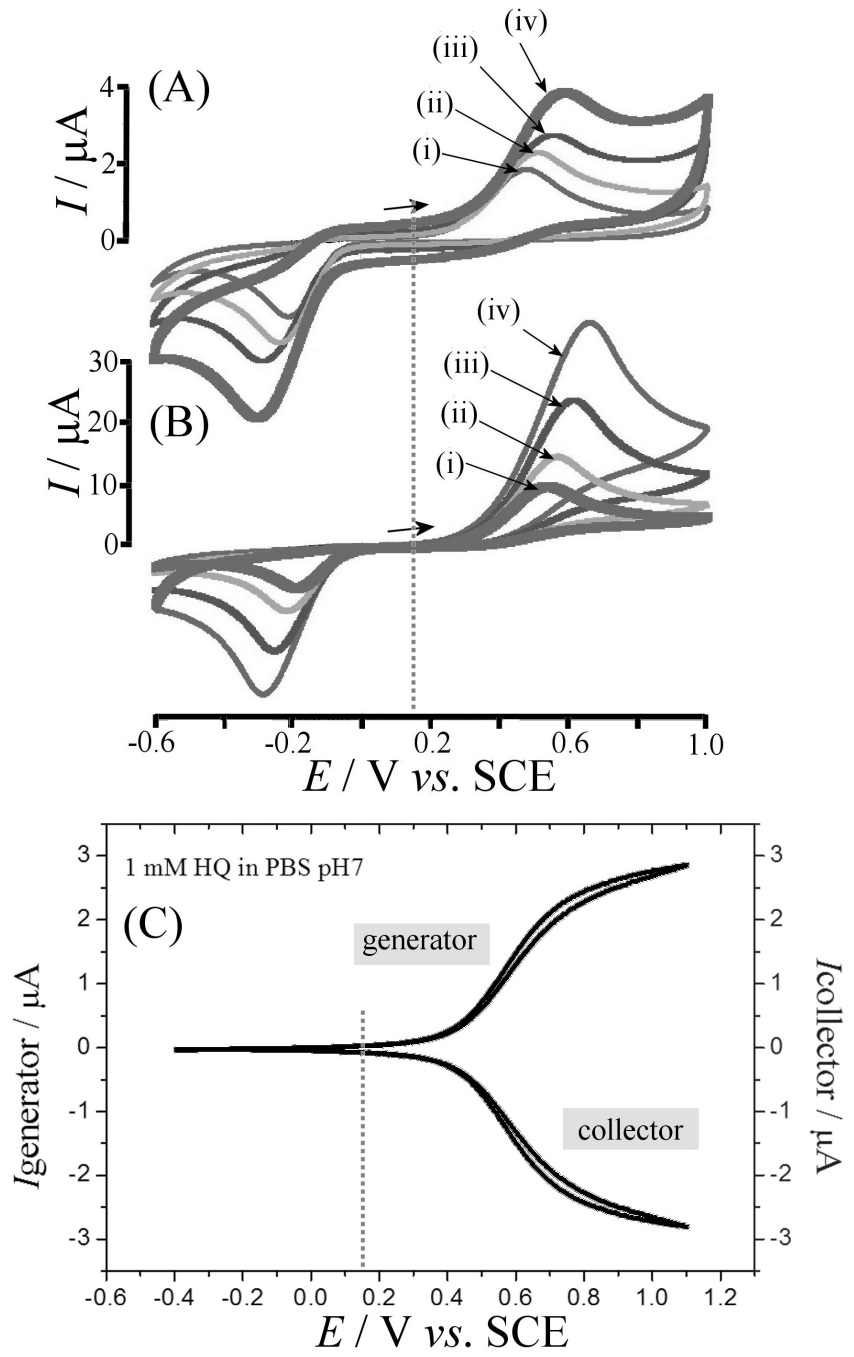


**Figure 6.4** (A, B) Cyclic voltammograms (scan rates (i) 20, (ii) 50, (iii) 100, and (iv) 200 $mVs^{-1}$) obtained at boron-doped diamond electrodes (5 mm × 5 mm active area) in 0.1 M phosphate buffer pH 7 for the oxidation of (A) 0.1 mM hydroquinone and (B) 1 mM hydroquinone. (C) Generator-collector voltammograms (scan rate 20 $mV^{s-1}$, collector potential -0.4 V vs. SCE) for the oxidation of 1 mM hydroquinone at a dual-plate BDD trench electrode immersed in 0.1 M phosphate buffer pH 7. The dotted line indicates the midpoint potential.

### 6.3.3 BDD-BDD Dual-Plate Generator-Collector Chronoamperometry I: Hydroquinone Oxidation under Flow Conditions without Feedback

Next, the oxidation of hydroquinone in 0.1 M phosphate buffer pH 7 is studied by chronoamperometry using flow conditions with a BDD dual-plate micro-trench electrode configured as shown in Figure 6.1. One of the two BDD working electrodes is active (connected to the potentiostat) and held at 1.0 V vs. SCE whilst the other electrode is inactive (not connected). At regular intervals, 20 μL injections of 1 mM hydroquinone solution are made, and clear peak currents are observed at two different flow speeds (see Figure 6.5A). The shape of peaks (in particular the width) is dependent on the flow rate of the analyte with peak broadening approximately inversely proportional to flow speed. This observation is consistent with a process where the analyte in the reservoir over the trench electrode (see Figure 6.1) is only partially consumed and diffusion towards the micro-trench (like a micro-band) dominates the detector current. Complete consumption for a 20 μL plug of liquid containing 1 mM hydroquinone would result in a peak with 3.8 mC charge. The charge under the peak for the analyte present in the liquid phase is typically 2.5 μC for a flow rate of 10 mL/h. Therefore only a very small fraction of the analyte can diffuse into the micro-trench under these conditions. From the peak duration (peak width at half height = 20 s at 2.7 $\mu Ls^{-1}$) the flow cross-sectional area for the detector can be estimated as $A_{flow} = \frac{delay\ time \times flow\ velocity}{length} = 6.8\,mm^2$ where the delay time is the peak duration, 20 s, minus the theoretical peak duration for a very short detector, 7.4 s.

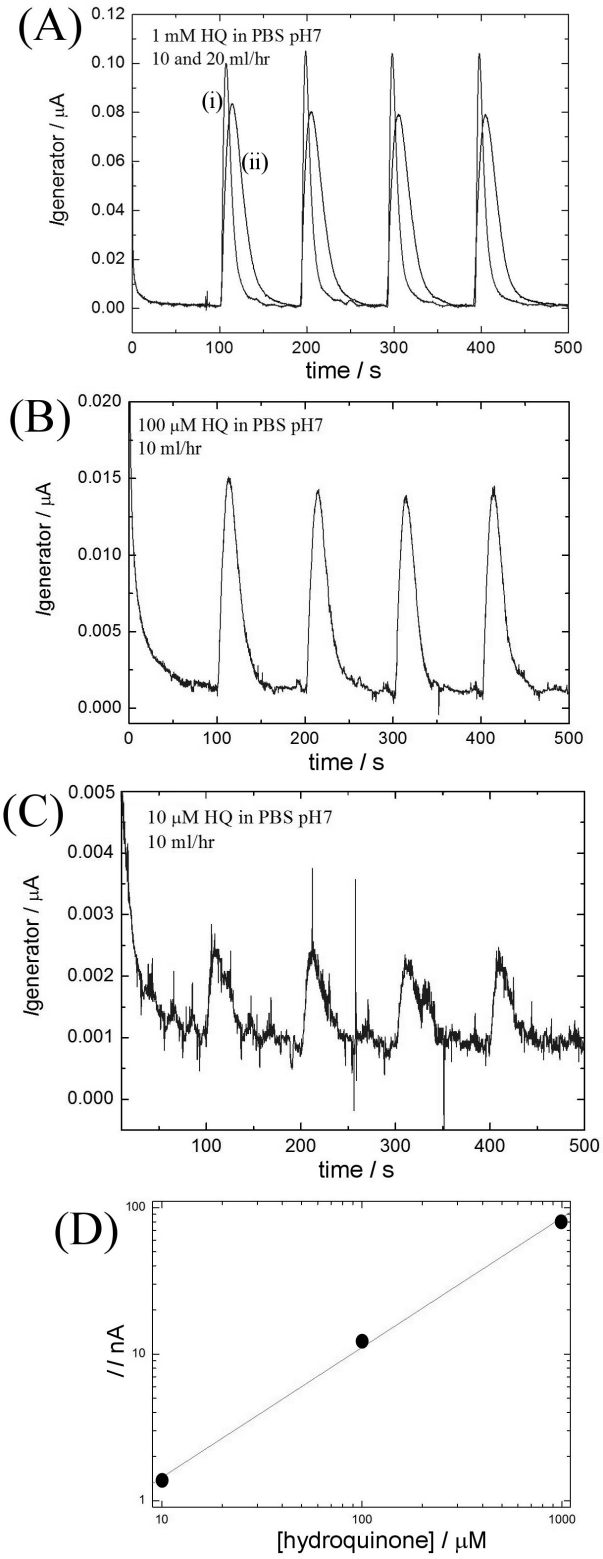


**Figure 6.5** (A) Chronoamperometry data (applied potential 1 V vs. SCE, flow rate (i) 20 mL and (ii) 10 mL per hour) obtained at a dual-plate BDD electrode with only one electrode connected in 0.1 M phosphate buffer pH 7 for the oxidation of 1 mM hydroquinone. (B) As above but for 0.1 mM hydroquinone. (C) As above, but for 0.01 mM hydroquinone. (D) Double-logarithmic plot of peak current versus hydroquinone concentration.

The effect of hydroquinone concentration is shown in Figure 6.5B and 6.5C. Well-defined peak responses for 1 mM, 100 μM, and 10 μM hydroquinone are observed and a double logarithmic plot (Figure 6.5D) shows linear dependence of hydroquinone concentration at 10 mL/h flow rate. The low concentration range signal is limited by background noise. The maximum peak current under these conditions can be related to the current towards a micro-band (here the micro-trench) as given in Equation 6.4 [1, 36, 42].

$$I_{peak,\ single\text{-}electrode} = nFD \times length \times c \times \left[ \frac{\pi e^{-2.5\sqrt{\frac{\pi Dt}{\delta^2}}}}{4\sqrt{\frac{\pi Dt}{\delta^2}}} + \frac{\pi}{\ln\left(\left[\frac{64e^{-0.577}Dt}{\delta^2}\right]^{1/2} + e^{5/3}\right)} \right] \quad (6.4)$$

In this equation *n* is the number of electrons transferred per molecule arriving in the trench, *F* is the Faraday constant, *D* is the diffusion coefficient for hydroquinone, *length* is the trench length, *c* is the (average) hydroquinone concentration, δ is the trench width, and *t* is the diffusion time. For a 10 mL/h flow rate the time between current onset and current peak is 4.4 s (see Figure 6.5A), which allows a peak current to be predicted. The calculated value 0.33 μA is approximately four times higher compared to the observed peak current for 10 mL/h flow. The main reason for this deviation is likely to be some mixing in the space over the micro-trench (see Figure 6.1) lowering the apparent concentration (*vide infra*).

Figure 6.5D does not take into consideration repeated results; the logarithmic plot is for one set of experiments (all the results seen in this chapter) using the same electrode. The newly designed electrode geometry was more fragile than previously expected and after

continuous use within the flow cell, the two boron-doped diamond electrodes started to pull away from one another. This could be attributed to the weakening of the SU-8-2002 photoresist that was used to glue the electrodes together, or from the attachment of the potentiostat connectors to the end of the BDD electrodes (the weight of each connector was possibly too heavy for the size of the BDD electrodes). The BDD-BDD dual-plate micro-trench electrodes were prone to damage during the initial production trials meaning I was unable to test the reproducibility between the electrodes that were made. If time permitted, the issues with the potentiostat connectors would be addressed and as the method for electrode production improved, further analysis would be carried out to check reproducibility between electrodes and with the same electrode for more reliable results.

### 6.3.4 BDD-BDD Dual-Plate Generator-Collector Chronoamperometry II: Hydroquinone Oxidation under Flow Conditions with Feedback

When the BDD dual-plate electrode is in generator-collector mode, both electrodes are "active", which changes the operational mode from external to internal diffusion control (diffusion within the trench rather than diffusion towards the trench) without significant consumption of the analyte in the flow space. Figure 6.6A shows current peak signals for 10 mL/h flow rate, with potentials applied to generator and collector of 1.0 V and -0.4 V vs. SCE, respectively. The peak current is amplified by an order of magnitude (compared to single electrode signals, see Figure 6.5A-C) with peak width and shape unchanged.

The magnitude of the peak current is now given by the internal mass transport which can be approximated by equation 6.5 [43].

$$I_{peak,\ dual\text{-}electrode} = \frac{nFD \times length \times depth \times c}{\delta} \qquad (6.5)$$

The anticipated peak current is 2.8 μA (see Figure 6.4C), which is approximately twice the experimental value (see Figure 6.6A). This discrepancy is likely to be associated with the lower apparent concentration in the trench (as well as in the space over the trench) at the time of the peak due to non-ideal flow of analyte (no ideal plug flow and some degree of mixing in the space over the micro-trench detector). Further evidence for this is obtained by changing the flow rate. In Figure 6.6B data for increased analyte flow rate are presented and the peak current can be seen to further decrease approximately inversely proportional to the flow rate. Therefore future improvements in the detector current signal are possible at lower flow rate and with more ideal flow geometry.

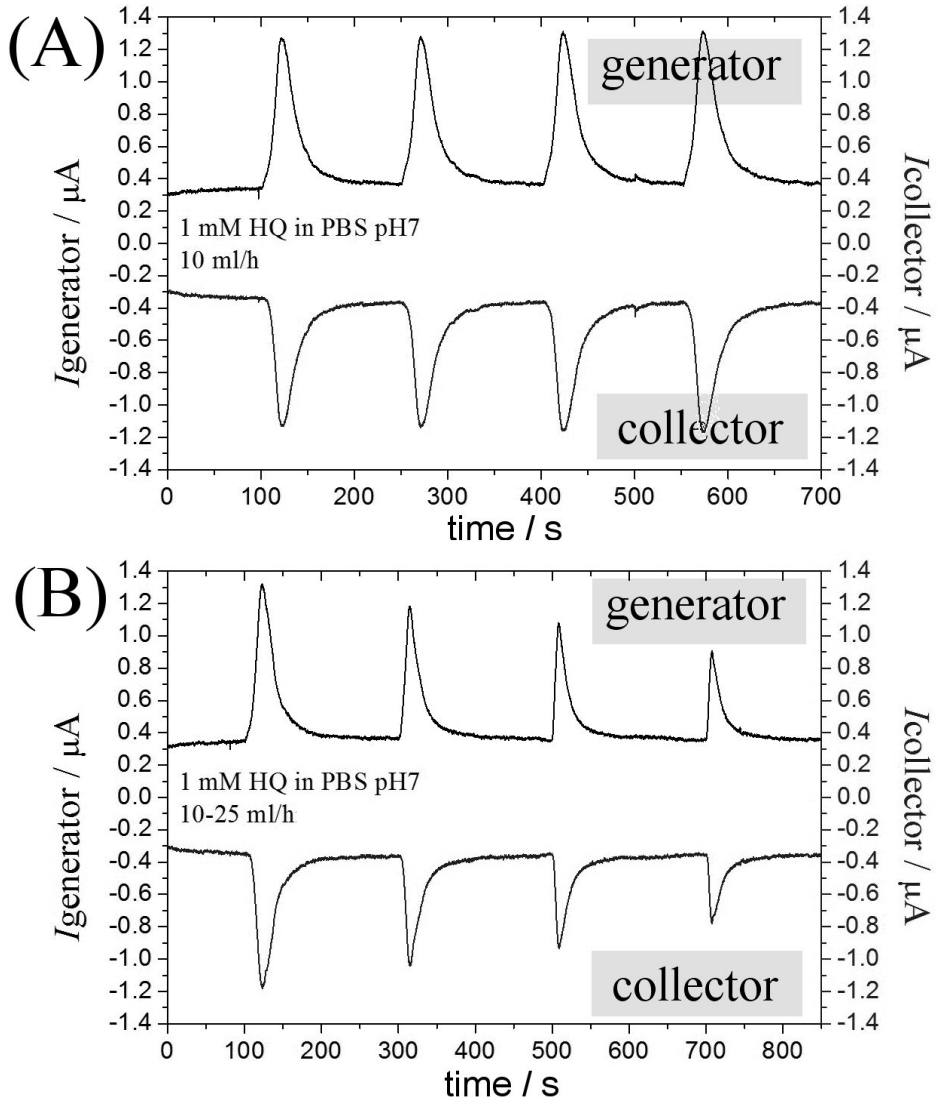


**Figure 6.6** (A) Chronoamperometry data (applied generator potential 1 V vs. SCE, applied collector potential -0.4 V vs. SCE, flow rate 10 mL per hour) obtained at a dual-plate BDD electrode with generator-collector feedback in 0.1 M phosphate buffer pH 7 for the oxidation of 1 mM hydroquinone. (B) As above but for a flow rate varying from 10 to 25 mL/h.

## 6.4 Summary and Conclusion

A simple flow injection cell with a BDD dual-plate micro-trench electrode detector has been successfully used for the flow injection electroanalysis of hydroquinone as a single working electrode detector and in generator-collector mode. The micro-trench geometry of the BDD dual-electrode enables the switching of the rate limiting diffusion process from outside to inside the trench, but unfortunately compromising the experimental peak current compared to theoretical values.

However, improvements in flow conditions and electrode geometry can further enhance the performance of this proposed flow injection device and obtain lower detection limits by:

(i) Reducing the trench width

(ii) Increasing the trench length or fabricate multiple parallel micro-trenches allowing for more analyte solution to be sampled

(iii) Increasing the trench depth

Detection limits of 1 μmol/L and lower would need to be achieved to ensure the device was comparable to other methodologies in the literature (see Table 1.3 in section 1.3.3).

Despite the limited sensitivity, BDD offers a robust electrode material where Piranha etch cleaning can maintain the functioning of the electrode and its wide potential window facilitates the detection of analytes at more positive potentials. This is desirable for environmental sensing as the lifetime of the electrode could ensure continual analysis rather than a one-use device and the wider potential window allows the detection of a greater number of contaminants.

An in situ flow injection device that offers continual real-time sampling of target contaminants is also advantageous in terms of cost and analysis time as it eliminates the need for:

(i) Sample collection

(ii) Storage and transport of materials

(iii) Preparation of samples before analysis

(iv) Trained professionals for sample analysis.

With this in mind, as a proof-of-concept, the BDD flow injection system described has the potential to be a useful new device for the detection of environmental pollutants such as hydroquinone, benzene and paracetamol and could possibly be incorporated with chromatography or other separation techniques for more sensitive and precise results.

## 6.5 References

1. Lewis, G.E.M., S.E.C. Dale, B. Kasprzyk-Hordern, A.T. Lubben, E.O. Barnes, R.G. Compton, and F. Marken, *Cavity transport effects in generator-collector electrochemical analysis of nitrobenzene.* Physical Chemistry Chemical Physics, 2014. **16**(35): p. 18966-18973.

2. Li, M., G.E.M. Lewis, T.D. James, Y.T. Long, B. Kasprzyk-Hordern, J.M. Mitchels, and F. Marken, *Oil vertical bar Water Interfacial Phosphate Transfer Facilitated by Boronic Acid: Observation of Unusually Fast Oil jWater Lateral Charge Transport.* Chemelectrochem, 2014. **1**(10): p. 1640-1646.

3. Gross, A.J. and F. Marken, *Boron-doped diamond dual-plate microtrench electrode for generator-collector chloride/chlorine sensing.* Electrochemistry Communications, 2014. **46**: p. 120-123.

4. Del Rio, R., F. Armijo, R. Schrebler, G. Del Canto, C. Vergara, and C. Gutierrez, *Modification of boron doped diamond electrodes with glucose oxidase, characterization by electrochemical techniques.* Journal of the Chilean Chemical Society, 2011. **56**(1): p. 621-624.

5. Toghill, K.E. and R.G. Compton, *Metal Nanoparticle Modified Boron Doped Diamond Electrodes for Use in Electroanalysis.* Electroanalysis, 2010. **22**(17-18): p. 1947-1956.

6. Strojek, J.W., M.C. Granger, G.M. Swain, T. Dallas, and M.W. Holtz, *Enhanced Signal-to-Background Ratios in Voltammetric Measurements Made at Diamond*

*Thin-Film Electrochemical Interfaces.* Analytical Chemistry, 1996. **68**(13): p. 2031-2037.

7. Yano, T., D.A. Tryk, K. Hashimoto, and A. Fujishima, *Electrochemical Behavior of Highly Conductive Boron-Doped Diamond Electrodes for Oxygen Reduction in Alkaline Solution.* Journal of the Electrochemical Society, 1998. **145**(6): p. 1870-1876.

8. Yano, T., E. Popa, D.A. Tryk, K. Hashimoto, and A. Fujishima, *Electrochemical Behavior of Highly Conductive Boron-Doped Diamond Electrodes for Oxygen Reduction in Acid Solution.* Journal of the Electrochemical Society, 1999. **146**(3): p. 1081-1087.

9. Pecková, K., J. Musilová, and J. Barek, *Boron-Doped Diamond Film Electrodes—New Tool for Voltammetric Determination of Organic Substances.* Critical Reviews in Analytical Chemistry, 2009. **39**(3): p. 148-172.

10. Klavarioti, M., D. Mantzavinos, and D. Kassinos, *Removal of residual pharmaceuticals from aqueous systems by advanced oxidation processes.* Environment International, 2009. **35**(2): p. 402-417.

11. Isarain-Chavez, E., R. Maria Rodriguez, J. Antonio Garrido, C. Arias, F. Centellas, P. Lluis Cabot, and E. Brillas, *Degradation of the beta-blocker propranolol by electrochemical advanced oxidation processes based on Fenton's reaction chemistry using a boron-doped diamond anode.* Electrochimica Acta, 2010. **56**(1): p. 215-221.

12. Martin de Vidales, M.J., C. Saez, P. Canizares, and M.A. Rodrigo, *Metoprolol abatement from wastewaters by electrochemical oxidation with boron doped*

*diamond anodes.* Journal of Chemical Technology and Biotechnology, 2012. **87**(2): p. 225-231.

13. Einaga, Y., J.S. Foord, and G.M. Swain, *Diamond electrodes: Diversity and maturity.* Mrs Bulletin, 2014. **39**(6): p. 525-532.

14. Jones, S.E.W. and R.G. Compton, *Stripping analysis using boron-doped diamond electrodes.* Current Analytical Chemistry, 2008. **4**(3): p. 170-176.

15. Honeychurch, K.C., G.C. Smith, and J.P. Hart, *Voltammetric behavior of nitrazepam and its determination in serum using liquid chromatography with redox mode dual-electrode detection.* Analytical Chemistry, 2006. **78**(2): p. 416-423.

16. Honeychurch, K.C., G.M. Davidson, E. Brown, and J.P. Hart, *Novel reductive-reductive mode electrochemical detection of Rohypnol following liquid chromatography and its determination in coffee.* Analytica Chimica Acta, 2015. **853**: p. 222-227.

17. Honeychurch, K.C., A.T. Chong, K. Elamin, and J.P. Hart, *Novel electrode reactions of diazepam, flunitrazepam and lorazepam and their exploitation in a new redox mode LC-DED assay for serum.* Analytical Methods, 2012. **4**(1): p. 132-140.

18. Hart, J.P., M.J. Shearer, and P.T. McCarthy, *Enhanced sensitvity for the determination of endogenous phylloquinone (Vitamin-K1) in plasma using high-performance liquid-chromatography with dual-electrode electrochemical detection.* Analyst, 1985. **110**(10): p. 1181-1184.

19. Voegel, P.D. and R.P. Baldwin, *Electrochemical detection in capillary electrophoresis with dual-parallel on-capillary electrodes.* Electrophoresis, 1998. **19**(12): p. 2226-2232.

20. Du, F.Y., S.N. Cao, and Y.S. Fung, *A serial dual-electrode detector based on electrogenerated bromine for capillary electrophoresis.* Electrophoresis, 2014. **35**(24): p. 3556-3563.

21. Zhong, M., J.X. Zhou, S.M. Lunte, G. Zhao, D.M. Giolando, and J.R. Kirchhoff, *Dual-electrode detection for capillary electrophoresis electrochemistry.* Analytical Chemistry, 1996. **68**(1): p. 203-207.

22. Sahlin, E., A. ter Halle, K. Schaefer, J. Horn, M. Then, and S.G. Weber, *Miniaturized electrochemical flow cells.* Analytical Chemistry, 2003. **75**(4): p. 1031-1036.

23. Albery, W.J. and Bruckens.S, *Ring-disc electrodes .2. Theoretical and experimental collection efficiences.* Transactions of the Faraday Society, 1966. **62**(523P): p. 1920-1931.

24. Albery, W.J., *Ring-disc electrodes .1. A new approach to theory.* Transactions of the Faraday Society, 1966. **62**(523P): p. 1915-1919.

25. Albery, W.J. and C.M.A. Brett, *The wall-jet ring-disc electrode .1. Theory.* Journal of Electroanalytical Chemistry, 1983. **148**(2): p. 201-210.

26. Albery, W.J. and C.M.A. Brett, *The wall-jet ring-disc electrode .2. collection efficiency, titration curves and anodic-stripping voltammetry.* Journal of Electroanalytical Chemistry, 1983. **148**(2): p. 211-220.

27. Unwin, P.R., *The ECE-DISP1 problem - general resolution via double channel electrode collection efficiency measurements.* Journal of Electroanalytical Chemistry, 1991. **297**(1): p. 103-124.

28. Fisher, A.C. and R.G. Compton, *Double-channel electrodes - homogeneous kinetics and collection efficiency measurements.* Journal of Applied Electrochemistry, 1991. **21**(3): p. 208-212.

29. Shrestha, B.R., A.P. Yadav, A. Nishikata, and T. Tsuru, *Application of channel flow double electrode to the study on platinum dissolution during potential cycling in sulfuric acid solution.* Electrochimica Acta, 2011. **56**(27): p. 9714-9720.

30. Fenn, R.J., S. Siggia, and D.J. Curran, *Liquid-chromatography detector based on single and twin electrode thin-layer electrochemistry - application to determination of catecholamines in blood plasma.* Analytical Chemistry, 1978. **50**(8): p. 1067-1073.

31. Anderson, L.B. and C.N. Reilley, *Thin-layer electrochemistry - steady-state methods of studying rate processes.* Journal of Electroanalytical Chemistry, 1965. **10**(4): p. 295-296.

32. Yildiz, A., Kissinge.Pt, and C.N. Reilley, *Evaluation of an improved thin-layer electrode.* Analytical Chemistry, 1968. **40**(7): p. 1018-1019.

33. Anderson, M.J. and R.M. Crooks, *High-Efficiency Generation-Collection Microelectrochemical Platform for Interrogating Electroactive Thin Films.* Analytical Chemistry, 2014. **86**(19): p. 9962-9969.

34. Amatore, C., N. Da Mota, C. Lemmer, C. Pebay, C. Sella, and L. Thouin, *Theory and Experiments of Transport at Channel Microband Electrodes under Laminar Flows. 2. Electrochemical Regimes at Double Microband Assemblies under Steady State.* Analytical Chemistry, 2008. **80**(24): p. 9483-9490.

35. Amatore, C., M. Belotti, Y. Chen, E. Roy, C. Sella, and L. Thouin, *Using electrochemical coupling between parallel microbands for in situ monitoring of flow rates in microfluidic channels.* Journal of Electroanalytical Chemistry, 2004. **573**(2): p. 333-343.

36. Bard, A.J. and L.R. Faulkner, *Electrochemical Methods*. 2001, New York: Wiley, p. 29.

37. Marken, F., J.C. Eklund, and R.G. Compton, *Voltammetry in the presence of ultrasound - can ultrasound modify heterogeneous electron-transfer kinetics.* Journal of Electroanalytical Chemistry, 1995. **395**(1-2): p. 335-339.

38. Hasnat, M.A., A.J. Gross, S.E.C. Dale, E.O. Barnes, R.G. Compton, and F. Marken, *A dual-plate ITO-ITO generator-collector microtrench sensor: surface activation, spatial separation and suppression of irreversible oxygen and ascorbate interference.* Analyst, 2014. **139**(3): p. 569-575.

39. Vuorema, A., M. Sillanpaa, L. Rassaei, M.J. Wasbrough, K.J. Edler, W. Thielemans, S.E.C. Dale, S. Bending, D. Wolverson, and F. Marken, *Ultrathin Carbon Film Electrodes from Vacuum-Carbonised Cellulose Nanofibril Composite.* Electroanalysis, 2010. **22**(6): p. 619-624.

40. Marken, F., C.A. Paddon, and D. Asogan, *Direct cytochrome c electrochemistry at boron-doped diamond electrodes.* Electrochemistry Communications, 2002. **4**(1): p. 62-66.

41. Adams, R.N., *Electrochemistry at Solid Electrodes*. 1969, New York: Marcel Dekker, p. 220.

42. Szabo, A., D.K. Cope, D.E. Tallman, P.M. Kovach, and R.M. Wightman, *Chronoamperometric current at hemicylinder and band microelectrodes - theory and experiment.* Journal of Electroanalytical Chemistry, 1987. **217**(2): p. 417-423.

43. Dale, S.E.C., A. Vuorema, M. Sillanpaa, J. Weber, A.J. Wain, E.O. Barnes, R.G. Compton, and F. Marken, *Nano-Litre Proton/Hydrogen Titration in a Dual-Plate Platinum-Platinum Generator-Collector Electrode Micro-Trench.* Electrochimica Acta, 2014. **125**: p. 94-100.

# Chapter 7

# Conclusion and Outlook

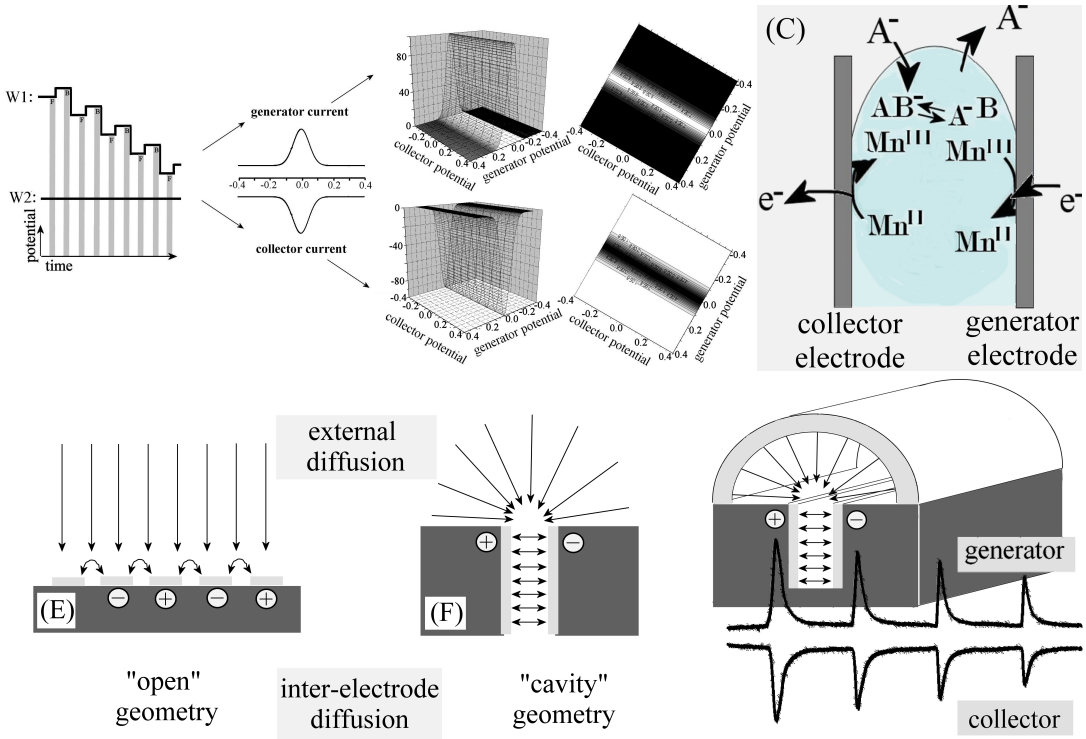


## Abstract

Presented here is an overview of the results found within this thesis and insights into future research.

# Conclusion and Outlook

The focus of this thesis has been upon generator – collector electro-analytical sensing with a view towards water quality monitoring. Current analytical techniques for the detection of contaminants in the aqueous environment are extremely successful with low detection limits and the ability to analyse complex matrices, however these methods are extremely time-consuming, costly and require a highly skilled labour force. Electrochemical sensing devices can offer a low cost alternative that is easily operated and benefit from i) fast response times; permitting real-time sampling, ii) the ability to miniaturize a system for portability, iii) low detection limits, and iv) wide linear range. This thesis investigates a variety of generator-collector electrode geometries, fabricated using low cost methods, to explore the detection of various environmental pollutants. The geometries used for this research were dual-hemisphere electrodes and dual-plate micro-trench electrodes that were fabricated in the laboratory and commercially produced interdigitated array electrodes were purchased for a comparison study. This chapter draws conclusions about the results in this thesis.

Chapter 3 demonstrated the use of square wave voltammetry in bipotentiostatic mode as a potential electrochemical method for sensing devices. It benefits from faster analysis compared to conventional cyclic voltammetry due to the shorter scan rates available (rate of voltage change over time), which enables the ability to detect short-lived intermediates, desirable for on-site analysis. The electrochemical analysis of indigo carmine using pulse voltammetry further explained this showing the distinction between reaction intermediates and the fully reduced/oxidised species by simply varying the pH environment. Difficulties arose however in un-buffered media, resulting in the mismatch of generator and collector signals from the changing pH gradients, but this

complexity provides a wealth of information regarding the kinetic mechanism and can be used for detecting the "fingerprint" region of complex analytes. Selectivity is important for environmental sensing applications and square wave voltammetry in generator-collector mode can provide more in depth detail about challenging redox reactions than a single voltammetric signal can. The electrode geometry used for these experiments was a gold-gold dual-hemisphere generator-collector electrode, fabricated using electro-deposition methods. Despite having a small inter-electrode gap, the fabrication method resulted in poor symmetry of the two hemispheres and a small active area for fast diffusion, giving low collection efficiencies. To further enhance on the sensitivity of these electrodes, small improvements to the geometry would prove beneficial.

The lab-bench fabrication of a gold-gold dual-plate micro-trench electrode (seen in Chapter 4) provided an electrode with a greater active area compared to that of the gold dual hemisphere electrode. Its electroanalytical performance was compared to a commercially produced gold interdigitated array electrode, exhibiting more stable steady state voltammetric responses when studying the reduction of nitrobenzene in aerated solution. The dual-plate electrode demonstrated more tolerance towards oxygen diffusing in from the bulk solution, illustrated by only a small shift in the electrochemical signal, and achieved a higher cavity transport coefficient, $\Phi_{cavity}$, indicating it was less sensitivity to convection in the bulk solution. These are ideal prerequisites for environmental detection that primarily involves analysis in complex media under less ideal conditions.

The success of the gold-gold dual-plate microtrench electrode in Chapter 5 saw the early development of a sensor for the detection of phosphate in water. The trench of the dual-plate electrode was filled to create a triple phase boundary reaction zone for

studying phosphate anion transfer, $H_2PO_4^-$. The process was made more selective by using a boronic acid facilitator and signals were amplified when using generator-collector voltammetry compared to using a single working electrode. Unfortunately, complex mechanistic and transport details remained unsolved, so further method development is needed to obtain a more robust sensor device (as mentioned in Chapter 5.4).

Chapter 6 demonstrated a novel boron-doped diamond dual-plate micro-trench detector for electrochemical flow injection was successfully employed for the electroanalysis of hydroquinone. Although the same electrode geometry was used in this study, the fabrication was improved to provide a more robust detector with smaller inter-electrode gap sizes. The previous method used a slow cure epoxy to glue the two electrodes together that acted as the spacer between them, but it was difficult to control the thickness of the epoxy layer, compromising reproducibility. The new method rectified this by spin coating a single layer of photo-resist, SU-8-2002, onto the two electrodes to produce a more precise thickness. Another modification made was the change in electrode material from gold to the more robust boron-doped diamond. It offers a wider potential window, enabling the detection of a greater selection of pollutants, and can be cleaned in strong reagents, such as Piranha solution, whilst still maintaining performance.

The flow injection system was used as a single working electrode detector and in generator-collector mode. With one working electrode ‘active’ the rate limiting process is primarily outside of the trench (diffusion towards the trench), with only a small fraction of the analyte entering the trench. To switch from an external to an internal process (diffusion within the trench), both working electrodes are ‘active’, in feedback mode, with only a small amount of the analyte in the external flow space being

consumed. The peak current is amplified by an order of magnitude compared to the single signals, with peak and width shape remaining, but this was lower than the theoretical value. This indicates that generator-collector electrochemical systems are an advantage over single working electrode devices and small improvements in the design could further enhance the performance to obtain the lower detection limits and match theoretical values. This proof-of-concept design shows promise for the continuous monitoring of emerging environmental pollutants and with changes to the electrode material and fabrication method, the lifetime of the detector is lengthened. Finally there is the possibility of combing the flow injection device with current analytical separation techniques for more sensitive and precise analysis.

The work in this thesis is preliminary in nature; it shows a variety of novel electrochemical sensing methods that have potential for the environmental monitoring of emerging pollutants. Future work includes the continual improvements in electrode geometry to provide smaller inter-electrode gap sizes with nano-meter distances for enhanced sensitivity and single molecule detection, experimental work in aqueous environmental matrices and interference studies to discover the selectivity of the devices against other emerging pollutants.